
Design considerations of a PAAm-PEGDA hydrogel wound dressing

-The release of anti-bacterial silver nanoparticles -

Master thesis

Lennart J. van Zanten and Marcus B. Frederiksen

Aalborg University
MATERIALS AND PRODUCTION



MATERIALS AND PRODUCTION

Aalborg University

<http://www.aau.dk>

AALBORG UNIVERSITY

STUDENT REPORT

Title:

Design considerations of a PAAm/PEGDA hydrogel wound dressing,- The release of anti-bacterial silver nanoparticles -

Theme:

Project Period:

9th/10th semester 2020/2021

Project Group:

5.319

Participant(s):

Lennart, J. van Zanten

Marcus Bevacqua Frederiksen

Supervisor(s):

Peter Fojan

Copies: 1

Page Numbers: 95

Date of Completion:

June 3, 2021

Abstract:

This project researches the diffusion of different shaped silver nanoparticles (Ag-NPs) through different concentration of PAAm/PEGDA gels. Mechanical properties of the different gels were tested by compression, elongation and rheology to see how the change in monomer and crosslinker concentration affected the strength of the gel. Swelling ratio of gels were measured too. SEM images were taken of both the gels and particles for characterization. The gels were loaded with prism, spherical shaped AgNPs and tetracycline and tested on *E. coli* and *S. cerevisiae* on agar plates and *E. coli* in LB-medium

More force is required to deform the gels when concentration of monomer and crosslinker is increased. The length of PEGDA does not affect the compression much. Gels cured with AgNPs become tougher compared to gels without nanoparticles. Elongation results showed with increased concentration of monomer and crosslinker more force are needed before the gels break but the stretchability decreases. The results from rheology and swelling were used to calculate mesh size and it showed the trend of increased concentration of PEGDA leads to smaller mesh sizes. The swelling further showed increased PEGDA concentration leads to decrease in swelling ratio. The gels cured with prism and spherical AgNPs had an comparable effect on bacterial growth with the normal gels.

The content of this report is freely available, but publication (with reference) may only be pursued due to agreement with the author.

Preface

This master thesis has been written by two master students, Lennart J. van Zanten and Marcus Bevacqua Frederiksen. The project period spanned from 3rd of September to 3rd of June under supervision from Peter Fojan. The 60 ects points project was developed at 3rd and 4th semester of the study program Nanobiotechnology, department of materials and production at Aalborg university.

The goal of this project was to control the mechanical properties of a PAAm/PEGDA hydrogel and further control the diffusion of silver nanoparticles to end up with a wound dressing which where able to diffuse antimicrobial agents.

IEEE citation style were used as references throughout the project meaning that text references is represented by numbers referring to the corresponding source in bibliography.

We would like to thank Dr. Peter Kjær for providing us with the SEM images of the produced nanoparticles used for the project. Furthermore, we would thank Thomas Sørensen Quaade for helping us with the compression and rheology equipment. Lastly we thank our supervisor professor Peter Fojan for the time he has spent helping us when needed.

Aalborg University, June 3, 2021

Lennart J. van Zanten
<lvanza19@student.aau.dk>

Marcus Bevacqua Frederiksen
<mfre16@student.aau.dk>

Summary

English

Chronic wounds can be a problem due to skin irritation and infection problems. Hydrogels are an efficient way to keep the wound clean and moist. If needed the gels can be loaded with antibacterial drugs with sustained release over a period, resulting in less dressing change and less stress for the wound. In this project the diffusion of prism and spherical shaped silver nanoparticles through different concentration of monomer (acrylamide) and crosslinker polyethylene glycol diacrylate (PEGDA) gels were investigated. Furthermore, the mechanical properties of the different gels were tested by compression and elongation to see how the change in monomer and crosslinker concentration affected the strength of the gel. Swelling ratio and rheology of the different gels were also measured and from the swelling and rheology results, mesh sizes were calculated. SEM images were taken of both the gels and particles to characterize them. AFM was also used to characterize the silver nanoparticles. The gels were loaded with the particles and tetracycline and tested on *E. coli* and *S. cerevisiae* on agar plates and *E. coli* in LB-medium

From the SEM analysis the prism and spherical shaped particles used in the gel had an average Feret's diameter of 59.8 ± 22.8 and 16.97 ± 12.37 nm, respectively. The pore size of the gels varied, and no conclusion can be made on how the concentration and length of PEGDA affect the size due to inhomogeneous crosslinking. From compression it was observed that more force is required to deform the gels when concentration of monomer and crosslinker is increased. The length of PEGDA does not affect the compression results compared to the change of PEGDA concentration. Compression and swelling testing were performed on gels cured with nanoparticles. The cured gels could withstand more applied pressure compared to gels without nanoparticles. Elongation results shows that with increased concentration of monomer and crosslinker more force is needed before the gels break but the Elasticity decreases. The results from rheology and swelling were used to calculate mesh size and it showed the trend of increased concentration of PEGDA leads to smaller mesh sizes. The swelling further showed increased PEGDA concentration leads to decrease in swelling ratio.

From diffusion experiment the gels consisting of 0.78% PEGDA and cured with tetracy-

cline released the most, no prism shaped nanoparticles were released and a low concentration of spherical nanoparticles were released. This explained the results when cured gels were tested on agar plates and in liquid medium. Only gels cured with tetracycline had a zone of inhibition for *E. coli* but when the cured gels were tested in medium all kinds of gels had an effect. The gels cured with tetracycline killed at lower concentration of *E. coli*. The gels cured with prism and spherical AgNPs had an comparable effect on bacterial growth with the normal gels.

Dansk

Kroniske sår kan være problematiske da hudirritation og infektionsproblemer kan opstå. Hydrogeler er en effektiv måde at holde såret rent og fugtigt på. Hydrogelerne kan yderligere effektiviseres ved at inkorporere dem med antibakterielle lægemidler, som kan frigive lægemidlet over længere tid. Dette resultere i mindre skift af bandage og er mere skånsom over for såret. Fokuset i dette projekt er at undersøge diffusion af prisme og sfæriske formede nanopartikler lavet af sølv. Yderligere vil vi prøve at kontrollere diffusion gennem gelerne ved at ændre på koncentrationer af monomer (akrylamid) og crosslinker (polyethylene glykol). Gelernes mekaniske egenskaber blev testet ved kompression og udstrukket til de gik i stykker for at se, hvordan ændringen i monomer og crosslinker koncentration påvirkede gelens styrke. Hvor meget gelerne udvidede sig i vand og rheologi for de forskellige geler blev også målt, og ud fra resultaterne blev gitterstørrelsen beregnet. Der blev taget SEM-billeder af både geler og partikler for at karakterisere dem. AFM blev også brugt til at karakterisere sølvnanopartiklerne.

Gelerne blev fyldt med sølvpartikler og tetracyclin og deres antibacterial effektivitet testet på *E. coli* og *S. cerevisiae* på agarplader og *E. coli* i LB-medium

Fra SEM-analysen havde prisme og de sfæriske formede partikler, der blev anvendt i gelen, en gennemsnitlig Feret-diameter på henholdsvis $59,8 \pm 22,8$ og $16,97 \pm 12,37$ nm. Porestørrelsen på gelerne varierede, og der kan ikke drages nogen konklusion om, hvordan koncentrationen og længden af PEGDA påvirkede størrelsen på grund af heterogene binding mellem crosslinker og monomer. Fra kompression blev det observeret, at der skal mere kraft til at deformere gelerne, når koncentrationen af monomer og crosslinker øges. Længden af PEGDA påvirker ikke kompressionsresultaterne sammenlignet med ændringen af PEGDA-koncentrationen. Test af kompression og gelens egenskab til at udvide sig i vand blev udført på geler med inkorporeret nanopartikler. De hærdede geler kunne modstå mere tryk samlignet med geler uden nanopartikler. Forlængelse af geler med viser, at med øget koncentration af monomer og crosslinker er der behov for mere kraft, før gelerne går i stykker, men deres evne til at forlænges mindskes. Resultaterne fra reologi og gelens evne til at udvide sig i vand blev brugt til at beregne gitterstørrelse, og det viste sig at øget koncentration af PEGDA fører til mindre gitterstørrelser. Evnen til at udvide sig i vand mindskes for gelerne når PEGDA koncentrationen øges.

Diffusionseksperimenterne viste at gelerne bestående af 0,78 % PEGDA og indeholder

tetracyclin frigav mest, ingen prisme formede nanopartikler blev frigivet, og en lav koncentration af sfæriske nanopartikler blev frigivet. Dette forklarede resultaterne, for gellerne testet på agarplader og i flydende medium. Kun geller med tetracyclin havde en hæmningszone for *E. coli* men når de samme geller blev testet i medium, havde alle typer geller en effekt. Gellerne med tetracyclin var de mest effektive til at slå *E coli* ihjel. Gellerne med prisme eller sfæriske nanopartikler havde en sammenlignelig virkning med de normale geller på bakterievækst.

AAM	Acrylamide
AFM	Atomic force microscopy
AgNP	Silver nanoparticles
AgNP_{prism}	prism shaped silver nanoparticles
AgNP_{spherical}	spherical shaped silver nanoparticles
LB	Lysogeny broth
NTA	Nanoparticle tracking analysis
O/N	overnight
PAAm	Polyacrylamide
PEG	polyethylene glycol
PEGDA	polyethylene glycol diacrylate
PEGDA₂₅₀	polyethylene glycol diacrylate average molecular length 250 Mn
PEGDA₅₇₅	average molecular length 575 Mn polyethylene glycol diacrylate
PEGDA₇₀₀	polyethylene glycol diacrylate average molecular length 700 Mn
PSSS	Poly sodium styrene sulphate
PVP	Polyvinylpyrrolidone
ROS	reactive oxygen species
SDS	Sodium dodecyl sulphate
TGA	Thermal gravimetric analysis
TPO	Trimethylbenzoyl-diphenylphosphineoxide
TSC	Trisodium citrate

Contents

Preface	v
1 Introduction	1
1.1 Polymers	2
1.1.1 Polymerisation of PAAm-PEG gels using TPO as photo initiator	3
1.2 Freeze drying of hydrogel	5
1.3 Hydrogel structure and diffusion	5
1.3.1 Hydrogel mechanics	5
1.3.2 Hydrogel structure	7
1.4 Antibacterial effect of silver	14
1.5 Synthesis and shape control of silver nanoparticles	15
2 Material and methods	19
2.1 Silver nanoparticle synthesis	19
2.1.1 Nanoparticle prisms	19
2.1.2 Ag nanospheres production method	19
2.1.3 Ag nanospheres production AG-ammonia complex method	20
2.2 Characterization of silver nanoparticles	20
2.2.1 UV-spectra of silver nanoparticles	20
2.2.2 AFM	20
2.2.3 Preparation of silicon wafers	20
2.3 TPO nanoparticles	21
2.3.1 TPO nanoparticle synthesis	21
2.3.2 Characterization of TPO nanoparticles	21
2.4 Hydrogel preparation and characterisation	21
2.4.1 SEM characterisation	22
2.5 Mechanical analysis	22
2.5.1 Compression	22
2.5.2 Elongation	22
2.5.3 Rheology	23
2.5.4 Swelling	23

2.6	Bacterial growth and preparation	23
2.6.1	Growth medium	23
2.6.2	Minimum inhibition concentration	23
2.6.3	Zone of inhibition	24
2.6.4	Segmented growth	24
2.7	Diffusion of particles	24
3	Results	27
3.1	Characterisation of nanoparticles	27
3.1.1	UV/Vis spectrum analysis of particles	27
3.1.2	Nanoprism	28
3.1.3	Ammonia complex spherical AgNPs	30
3.1.4	Scaling reaction volumes	31
3.2	TPO nanoparticles characterisation	33
3.3	Hydrogels	35
3.3.1	SEM image of hydrogels	35
3.3.2	Compression	39
3.3.3	Elongation	42
3.3.4	Rheology	45
3.3.5	Hydrogel swelling	46
3.4	cross-link dependent diffusion	47
3.5	Bacterial growth and inhibition	50
3.5.1	Minimal inhibitory concentration	50
3.5.2	Zone of inhibition	51
3.5.3	Segmented growth experiment	52
4	Discussion	57
4.1	Particle synthesis	57
4.1.1	AgNP synthesis	57
4.1.2	Spherical particles	58
4.1.3	TPO nanoparticles	58
4.2	Mechanical characteristics of PAAm/PEGDA hydrogel	59
4.3	Swelling of hydrogels	61
4.3.1	Diffusion through PAAm/PEGDA gels	62
4.4	Polymer network structure	63
4.5	Antibacterial effect PAAm/PEGDA hydrogel	67
4.6	Particle interaction with PAAm/PEGDA network	69
5	Conclusion	71
	Bibliography	73

Contents	xiii
A Particle shape and size characterisation	81
B Nanoparticle AFM and SEM image analysis	85
C SEM images and histogram of pore size	89

Chapter 1

Introduction

Chronic wounds such as pressure ulcers and burn wounds require proper attention. For these wounds traditional wound dressing such as gauze is not sufficient. Gauze can attach to the wound and this results in tissue damage when the bandage is replaced, causing pain and delay of the healing process [1, 2, 3]. Frequent contact with the wound adds increased risk of infection and it is a well known phenoma with chronic wounds. Therefore, there is a high demand for low-adherence antibacterial wound dressing.

Depending on the polymers used in the polymer network for hydrogels, they can have a strong adhesion to surfaces, mediated through hydrogen bonding and capillary adhesion [4]. Hydrogels posses strong sorption capabilities which help in debridement of the wound and removal of wound excudate of chronic wounds[2]. Debridement of wound area is the removal of death, necrotic tissue and bacterial cells, reducing inflammation of the wound area which helps with the wound healing process [1]. Since wound excudate contains inflammatory elements and enzymes that hinder wound repair, removal of the excudate is positive for wound healing [2, 1, 3]. Hydrogels also provide a sealed environment which protects wounds against anti-microbial migration to the wound area [1]. While sealing the area, it provides a moisture for the wound. They can increase the wound healing actively and passively by incorporation of natural polymers [3]. These natural polymers can mimic signals that increase wound repair processes. Synthetic polymers can still help the wound repair passively by covering the wound with high water content. A wet environment has been shown to be enough to speed up the wound healing process and is considered essential for burn and chronic wounds [3, 1]. In addition, hydrogels are versatile in development, where stimulating drugs for healing, enzymes and antibacterial agents such as antimicrobial peptides and silver nanoparticles can be incorporated. [5, 3, 2].

Polymers can either be biological or synthetic, depending on the chosen polymer different properties can be controlled such as stiffness, pore size, and the polymers interaction with the environment. The control of properties makes hydrogels useful in biological field such as tissue engineering, drug delivery or wound dressing [6, 7]. Hy-

drogels are used in tissue engineering to mimic extracellular matrices. Since the cells differentiate depending on stiffness and chemical stimuli [8, 9].

Drug delivery is also possible with hydrogels, since the drug can either be released through diffusion or the gel can react with the environment and release insulin or other drugs to the body [8, 10, 11]. Hydrogels are useful as wound dressing due to the large amount of water that can be absorbed by the gels which keeps the wound moist. Furthermore, the gel can work as a barrier for invading microorganism. Some synthetic polymers do not interact with the underlying tissue, which means it can be taken off without damaging the healing wound. With the right choice of polymer the hydrogel can also enhance the wound healing as seen when comparing chitosan based gels with chitosan free gels [2]. The presence of chitosan can elevate cell proliferation. Other natural polymers such as collagen and hyaluronic acid show similar effects. Another possibility is to mix the dressing with bactericidal agents such as antimicrobial peptide or metal nanoparticles. Wound dressing can be used as a drug delivery system keeping the wound clean while improving the healing process [2].

Although, hydrogels are already commercially available for difference usage like contact lenses and aforementioned biological fields, research is still necessary to increase understanding of how to modulate the drug release by changing cross-linker or monomer concentration used in hydrogels [12].

1.1 Polymers

Polymers can be classified by their origin which is either natural or synthetic. Each of them having their advantages. Natural occurring polymers are often used in tissue engineering since they either are components of or have similar properties as the extracellular matrix. Synthetic polymers on the other hand are controllable and reproducible. Thus it is possible to control cross-linking density, mechanical strength, gel formation dynamics and degradation properties. This is done by producing different molecular weights, block structures and cross-linking modes [13].

Often wound dressing consist of a combination of both natural and synthetic polymers to get the advantages of both. Synthetic polymers do not actively help with wound healing as natural polymers do. However, synthetic polymers does not get degraded either. They can help with the stabilisation of the wound dressing and are often more cost effective [1, 2, 13].

One of the most common synthetic polymer is acrylamide, often used in materials such as contact lenses and gels used for protein separation. Acrylamide advantages is its low cost, hydrophilicity and it does not interact with biological tissue. Mechanical strength (Young's modulus) of hydrogels made out of AAm can be tuned from 0.1 to 300 kPa. This can be done by increasing the monomer concentration, resulting in a higher w/w% polymer-water concentration. In addition the amount of cross-linking can be increased.[14, 15]. An advantages of being able to tune Young's modulus is the ability to

emulate soft tissue such as organs. The brain for example has a Young's modulus on 100 Pa whereas soft cartilage is 100 kPa. PAAm gels is also used to study stiffness-dependent cell behavior. [15, 16].

Poly ethylene glycol like acrylamide is bioinert and used in biological fields. The molecular weight can differ and is a useful tool to change gel properties [14]. Caykara et al. [17] studied PAAm-PEG gels with a difference in concentration and molecular size of PEG (4000, 6000 and 10000 g/mol). They observed that the increase of molecular weight led to larger pores and faster swelling. The change in concentration did not affect the swelling ratio as much as the effect of the molecular weight.

Furthermore, an increase in polyethylene glycol diacrylate (PEGDA) concentration increases the gel stiffness, therefore, decreasing the elasticity. This is due to higher cross-linking density which results in a smaller distance between cross-linking points. The smaller distances between cross-linking points does not only lead to a tougher gels, the mobility of polymer chains is inhibited as well. This means the polymer chains cannot stretch as much, meaning it takes up less water [17, 18, 19].

High concentration of cross-linker leads to a rigid gel due to inhomogeneous structure. When decreasing the cross-linker concentration the gel have more mobility which result in better dissipation of the applied stress. Norioka et al. [20] used PAAm and *N,N'*-methylenebisacrylamide as cross-linker. They discovered that high concentration of monomer (5 mol/L) and a small concentration of cross-linker (0.005 mol% cross-linker content) was the best way to make a stretchable and tough gel. They attributed this toughness to physical chain entanglement of PAAm acting as mobile cross-linkers. Another factor concerning hydrogel toughness besides length and concentration of cross-linker is the amount of cross-link binding sites. For example Browning et al. [21] tried to incorporate a 4-arm PEG cross-linker. The point was to make a tough gel without decreasing the mesh size due to higher cross-link density which is controlled by decreasing molecular weight or increased concentration of cross-linker. An affect of mesh size was observed with a 4-arm PEG cross-linker but to a smaller degree compared to change in molecular weight and concentration of PEGDA. Still by using the 4-arm PEG it was observed by tensile and compression testing the gel was tougher compered to gels with the same amount of linear PEGDA [21].

1.1.1 Polymerisation of PAAm-PEG gels using TPO as photo initiator

Polymerisation of gels can be done in two ways either by physical or chemical cross-linking. Physical cross-linking is binding of the polymers due to molecular interaction such as electrostatic, hydrophobic and H-bonding.

Chemical cross-linking polymers creates the most stable gels due to the formation of covalent bonds between polymers. However, the cross-linking initiators used is often toxic, meaning it needs to be washed out before the gel can be used [22].

Trimethylbenzoyl-diphenyl phosphine oxide (TPO) is a water insoluble photo initia-

tor (the cross-linking agent) and used to chemically cross-link the PAAm/PEGDA gels. Before the cross-linking process can happen the TPO is made water soluble. For this to happen, the TPO molecules are encapsulated by amphiphiles such as sodium dodecyl sulphate (SDS) to increase solubility in water and Polyvinylpyrrolidone (PVP) to avoid crystallization of organic compounds in water [18, 23]. (see fig. 1.1)

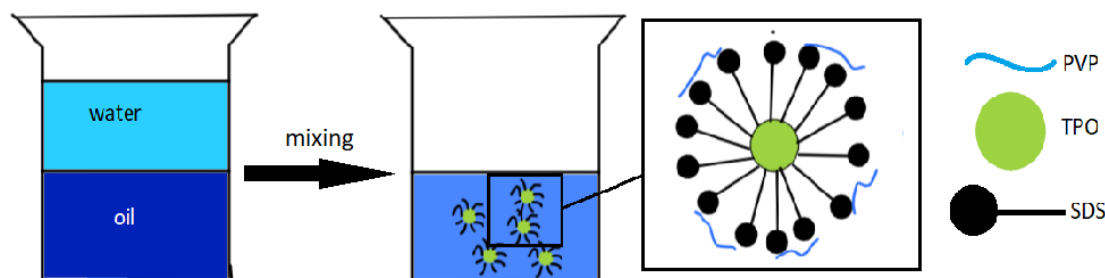


Figure 1.1: Water soluble TPO NPs

By encapsulating the TPO into micelles the water solubility is increased by 100 times compared to bulk TPO. Furthermore, TPO is also efficient at visible range 400 to 420 nm [23]. When TPO is exposed to light it creates radicals due to photo cleavage between the carbon-phosphorus bond resulting in two initiating radicals (see fig. 1.2). [24].

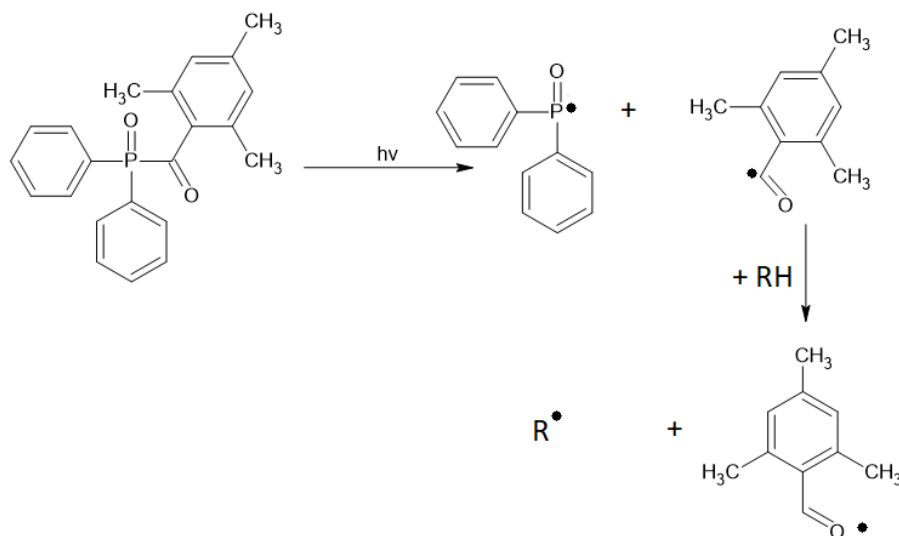


Figure 1.2: Homolytic cleavage of TPO between phosphor and carbon creating two radicals adapted from [24] chemsketch was used to draw the molecular structure [25].

The initiating radicals will propagate through the system and open the double bonds on the acrylate groups of both PEGDA and PAAm forming permanently cross-linked network as seen in fig. 1.3. Eventually the polymer solution will become a hydrogel. The

termination step occurs when the radical react with another radical canceling each other or the radical get entrapped by the entanglement of the cross-linked gel [18, 24].

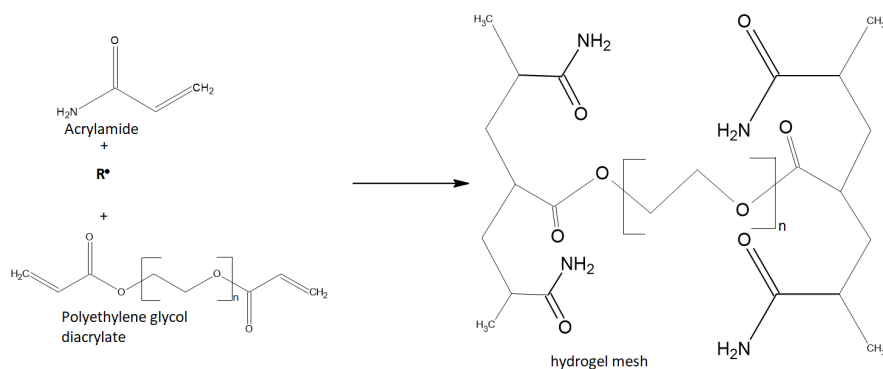


Figure 1.3: The chemical structure of acrylamide (monomer) and polyethylene glycol diacrylate (PEGDA) (cross-linker). R is the radical reacting with both polymers. n stands for the amount of ethanol group in the PEGDA chain. Image on the right is how the polymers are chained together (adapted from [24] and drawn with chemsketch [25]).

1.2 Freeze drying of hydrogel

SEM is used for imaging the morphology of hydrogels. Since vacuum is needed for SEM imaging, the gels needs to be dried after polymerisation. Freeze drying is an opportunity to both dry and change the morphology of the gel by adjusting freezing temperature [26, 27]. At high freezing temperatures (-20 °C) the ice crystals grow slower and bigger crystal are formed, which leads to larger pores on the gel after freeze drying. At colder temperature e.g. when gel is submerged in liquid nitrogen (-196 °C) the freezing results in many ice nuclei which further results in small ice crystals [28]. Problems that can occur during freeze drying is collapsing of the pores at the surface due to interfacial tension caused by the evaporation [27].

1.3 Hydrogel structure and diffusion

1.3.1 Hydrogel mechanics

When hydrogels are considered for wound dressing their mechanical properties are of importance. A strong elastic gel, with a decent adhesion to the skin is preferred as wound dressing. This adhesion should only be due to mechanical attributes such as capillary adhesion and hydrogen bonds formed between the water contained in the gel and the surface it comes into contact with [4]. Strength ensures that a gel does not break easily when applying it to a wound. Elasticity is nice for wound areas in places where the

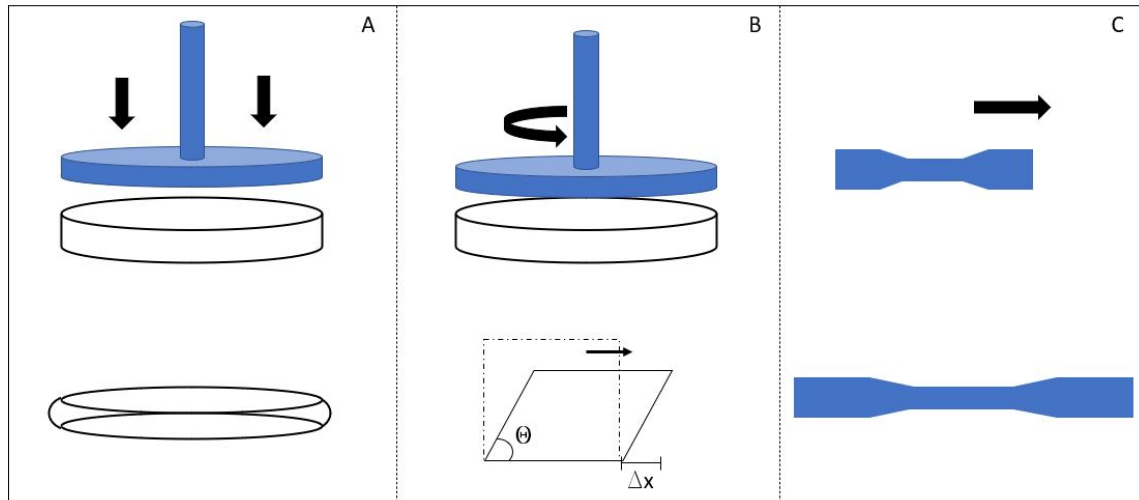


Figure 1.4: Different methods and forces used in measuring hydrogel/material strength

skin stretches, such as joints. By using compression, elongation testing and rheological measurements a good mechanical impression can be derived from the gel.

In compression the gel is compressed by a uni-axial force (fig. 1.4 A). Resulting in a negative deformation, where the reduction in height of the sample is taken as the deformation. By dividing the applied force with the deformation, pressure is derived expressed normally in Pascals.

$$\sigma = F/A \quad (1.1)$$

$$\epsilon = \Delta L/L \quad (1.2)$$

$$(1.3)$$

$$E = \frac{\sigma}{\epsilon} \quad (1.4)$$

In elongation (fig. 1.4), the gel is pulled by an uni-axial force, where the deformation is the length increase. From this follows a stress strain curve, Stress, σ is the amount of force applied on the cross sectional area. Strain, ϵ is the amount of deformation that occurs in the structure as it elongates, given by the percentage increase in length, $\Delta L/L$ [29].

For both compression and elongation a modulus can be given, which is a measure of force per area vs deformation. In case of compression this would be the modulus of compression to see how stiff a gel/material is. For elastic modulus it shows how far a gel can be elongated with a certain force and thus how elastic this material is. The Compression and elastic moduli are both considered to be the Young's modulus[29].

Aside from the elastic modulus, rheology can be used to investigate the shear modulus (fig. 1.4 B). The shear modulus is another measure of how elastic or rigid the a

material is [29]. With this method it is possible to investigate the viscosity of an material and often used to see the conversion rate, or polymerization rate, of hydrogels. Here again a force is applied that deforms the structure. instead of regarding the deformation in 1 direction, the force is applied on parallel planes in opposite direction. When we regard this on a square, where the force is applied on the top and bottom in opposing sideways direction. The angle between the two perpendicular planes will increase/decrease forming a parallelogram. The deformation is assessed by the transverse displacement, Δx , in a length measurement. In rheology this is done by having a bottom plate and the placing of a plate on top. The top plate is oscillating in both sideways directions changing the Δx , measuring the applied force over the sample area times Δx over the original height of the sample, Resulting in the G modulus.

$$G = \frac{Fl}{A\Delta x} \quad (1.5)$$

There exist a relationship between the Shear modulus and elastic modulus which uses the Poisson ratio, the measure of how much a material will deform perpendicular to the applied force.

$$E = 2G(1 + \nu) \quad (1.6)$$

ν is the poison ratio which for hydrogels is often taken as 0.5 due to a high amount of deformation upon stretching [29]. This leads to a relation: $E=3G$ for hydrogels. These moduli give a description of the forces the hydrogels can withstand and thus can be used as a measure of their strength. In addition they can be used to calculate other parameters of hydrogels such as the mesh size section 1.3.2.

1.3.2 Hydrogel structure

Hydrogels consist of polymers and water. These polymers form a network that retains the water, hydrophilic nature of the network is decided by the used polymers. There are different ways of making this network, either a pure polymer is used, an interpenetrating network or a cross-linked network. Since the gels are designed to be wound dressings, containing AgNPs, diffusion speed of these particles through the network is relevant for their release rate. By knowing the mesh size in the polymer network the diffusion can be estimated (fig. 1.5 A)

Before diffusion can be calculated the size of these pores need to be determined, this is done by calculating the average distance between the cross-linkers, mesh size. There are several ways to find values for this mesh size, one is from the swelling ratio and the other is by using the G' , storage modulus, which is part of the shear modulus which tells us how much energy is required to stretch the polymer network.

Swelling studies can be used to find the swelling ratio of the hydrogels. Placing the gels of a certain weight in water and measuring the weight over the coming days till it

reaches equilibrium. Rheology can be used to find the values for the G' modulus, where E modulus can be found with uni-axial elastic testing of hydrogels [30, 31, 32].

Mesh size swelling

According to Peppas [31] the mesh size can be determined by the root mean square of the un-perturbed end-to-end distance of a polymer chain.

$$\zeta = a\sqrt{\langle r^2 \rangle} \quad (1.7)$$

a is the length of deformation in the polymer network. Since Peppas et al. used the swelling of hydrogels to derive the equation a represents the change in volume in a gel. Where there is a change in every axis, $a_x a_y a_z$ for hydrogels the change in every axis is assumed to be homogenous, $a_x = a_y = a_z$ and thus leads to an increase of volume (fig. 1.5 B), $a^3 = V/V_0$. By taking the cubic root of the polymer volume fraction [31]:

$$a = v_{ps}^{-\frac{1}{3}} \quad (1.8)$$

The increase in lattice length is found which is proportional to the increase of polymer network volume of a swollen gel in equilibrium ($\langle r^2 \rangle$). Where $\langle r^2 \rangle$ can be expressed as for any specific polymer by:

$$\langle r^2 \rangle = nl^2 C_\infty \quad (1.9)$$

n is the number of bonds in the polymer chain and l is the length of the bonds in the polymer backbone. In the case for acrylamide this is C-C bond, which has a bond length of 0.154 nm. C_∞ is the characteristic ratio specified for the monomer used, AAm, and was taken as 12.5 [33]. It is an empirical measure for how rigid a polymer chains is. To know the length or distance in between cross-linking points we need to find the number of bonds in between the cross-linking location.

$$n = \frac{2M_c}{M_r} \quad (1.10)$$

The fraction finds the number of monomers, M_r , based on mass, in between cross-linking points, M_c and considers PAAm which has 2 C-C bonds per monomer in the polymer backbone.

Substituting equation eqs. (1.8) to (1.10) into eq. (1.7) allows for the calculation of mesh size based on the M_c .

$$\zeta = v_{ps}^{-\frac{1}{3}} l \left(\frac{2M_c}{M_r} C_\infty \right)^{1/2} \quad (1.11)$$

The number of bonds per molecular weight in between cross-linking points, can be approximated from the the w/w% between PAAm/PEGDA.

$$n = 2 \frac{w\%_{AAm}}{M_{AAm}} / \frac{w\%_{PEGDA}}{M_{PEGDA}} \quad (1.12)$$

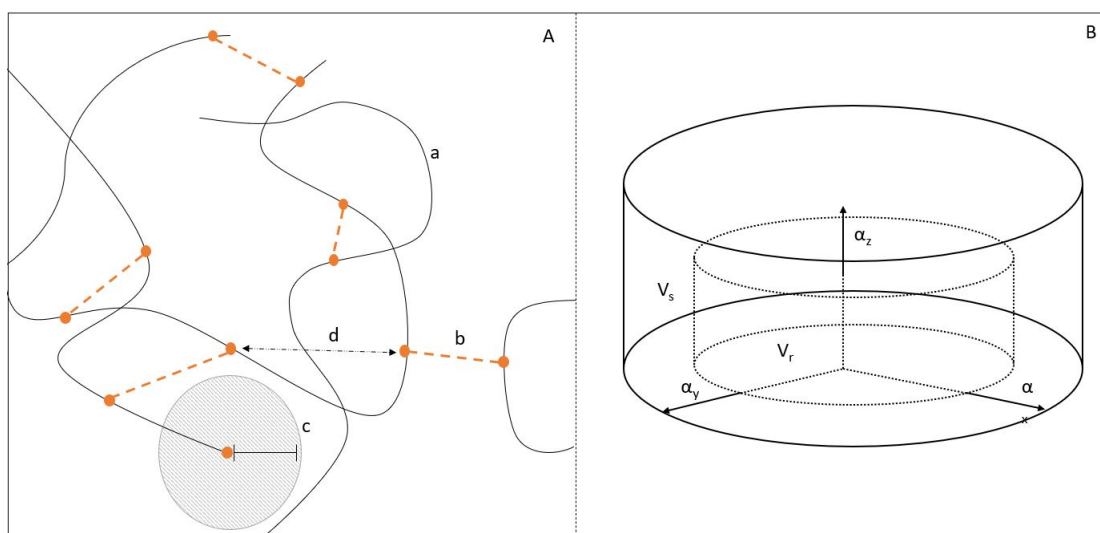


Figure 1.5: A) Schematic representation of a cross-linked hydrogel network. Where polymer strands of AAm (a) are cross-linked with PEGDA (b) to other PAAm strands. cross-linking points are assumed to be evenly spaced resulting in the M_C (d), from which the distance between links can be calculated. During polymerization there is a range a PAAm strand can grow in which is the root mean square unperturbed end-to-end distance (c), for cross-linked networks, that use a separate molecule as cross-linker the same is used to approximate the mesh size. B) A schematic of a swollen gel that swells equally in $a_x a_y$ and a_z and that a^3 is the increase in volume due to swelling V_r is the original volume and V_s is the volume after swelling.

M_{AAm} is the molar mass of AAm and M_{PEGDA} is the molar mass depending on the M_n of PEGDA. Where the molar ratio can be derived and thus the number of monomers per cross-linker. From this number the number of bonds is determined.

Mesh derived from swelling ratio

Finding the molecular weight between cross-linking points from swelling ratios requires a more complex calculation based on the volume fractions of polymer. To derive the M_C from a equilibrium swollen gel was discussed by Flory and Rehner back in 1943 [34, 30]. They derived the entropy of swelling in a polymer network based on 4 principles. 1) dilution of active chains with a number of solvent molecules. 2) cross-linking of chains in the presence of a solvent. 3) conversion of the cross-linked groups to polymer network in the presence of a diluent/solvent and 4) Formation of long polymer chains, since rubber molecules cross-link with the end of the chains increased length of the existing polymers would lead to a decreased number of cross-links.

Flory and Rehner assumed that polymer chain configuration was not altered by the swelling which allowed them to derive the length of the chains based on the swelling deformations [34, 30]. With this assumption they constructed the entropy contributions in the system based on swelling of polymer networks. Step 2 (S_A), 3 (S_B), and 4 (S_C)

represent the constraints of the model in a swollen state, where 1 (S_D) represents the change in network volume based on the added number of solvent molecules.

$$\Delta S_{swelling} = \Delta S_D + \Delta S_A + \Delta S_B - \Delta S_C \quad (1.13)$$

$$\Delta S_{relaxed} = \Delta S_A + \Delta S_B - \Delta S_C \quad (1.14)$$

They subtracted the entropy in a swollen gel from the entropy in a polymer network before swelling, which results in the total entropy contributed by the swelling.

$$\Delta S = \Delta S_{swelling} - \Delta S_{relaxed} \quad (1.15)$$

The components of $\Delta S_{swelling}$ use volume constraints for the model regarding the amount of swelling, solvent molecules are added. Then subtracting $\Delta S_{relaxed}$ from the entropy from swelling results in ΔS_D minus the volume difference produced between the network before and after swelling. Resulting in the total entropy contribution of a swelling network:

$$\Delta S = -kN \ln \left[\frac{N}{N + Zv} \right] - \frac{3}{2} k v \left[\frac{V_s}{V_p 1}^{\frac{2}{3}} - 1 \right] \quad (1.16)$$

k is the Boltzmann constant, N the number of cells and Z the number of elastically active chains in the gel. v is the specific polymer volume, the latter term therefore gives the volume fraction of polymer depending on the number of solvent molecules added and represents the contribution of the elasticity of the polymer chains to entropy. The first term is the contribution of thermodynamic mixing by dilution of polymer chains. Differentiation with respect to N , number of solvent molecules for the first term:

$$\begin{aligned} \frac{\partial \Delta S}{\partial n} - kn \left[\ln \left(\frac{n}{n + Zv} \right) \right] &= -R \left[\ln \left(\frac{n}{n + Zv} \right) - \frac{1}{n + Zv} \left(\frac{1}{n + Zv} - \frac{n}{(n + Zv)^2} \right) \right] \\ &= -R \left[\ln \left(\frac{n}{n + Zv} \right) - \left(1 - \frac{n}{n + Zv} \right) \right] \end{aligned} \quad (1.17)$$

$\frac{n}{n + Zv}$ represents the solvent volume fraction and can be written as the volume fraction of polymer $1 - \frac{Zv}{n + Zv}$, therefore,

$$-R \ln \left(\frac{n}{n + Zv} \right) - \left(1 - \frac{n}{n + Zv} \right) = -R \left[\ln \left(1 - \frac{Zv}{n + Zv} \right) + \frac{Zv}{n + Zv} \right] \quad (1.18)$$

For the second term the derivative in respect to N :

$$\begin{aligned}
\frac{\partial \Delta S}{\partial n} - \frac{3}{2}kv\left(\frac{n + Zv^{\frac{2}{3}}}{Zv} - 1\right) &= -\frac{3}{2}Rv\left(\frac{2}{3}\frac{1}{Zv^{\frac{2}{3}}}\frac{1}{(n + Zv)^{\frac{1}{3}}}\right) \\
&= -Rv\frac{1}{Zv^{\frac{2}{3}}(n + Zv)^{\frac{1}{2}}} \\
&= -\frac{Rv}{Zv}\left(Zv\frac{1}{Zv^{\frac{2}{3}}(n + Zv)^{\frac{1}{2}}}\right) \\
&= -\frac{R}{Z}\frac{Zv^{\frac{1}{3}}}{n + Zv}
\end{aligned} \tag{1.19}$$

combining the two terms:

$$\begin{aligned}
\frac{\partial \Delta S}{\partial n} &= -R\ln\left(1 - \frac{Zv}{n + Zv}\right) + \frac{Zv}{n + Zv} - \frac{R}{Z}\left(\frac{Zv}{n + Zv}\right)^{\frac{1}{3}} \\
&= R[n(1 - v_{ps}) + v_{ps}] - \frac{R}{Z}v_{ps}^{\frac{1}{3}}
\end{aligned} \tag{1.20}$$

Where v_{ps} is the polymer volume fraction in swollen state.

The above statement includes the contributions of thermodynamic mixing of solvent-polymer interaction and swelling of the polymer network to the total entropy, therefore, we can substitute eq. (1.20) into eq. (1.21) which represents the change in free energy in the system.

$$\Delta F = -T\Delta S\Delta H \tag{1.21}$$

$$\Delta H = BV_1v_2^2$$

$$K = \frac{2BV_1}{RT}$$

Flory and Rehner Incorporated the enthalpy which is dependent in the thermodynamic mixing term of the swelling entropy signified by K and ended up with eq. (1.22).

$$\Delta F = RT(Kv_2^2/2 + \ln(1 - v_2) + v_2 + (\rho V_1/M_c)v_2^{\frac{1}{3}}) \tag{1.22}$$

From the change in free energy we can calculate the M_c of a swollen gel in equilibrium state, $\Delta F = 0$

$$0 = RT(Kv_2^2/2 + \ln(1 - v_2) + v_2) + (RT\rho V_1/M_c)v_2^{\frac{1}{3}}$$

$$(-RT\rho V_1v_2^{\frac{1}{3}})/M_c = RT(Kv_2^2/2 + \ln(1 - v_2) + v_2)$$

leading to an expression for the M_c which can be calculated from the entropy in the system eq. (1.23).

$$M_c = -\frac{\rho V_1 v_2^{\frac{1}{3}}}{K v_2^2 / 2 + \ln(1 - v_2) + v_2} \quad (1.23)$$

$$\frac{1}{M_C} = \frac{2}{M_n} - \frac{\frac{v}{\bar{V}_w} [\ln(1 - v_{ps}) + v_{ps} + \chi v_{ps}^2]}{v_{ps}^{\frac{1}{3}} - \frac{v_{ps}}{2}} \quad (1.24)$$

Where v is the specific volume of the polymer in other words, the reciprocal of the density. M_C the molecular weight between cross-links, M_n is the average molecular weight of polymers in the solution.

This model by Flory and Rehner considered a polymer network where rubber was vulcanized. Vulcanisation is a process where rubber is treated at very high temperatures to cross-link the ends of already formed polymer chains. Aside from treatment, the assumption this model gives is that it does not account for solvent molecules that are present in the initial volume, cross-linking in solid state. After cross-linking they apply stresses to the system due to swelling. Bray and Merrill [35] modified Flory and Rehners [30] work on swelling entropy with a reference point for volume where the cross-linking occurs, a so-called relaxed state, already including solvent models in the initial volume which can be also applied to hydrogels.

$$\frac{1}{M_C} = \frac{2}{M_n} - \frac{\frac{v}{\bar{V}_w} [\ln(1 - v_{ps}) + v_{ps} + \chi v_{ps}^2]}{v_{pr} [v_{pr}^{\frac{1}{3}} - \frac{v_{ps}}{v_{pr}}]} \quad (1.25)$$

Here the polymer volume fraction in a swollen gel, v_{ps} is related to the polymer fraction in relaxed state, v_{pr} . Both models assume that there are already preformed polymers in the solution of M_n . In the case of condensed cross-linked hydrogels this is not the case. There are monomers present and cross-linkers of an M_n weight, in this sense the equations proposed by Flory & Rehner and Bray & Merrill do not apply in full, since they state that polymers are present before cross-linking. Aside from that they also used this model to describe polymer networks of 1 polymer, either rubber or PVA, not including other molecules that are used to cross-link. M_n can be used to calculate the number elastic active chains together with the average molecular weight, M_n between the cross-links [36, 35].

$$\frac{1}{M_C} - \frac{2}{M_n} = v_e \left(\frac{v}{V_p} \right) \quad (1.26)$$

Substituting eq. (1.26) in eq. (1.25) it becomes:

$$v_e \left(\frac{v}{V_p} \right) = -\frac{\frac{v}{\bar{V}_w} [\ln(1 - v_{ps}) + v_{ps} + \chi v_{ps}^2]}{v_{pr} [v_{pr}^{1/3} - \frac{v_{ps}}{v_{pr}}]} \quad (1.27)$$

Rewriting eq. (1.27) in terms of v_e

$$v_e = -\frac{V_p}{V_w} \frac{[\ln(1 - v_{ps}) + v_{ps} + \chi v_{ps}^2]}{v_{pr} \left[\frac{v_{ps}^{1/3}}{v_{pr}} - \frac{v_{ps}}{v_{pr}} \right]} \quad (1.28)$$

Elbert et al. made a statement that the v_e can be calculated from the total molecular weight of polymer and the average weight between cross-links [36].

$$v_e = \left(\frac{v}{V_p} \right) / M_C \quad (1.29)$$

This allows for the calculation of the number of elastic chains, dividing this number by the polymer mass should allow us to calculate the molecular mass in between cross-linking without using the number average molecular mass of polymers already present in the solution.

Therefor,

$$\zeta_{swelling} = v_{ps}^{-1/3} l \left[\frac{2 \left(\frac{v}{V_p} / v_e \right)}{M_r} C_\infty \right]^{1/2} \quad (1.30)$$

mesh calculation based on G storage modulus

Another way to approach the mesh size is based on the G' . By the equation from Peppas eq. (1.7) [31], where we know that the mesh of a swollen gel can be derived from the length of deformation and the root mean square length of unperturbed chains. For rheological measurements a gel is used after cross-linking without swelling. Therefor, there is no change in deformation $a = a_0$, so the mesh size becomes equal to the $\sqrt{r_0^2}$. Resulting in a similar formula seen in swelling (eq. (1.11))

$$\begin{aligned} \zeta_{rheology} &= \sqrt{r_0^2} \\ &= l \left(\frac{2M_c}{M_r} C_\infty \right)^{1/2} \end{aligned} \quad (1.31)$$

Flory et al. used a definition by Khun et al. to express a modulus of elasticity in terms of M_c [34].

$$\begin{aligned} \epsilon &= \frac{3RT\rho}{M_c} \\ M_c &= \frac{3RT\rho}{\epsilon} \end{aligned} \quad (1.32)$$

I was not specified which modulus should be used, however, multiple papers have used the G modulus in combination with this expression [32, 37]. Although Flory introduced the deformations in terms of uni-axial deformation, where the difference in length was specified. Indication that the Young's modulus should be used [30, 38]. Since eq. (1.6)

exists the G modulus can still be used to calculate the average mesh size by substituting equation eq. (1.32) into equation eq. (1.31) the mesh size from the elastic modulus can be calculated.

$$\zeta_{Rheology} = l \left(\frac{6RT\rho}{M_r \epsilon} C_\infty \right)^{\frac{1}{2}} = l \left(\frac{6RT\rho}{M_r G} C_\infty \right)^{\frac{1}{2}} \quad (1.33)$$

Since the ρ in eq. (1.32) was originally added as the density of a rubber network, it is replaced for the concentration of PAAm/PEGDA molecules in the hydrogel, $c = \rho v_{pr}$.

$$\zeta_{Rheology} = l \left(\frac{6RTc}{M_r G} C_\infty \right)^{\frac{1}{2}} \quad (1.34)$$

and for the elastic modulus

$$\zeta_{Rheology} = l \left(\frac{6RTc}{M_r G (2(1 + \nu))} C_\infty \right)^{\frac{1}{2}} \quad (1.35)$$

1.4 Antibacterial effect of silver

Silver nanoparticles (AgNPs) have seen a resurgence in their use as biomedical application. In the past decades investigation has been renewed into silver and its antimicrobial activity, this includes the use of AgNP in wound treatment. AgNPs are a good alternative to antibiotics in treating antimicrobial infections. With a wide spread in effectiveness against gram-positive, gram-negative and fungi, some of which are common in chronic wounds [39, 40].

The wide killing range of AgNP is due to the mechanism through which they trigger cell death, production of radical oxygen species (ROS) species. Literature describes the rapid production of ROS species by Ag^+ ions that accumulate in the cytoplasm which results in apoptosis [41]. In addition, DNA damage and the inhibition of important proteins, such as the reductases of the oxidative phosphorylation chain, have been named. How the ROS is initiated is not fully understood.

Beer et al. [42] showed that the effect of large particles $\sim 70\text{nm}$ is mostly dependent on the ions in the supernatant. In additions they show that smaller particles 15nm do have an effect that does not rely on the ion concentration. This would mean another mechanism is in play, the interaction between the AgNP and the cell wall/membranes of organisms. The nanoparticles form pores in the cell wall and the membrane through which the cytoplasmic content leaks out of the cells [43, 44].

The efficiency of AgNPs has been linked to their size and shape. The results summarized in Liao et al. [41] show that particles below 15nm in size have a strong killing effect. However, there are studies that also show an effect with larger particles [42, 43, 45, 46]. Although larger particles are still able to inhibit growth, the effective concentration increases significantly with size. Where smaller particles are more effective either due to

the increased release of Ag^+ ions due the large surface to volume ratio, or the increased contact of the AgNP to the cell wall [41].

It has been described that the shape of AgNP can have a significant effect on the bactericidal effect. Pal et al. [45] compared rod-shapes, triangular-shaped/prisms and spherical particles (~50nm) in their ability to inhibit cell growth and showed that prisms were more potent than spherical particles, whereas the rod-shapes barely showed any effect. The increased effect of AgNP_{prism} was ascribed to the {111} facet of the AgNP crystal which is responsible for a stronger interaction with the cell surface of bacterial cells [45, 46]. The {111} facet of the crystal has the most densely packed atoms and covers most of the surface of AgNP_{prism} , whereas the rod shaped particles have {111} facet on the smaller ends, correlating with the effect. Raza et al. [46] showed a difference in shape as well, using large AgNP_{prism} (~150nm edgelenh). These particles showed a stronger effect in a disk diffusion experiment compared to spherical particles (~10-90nm). Where the difference was more pronounced against *Psuedomonas aeruginosa* then *Escherichia coli*. Ferrag et al. demonstrated the diffusion of differently shaped particles and the effect against *e.coli* [47]. Where they demonstrate again the effect of prisms vs spherical vs rod-shaped particles. Where rod-shaped showed the least effect.

In addition to the shape and size of AgNP the surface charge plays a big role and can be positive or negative. This surface charge is dependent on the the capping agent used to stabilize AgNP (section 2.1). These capping are often molecules that adhere to the AgNP surface and carry a charge. Such as citrate which is a negatively charged molecule, this results in a negative charge on the surface of AgNPs ensuring the dispersion of AgNPs by electrostatic repulsion.

The relation between surface charge and toxicity /antimicrobial effect has been demonstrated by Abbaszadegan et al. [48] whom showed increased effect of positively charged particles in killing a range of gram-positive and negative bacteria. A suitable explanation would be the negatively charged membranes of organisms, which would lead a stronger attraction to positively charged particles, hence the increased effect of a positive surface charge. A similar finding was reported before by Badawy et al. [49]. Where AgNP with a citrate capping showed a decreased effect compared to neutral charge AgNP, capped with Polyvinylpyrrolidone [49]. Cytotoxicity is something that has to be considered when changing the capping agents. Since AgNP, as discussed before, have a broad distribution in cytotoxic effect, including mammalian cells where the effect seems indiscriminate [50]. Increasing the effect against prokaryotic cells based on the charge of the capping agent should also increase the effect against mammal cell.

1.5 Synthesis and shape control of silver nanoparticles

There are multiple methods of synthesizing AgNPs such as physical deposition, wet chemical and bio-based production. This report shall focus on the wet chemical synthesis of spherical and prisms AgNPs. Wet synthesis was chosen, since it is a relatively easy

process which requires a few steps. Although size distribution is easier to control with physical synthesis and production is higher with bio-based synthesis methods, chemical synthesis gives more control in shaping the particles [51]. Shape deciding components of the synthesis are most commonly polymers that adhere to the surface and block growth on one of the crystal faces more efficiently than other facets leading to an a-symmetric growth of particles and thus different shapes [52, 53, 54, 55]. Synthesis of particles require silver ions, Ag^+ which are normally added in the form of a silver salt such as $AgNO_3$.

In solution the silver ions Ag^+ are reduced to Ag^0 and loses its solubility leading to agglomeration with other neutral silver atoms forming nuclei. These nuclei cluster together to form colloidal silver particles [56]. The use of capping agents in this process is important to prevent the precipitation of silver metal from the solution. These capping agents are often polymers or surfactant molecules such as citrate [57]. Adding a charge to surface of the Ag colloid will increase the repulsion between particles, preventing further agglomeration between particles and keeps the particles water soluble.

To control the size of particles the strength of the reducer is the determining factor. Fast nucleation results in a relative monodisperse population of small particles, generally in the range of 5-10 nm. When a weaker reducer is added, the nucleation process and subsequent clustering occurs slower. Larger AgNPs with a lower monodispersity are produced in this fashion [56, 58]. Controlling the monodispersity of larger AgNPs is, therefore, often done through seed mediated growing of particles. First seeds (small AgNPs) are produced, $AgNO_3$ reduced with sodium borohydride. In a second reaction silver ions are reduced by a weaker reducer and the seeds are used to form bigger AgNPs. The reason this works is the slow reduction of Ag^+ and having the available nuclei in solution which form centers the silver can aggregate around [58]. Resulting in the growth of the existing seeds and the formation of relatively monodisperse nanoparticles.

Majority of the shapes are dictated by the capping agent and the interactions it has with the crystal facets of the AgNP crystal. When capping agents such as trisodium citrate have a stronger preference to bind to a specific facet. The growth on this facet will be blocked and growth follows another direction. In the case of citrate this would be flat and it blocks the {111} facet, creating flat triangular and hexagonal plates [52, 54]. A combination of citrate and PSSS can be used to form silver nanoprisms, $AgNP_{Prism}$. Citrate Binds to {111} facet, hindering Ag atoms from attaching to this side, increasing the rate of adsorption on the {100}, resulting in particle growth in that direction [52]. In addition to this the PSSS is determining in increasing the percentage of $AgNP_{Prism}$ formed by disrupting the lattice formation in the earlier stages of seed formation. Although, PSSS alone is not enough to form triangular NP, it does considerably reduce the amount of trisodium citrate required [52]. By adjusting the seed volume it becomes possible to control the size of $AgNP_{Prism}$. Spherical particles, $AgNP_{Spherical}$ can be made with citrate as well. Since citrate has a strong binding to the {111} facet, these particles become quasi-spherical. Xing et al made use of ions to increase the ellipticity of the parti-

cles by providing a more evenly distributed capping during particle synthesis, from this they selected Cl^- as most effective [59, 60]. Further optimisation of these particles was done by reducing the chemical potential of silver salt added, AgNO_3 . Adding ammonia to this salt resulted in formation of ammonia-Ag complexes.

Combining both AgNP and PAAm/PEGDA leads to the formation of a AgNP-composite hydrogel with a potentially increased antibacterial effect. Thoniyot et al. [5] mentioned multiple methods to embed hydrogels with nanoparticles. 1) Swelling hydrogels in a NP solution. Subsequent deswelling in acetone removes water while keeping NP in [47, 61]. Repeating these steps to increase the concentration of silver in the gel further, 2) physically embedding of NPs after polymerization, 3) NP formation in the gel, 4) cross-linking using NPs and 5) using polymer, NPs and a gelator molecule and 6) polymerizing hydrogels in the presence of AgNPs, forming AgNP-hydrogel composites. The idea of producing AgNP-hydrogel composites is to stabilise the AgNPs and control their release by controlling the diffusion through the gel, by adjusting cross-linking densities. This creates a wound dressing that provides microbial protection over time, meaning less frequent changing of wound dressings and less interaction with the wound [62]. The researchers goal is to find a combination of polymers optimal for wound dressing while also providing control of AgNPs release. Previous attempts have been made with alginate [63] and a combination of chitosan with polyvinyl alcohol [64].

AgNPs, beside being an antibacterial drug can also increase the mechanical properties of the hydrogels. This might be due the interaction of the AgNPs with the hydroxyl group of PEG or physical entanglement with the polymers [65, 66]. In addition to the antimicrobial effect of AgNPs, it was shown that AgNP improve the wound healing too. [62, 65, 67].

Masood et al. [65] tested Chitosan polyethylene glycol (PEG) gel as wound dressing on rabbits and observed that wounds healed faster by using the same wound dressing infused by AgNPs. They, however, did not identify why the AgNPs assist in the wound healing. Tian et al. [67] tried to check if the aid in healing was solely due to antimicrobial effect they compared AgNPs to amoxicillin and metronidazole, and still saw a faster contraction of the wound. They conclude that AgNPs also has an effects on the inflammatory phase of wound healing due to modulation of cytokines.

the aim of this study is to understand the diffusion of differently shaped AgNPs through a hydrogel consisting of polyacrylamide (PAAm) and polyethylene glycol (PEG). The release of AgNP is modulated by manipulating cross-linking density in order to produce a long lasting wound dressing for medical application of chronic wounds.

Chapter 2

Material and methods

2.1 Silver nanoparticle synthesis

2.1.1 Nanoparticle prisms

To make Ag nanoprisms a seed solution was prepared. This seed solution contains small spherical nanoparticles which provide a basis for Ag⁺ ions to aggregate. The solution was made by adding 0.25 mL 0.5g/L Poly(Sodium StyreneSulphate) (PSSS) and 0.3 mL 10 mM Sodium Borohydride (NaBH₄) to 5 mL 2.5 mM Trisodium Citrate. 5 mL 0.5 mM Silver Nitrate Was added dropwise trough a burette at 2 mL/min. When the complete volume of AgNO₃ was added the seed solution was ready. Final color of the mixture was a dark yellow color. For a further reaction to attain the Ag nanoprisms a new reaction container was filled with 5 ml of MiliQ water, 75 μ L of 10 mM Ascorbic Acid as the reducing agent and different volumes of seed solution were added. Bigger nanoprisms need a lower concentration of seed, smaller prisms a higher concentration. To this mixture 3mL of 0.5 mM AgNO₃ was added dropwise at 1 mL/min. The reaction was finished when the total volume of AgNO₃ was added. The reaction volumes changed in color in respect to nanoprism size (bigger particles show a blue/light blue color, whereas the smaller particles show a red/orange/pink color). 0.5 mL of 25 mM Trisodium citrate was added to stabilize the particles.

2.1.2 Ag nanospheres production method

Nanospheres were produced by reducing a 10 mM SN solution with 10 mM Sodium Borohydride in the presence of a stabilising agent, PSSS. An 10 mL 0.5 mM SN solution was prepared and 1.5 ml 0.1mg/ml PSSS was added. The Solution was stirring vigorous when the NaBH₄ was added dropwise from a burette at a speed of 1 mL/min. A total volume of 10 mL SBH was added. The color of the solution turned Dark yellow.

2.1.3 Ag nanospheres production AG-ammonia complex method

A different synthesis for spherical particles was approached. Here the precursor AgNO₃ was mixed with 28-30% ammonia to form Ag-ammonia complex. Slowing the reaction rate of Ag⁺ reduction to Ag atoms. First a seed solution was prepared in 23.75 mL MiliQ water which was brought to boil, 40 μ L 0.1 M ascorbic acid was added. After 1 minute a mixture of 500 μ L 1 wt% Sodium citrate, 125 μ L 1 wt% AgNO₃ and 100 μ L 20mM NaCl which was mixed for 2 minutes. A second reaction was made for particle growth. Here the 200 μ L seed volume was added to 4.73 mL MiliQ. For different sized particles different concentration seeds were used, where the seed solution was centrifuged at 6000 rcf (Eppendorf centrifuge 5804 R). 70 μ L of the Ag-ammonia complex was added to the reaction volume. Finally 2 mL of 2.5 mM Ascorbic acid was added to the reaction volume through a burette. For increased reaction volumes of 20 mL the ratio between miliQ water, seed concentration and Ag-ammonia were kept the same. The ascorbic acid concentration was reduced to 1 mM and the addition speeds was also kept the same.

2.2 Characterization of silver nanoparticles

2.2.1 UV-spectra of silver nanoparticles

The samples prepared as described in section 2.1 were characterized by measuring absorbance spectra. The absorbance measurement were made with the UV-1800 Shimadzu UV-spectrometer. absorbance spectra measured ranged from 300 nm to 1000 nm.

2.2.2 AFM

3 ml of the AgNP samples were centrifuged in eppendorf centrifuge 5804 R for 25 min at 3500 rcf. After centrifuging the liquid was split in supernatant and liquid pellet (precipitate). 5 μ L of the precipitate was deposited on to a clean silicon wafer (see section 2.2.3) and placed for 10 min before gently blow drying the wafer with nitrogen.

The AFM, Solver from NT-MDT was used, and the resolution of the AFM pictures was set to 512 X 512 pixels. For characterisation of the nanoparticles a software WSXM [68] was used. The AFM samples were further used in SEM (Zeiss gemini SEM). For analyse the SEM images, ImageJ was used to measure Feret diameter.

2.2.3 Preparation of silicon wafers

Silicon wafers were sonicated for 15 min in acetone than 15 min in ethanol afterwards. The wafers were put in a ozone chamber for 30 minutes. The surface was treated with a drop of 25/75% APTMS/Tolene solution for 30 minutes in a vacuum chamber. The vacuum chamber was flowed through 3 times with argon. at 5 minutes interval to create an inert atmosphere. The particles were centrifuged and the pellet was deposited on the

wafers, particles were adhered to the surface after 30 minutes. The wafers were rinsed with milliQ and dried before use on the AFM or SEM.

2.3 TPO nanoparticles

2.3.1 TPO nanoparticle synthesis

The amount of chemical used to make TPO particles presented here is for a 50 mL 10% TPO NP-solution and the recipe is from [23] 3.75 g of PVP was added to 13.375 mL isopropanol in a bluecap bottle and stirred. The solution was heated to 50 °C to melt the PVP for 30 min. When the PVP was melted 12.64 mL of butyl acetate, 3.75 g of pulverized SDS and 0.85 g of TPO was added under continues stirring till SDS was dissolved (~ 60 minutes). Next, 20 mL of water is added and an oil phase and water phase was obtained. Stirrer the mixture until a clear solution with only one phase was visible and clear. The solution was frozen in liquid nitrogen and freeze dried over night at 0.001 mbar (Christ Alpha 1-4 LD plus).

2.3.2 Characterization of TPO nanoparticles

For the characterization of TPO NPs, the nanoparticle tracking analysis (NTA) NanoSight LM12 were used. Firstly the freeze dried TPO NPs got dissolved in 75 mL milli-Q water to make a stock solution. 1 mL of stock solution and a 1:4 dilution were made in eppendorf tubes for measurement. The samples got further diluted 1:10 in the syringe used for sample insertion. A laser beam gets through the sample to detect the Brownian motion of the particles. After the first batch ran dry, the other TPO solution made were filtered with 400 μ m filter to removes excess polymers or amphiphiles and analysed with a spectrophotometer (Shimadzu UV1800) to see if the wanted TPO particles were present.

2.4 Hydrogel preparation and characterisation

To investigate the influence of AAm and PEGDA concentratoins on mechanical properties. Gels with varying AAm concentration and PEGDA concentrations were made. The first gels made consisted of 20, 15, 10 and 5 % AAm with a 1.56 % PEGDA/AAm ratio with the number average molecular weight of 575 Mn. The next bunch of gels consisted of 15 % AAm and either 0.78, 1.56, 2.34 and 3.12% PEGDA/AAm ratio (table 2.1. The different length of PEGDA was 250, 575 or 700 Mn. PEGDA₅₇₅ was used for when either changing the monomer or cross-linker concentration. For gels with either PEGDA₂₅₀ or PEGDA₇₀₀ only 0.78 and 3.12 % PEGDA/AAm ratio where made for further experimentation, and it was assumed that 1.56 and 2.34 % PEGDA would give a result in between those two extremes. The stock solution of AAm was 50 % monomer in water.

Table 2.1: The amount of added chemicals to make different w/w% gels for a volume of 2 ml

AAM[%]	Aam[ml]	PEGDA[μ L]	TPO NP[mL]	milli-Q water[mL]
20	0.8	6.24	0.827	0.375
15	0.6	4.68	0.62	0.78
10	0.4	3.12	0.413	1.187
5	0.2	1.56	0.207	1.593
PEGDA [%]	Aam[ml]	PEGDA[μ L]	TPO NP[mL]	milli-Q water[mL]
3.12	0.6	9.36	0.62	0.78
2.34	0.6	7.02	0.62	0.78
1.56	0.6	4.68	0.62	0.78
0.78	0.6	2.34	0.62	0.78

The gels were made either in a syringe for compression testing, in a dogbone mold for elongation test and petridishes for diffusion testing. After mixing the solvents, it was placed in the desired mold depending on the usage. The mold where placed in Anycubic wash and cure and cured at 405 nm UV-light until the solution became solidified gels.

2.4.1 SEM characterisation

hydrogel samples were frozen in liquid nitrogen (-196 °C before freeze drying at 0.001 mbar (Alpha 1-4 LDplus). Other samples were prepared as follows. The gels were frozen than snapped before freeze drying. To make SEM measurement possible the gels were goldsputtered for 1.5 minutes. The sizes and Feret diameters of the pores were analysed by using ImageJ [69]. Both results were used to compare SEM result with calculated mesh size.

2.5 Mechanical analysis

2.5.1 Compression

The hydrogels were compressed in DMA 850 by the company TA instruments. Before compression 5mm thick disks with a diameter of 15 mm were cut and placed in the apparatus. The DMA was set to apply force with incremental steps of 1 N/min starting from 0 N and ending at 15 N.

2.5.2 Elongation

Gels polymerized in a 3D printed mold were manually elongated with 3D printed clamps (Anycubic Photon 3D printer). Keeping one clamp stationary alongside a ruler and pulling the other clamp in one direction with a newton meter. This allows for length measurement and corresponding force measurements. These experiments were filmed

and later analysed frame by frame producing a elongation force curve. The dog bone had a middle part with the dimension $3 \cdot 1 \cdot 0.29 \text{ cm}^3$ and two identically squares at the ends with dimension of $2 \cdot 1.5 \cdot 0.29 \text{ cm}^3$

2.5.3 Rheology

Rheology measurements were done with AR-G2 (TA instruments) on the 10, 15, 20% AAm gel plus all of the PEGDA gels. 2.5 mL of the gel solutions were made and cured in petridishes (diameter of 35 mm). Each of the gels were cut to the same size with a water bottle cap. After the cutting the gels were placed on the AR-G2, where first oscillation amplitude was measured followed by the frequency sweep with 1% strain through out the measurement, the sweep ranged from 100 rad/s to 0.1 rad/s. Amplitude test were done from 0.1% to 100% strain, where storage modulus and storage loss were assessed.

2.5.4 Swelling

The swelling test was done on gels with different concentration and length of PEGDA and 15 % PAAm. The gels were made according to table 2.1 and cut into discs, 1.5cm in diameter and 3 mm high and weighing 0.15-0.2 g. Gels were kept in petridishes with abundant water and were weighed every hour for the first 8 hours, before measuring them once daily for 48 hours. Weighing was done by placing the gel on a tissue paper, removing all remaining liquid before putting it on the scale.

2.6 Bacterial growth and preparation

2.6.1 Growth medium

Two growth medium were prepared one for *E. coli* and *S. cerevisiae*. 1 L Lysogeny Broth (LB)-medium was prepared by measuring 10 g of tryptone, 10 g of NaCl and 5 g of yeast extract. The three compounds were added into a 1 L blue cap bottle and 1 L of milli-Q water was added to the mixture and shook for a few seconds. For LB-agar plates 15g of agar is added

For yeast culture 1L of YPD-medium was made with 20g of dextrose and peptone. 10g of yeast extract was added and for plates 20g of agar was used.

Both YPD and LB-medium were autoclaved at 121 °C for 30 min under 1 bar pressure, where all compounds got dissolved. The liquid medium was stored at 4 °C and agar medium was stored at 60 °C until usage.

2.6.2 Minimum inhibition concentration

5 mL of O/N *E. coli* culture was incubated for 24 hours. 100 μL of the *E. coli* culture were transferred to 9 new tubes with 4 mL of LB-media and incubated at 37 °C for 2 hours.

After 2 hours the cultures were taken out of the incubator and 1 mL of either spherical or AgNP_{prism} solutions was added. 4 different particle concentrations were taken per shape, 2x concentrated, 1x, 0.5x and 0.25x. the cultures were incubated for 16-20 hours at 37°C. After two hours 100 μ L of each culture tubes where spread on agar plate for counting the next day.

2.6.3 Zone of inhibition

The antibacterial effect of the gels were also tested on both LB-agar and YPD-agar plates. First an O/N culture was made for both *E. coli* and *S. cerevisiae*. 200 μ L of the cultures were spread on the plates and the plates were placed in incubator for 30 minutes before a gel was placed upon the agar plates. The gels were loaded with prism NPs, spherical NPs or tetracycline in them. After the gel where placed on the agar plates, they were put back in the incubator overnight to be checked the next day. Images were taken and the zone of inhibition was measured with ImageJ [69].

2.6.4 Segmented growth

The gels have been tested on dry medium (agar plates), however also in liquid medium. For this experiment an O/N culture of *E. coli* was grown in 5 ml LB-medium, and gels for the experiment were made. Only one concentration of gel was made to make the experiments more comprehensible. The concentrations used were 0.78% PEG and 15% AAm, they where made with either prism, spherical NPs, tetracycline or just water. 3 ml of the gels where made in syringe with a 8 mm diameter.

The next day the O/N culture was used to make a serial dilution ($10^{-1} - 10^{-8}$) in 4.5 ml LB-medium and the different gels where placed inside the dilutions. OD_{600} was measured at 0 hours, 2 hours and every following hour, up to eight hours. After eight hours the different cultures were left overnight to see if growth would still occur the next day.

Eight dilutions, each with either prism NPs, spherical NPs or tetracycline gave 24 samples + 4 samples with normal gels. To make it easier and more comprehensible the repeating of the experiment was done with dilutions of $10^{-2} - 10^{-7}$. At the start of every experiment, 100 μ L of the dilutions from the negative control got plated for counting of colony forming units (CFU).

2.7 Diffusion of particles

To understand how particles move trough the gel, 3 gels were made with quasi spherical AgNP, Prism AgNP and tetracycline. Particles were made according to section 2.1 and up concentrated by centrifugation (5500 rcf for Ag_{Prisms} and 6000rcf for AgNP_{Spherical} in eppendorf centrifuge 5804 R) and adjusting the supernatant volume to the desired

concentrations, prisms 1:5 and spherical 1:3. A tetracycline solution was made of 0.2 mg/mL in MiliQ water. Gel solutions were made according to table 2.1 were particle and tetracycline solutions replaced the water volume. The gel solutions were poured into a petridish 4 cm in diameter and polymerized with 405 nm light emitted from anycube for 6 minutes. From this gel smaller gels were cut (0.2–0.3 gram), weighted and put into cuvettes. 2 mL water was added to start the diffusion of the gel content. Measurements were taken every hour for a duration of eight hours, followed by 1 measurement every 24 hours for 1 week.

Chapter 3

Results

3.1 Characterisation of nanoparticles

Characterisation of nanoparticles was done with AFM and SEM each instrument has their advantages. AFM where used to measure height and SEM for width of the nanoparticles. UV/vis measurements were conducted on the different sized of prism and spherical AgNPs solutions to asses the maximum absorbance, giving information about shape and size.

3.1.1 UV/Vis spectrum analysis of particles

UV/Vis spectra was used to get a fast insight in the particle dimensions and can be used as an indication for particle shape. Trisodium citrate was used together with PSSS as capping agents to produce AgNP prisms. The spectra of particle solutions where a different seed particle quantity was used is shown in fig. A.1. Here it can be seen that synthesis with decreasing seed volume results in a red shift of the maximal absorbance peak. This can also be observed in table 3.1 where the maximum absorbance has been linked to the wavelength. Prism_{25 μ L} shows a broad absorbance of low intensity with a maximal absorbance at 606 nm. Prism_{50 μ L} maximally absorbed at 809 nm. An overall wide ditribution was seen for Prism_{25 μ L} where less than 200 μ L seeds were used. Prism_{100 μ L} had a maximum abosorbtion at 684 nm where Prism_{150 μ L} absorbed at 645 nm. Maximal absorbance continued to decrease for Prism_{200 μ L}, 559 nm, Prism_{400 μ L} 520 nm and 518 nm for Prism_{600 μ L}.

It is common that AgNP are not stable over a longer period of time, therefor, the solutions were measured again with UV/vis after two months. The resulting maximal absorbance peaks are broad, where the maximal signal is spread over a range of wavelengths. in the 50, 100 and 200 μ L seed synthesis solutions, only 1 peak could be observed. The maximum absorbance was increased for all particles except for Prism_{150 μ L}, which remained the same and Prism_{600 μ L} where the absorbance had decreased.

Table 3.1: Table describes the maximal absorbance measured for the different NP solutions. For this maximal absorbance the wavelength was given. New spectra were recorded after 2 months.

	25 μL Prism	50 μL Prism	100 μL Prism	150 μL Prism	200 μL Prism	400 μL Prism	600 μL Prism
Wavelength	606	809	684	645	559	520	518
Wavelength 2 Months	614	824	677	645	565	537	502

3.1.2 Nanoprism

Height of the different was successfully measured with AFM, topography were used to produce height histograms for the different sized prism particles (fig. 3.2). heights are given in table 3.2, for Prism_{50 μL} , Prism_{100 μL} , Prism_{200 μL} and Prism_{400 μL} . The height for these prisms were 6 ± 5.5 , 7.18 ± 3.68 , 3.11 ± 2.56 and 3.2 ± 1.56 nm respectively (table 3.2.) The height was taken as the average of the histogram data, fig. 3.2 C for 400 μL , for the other samples topographies were used in the same way appendix B.

SEM images were taken of nanoprisms produced with different amounts of seed (appendix fig. A.2. From these images histograms of the Feret's diameter were made fig. 3.1. This diameter represents the edgelength of AgNP_{Prism} and were used to compare size. The average Feret diameter found for Prism_{50 μL} , Prism_{100 μL} , Prism_{200 μL} and Prism_{400 μL} ul were, 47.19 ± 36.8 , 39.41 ± 18.28 , 24.89 ± 9.77 and 15.05 ± 7.13 nm, respectively. For AgNP_{Prims50} a high distribution is seen, both visible on the histogram and in the standard deviation (fig. 3.1 A). More clear populations are seen in AgNP_{Prims100,200,400} where the distributions are still high, clear peaks are visible (fig. 3.1 B-D).

Table 3.2: The mean height of the different NP samples and the amount of seed solution used to make them.

Shape	Seed solution [μL]	mean height
Prism	400 μL	3.2 ± 1.56 nm
Prism	200 μL	3.11 ± 2.56 nm
Prsim	100 μL	7.18 ± 3.68 nm
Prsim	50 μL	6 ± 5.5 nm height

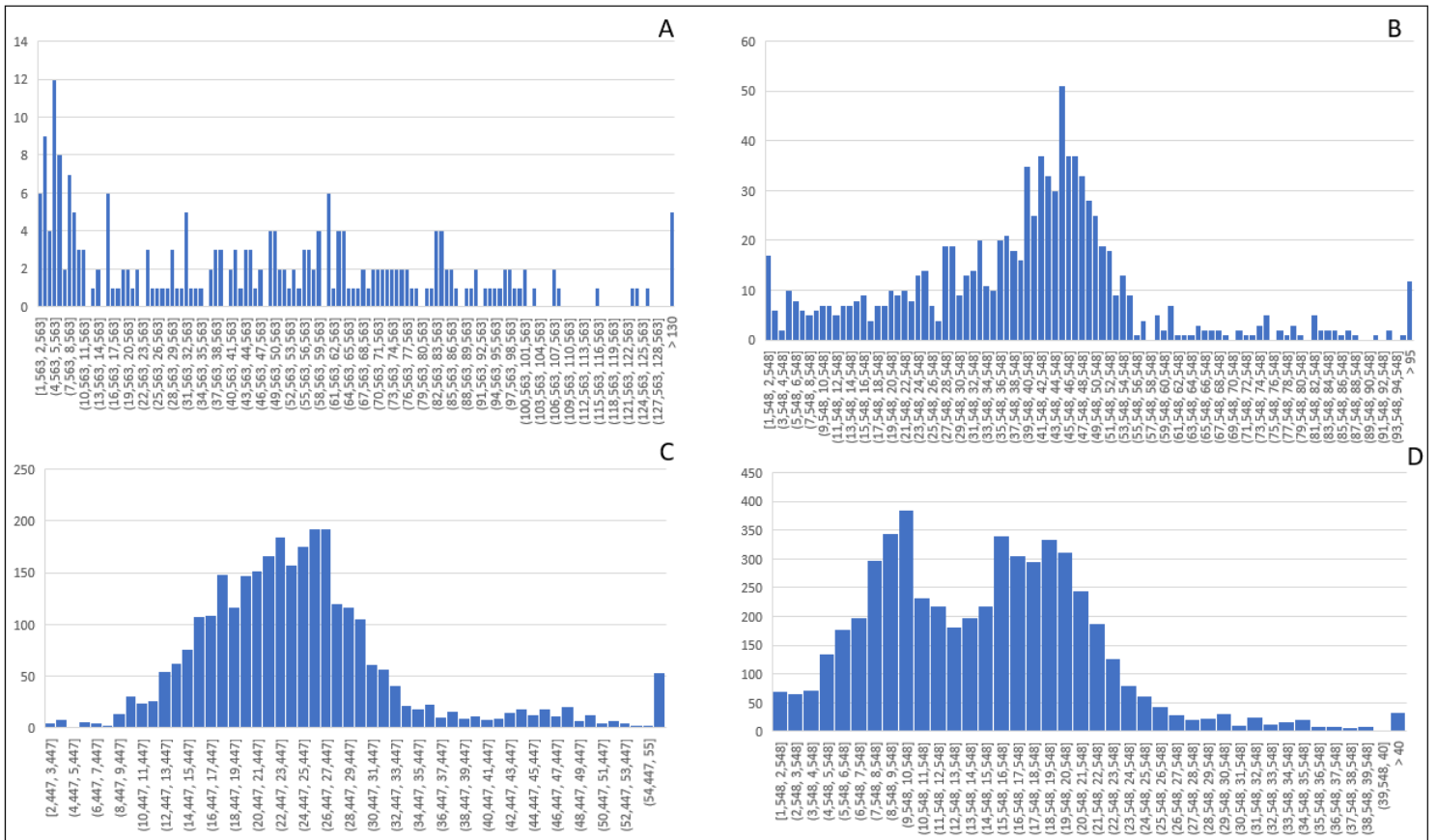


Figure 3.1: The Feret diameter distribution for the nanoparticles prism made with different amount of seeds. A) 50 μL , B) 100 μL , C) 200 μL , D) 400 μL

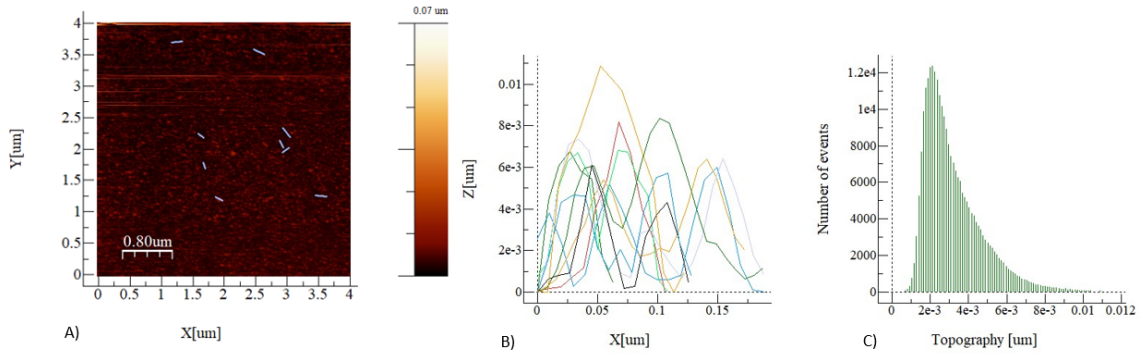


Figure 3.2: AFM image ($4 \times 4 \mu\text{m}^2$) of prism nanoparticles made with 400 μL seed solution is seen in A). Height measurement of selected particles is seen in B) where the selected particles measured is seen by the blue line in A). Height distribution of pixel is seen in C)

3.1.3 Ammonia complex spherical AgNPs

Spherical particles were produced with citrate capping, from ammonia-silver complexes. These particles were grown with different seed volumes to produce varying sized particles. Both SEM and AFM were used for analysing the particle size. AFM was useful measuring heights whereas SEM could measure width. From AFM images histograms were made and average sizes were calculated fig. 3.3, for AgNP₄₅, AgNP₆₀, namely 40.23 ± 10.80 and 44.62 ± 15.03 .

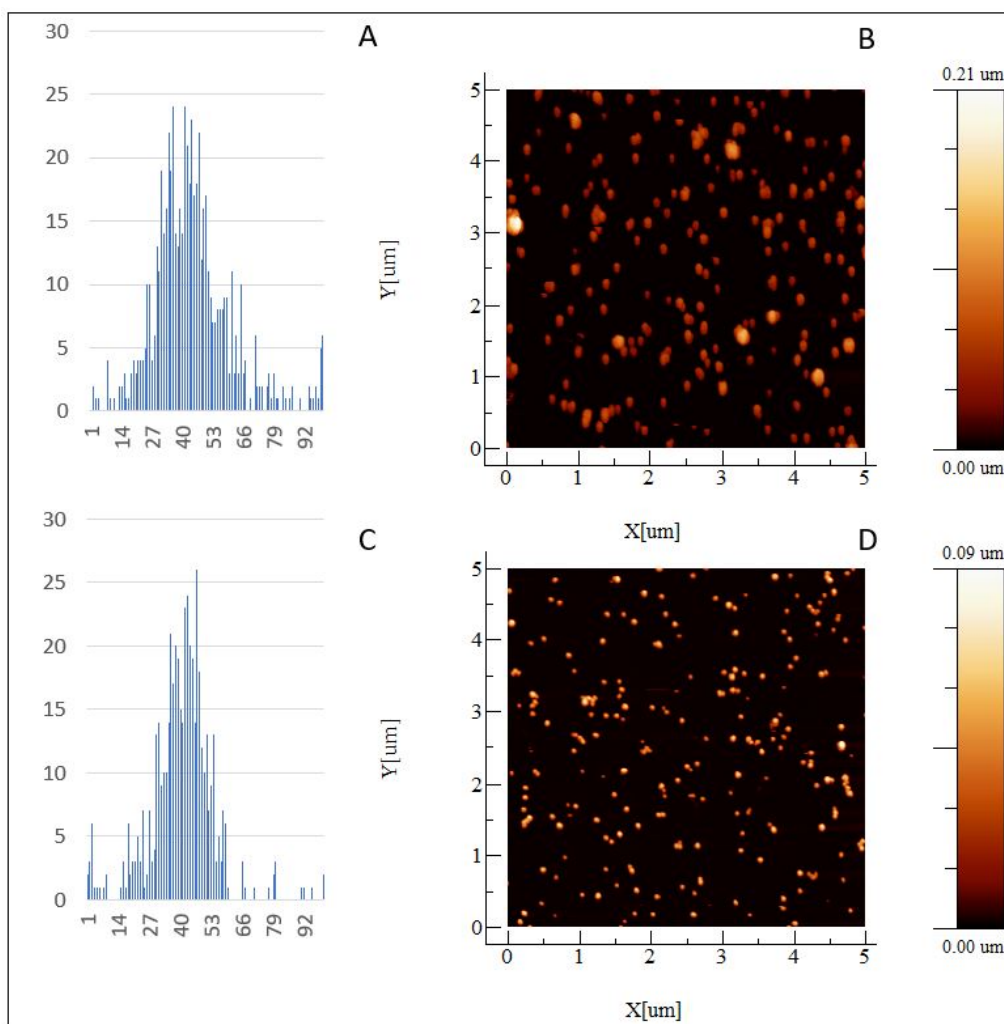


Figure 3.3: The distribution of particles size for A) AgNP₄₅ and c) AgNP₆₀ belonging to the AFM image B) and D), respectively.

Additional SEM images were taken of AgNP₄₅ and AgNP₆₀, however, the particle count was too low. No average Feret's diameter was reported for these particles. SEM images of seed particles were taken with high enough of count. A histogram was plotted

and an average Feret's diameter of 48.023 ± 15.301 was obtained (fig. 3.4).
fig. 3.6.

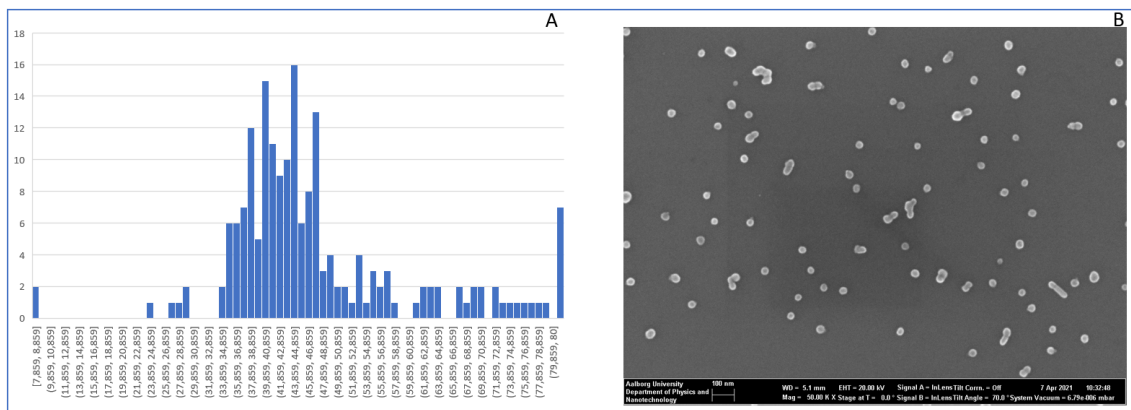


Figure 3.4: A) The Feret diameter distribution for the spherical nanoparticles. B) SEM image used to derive the histogram of spherical nanoparticles

3.1.4 Scaling reaction volumes

Big batches were made for the prisms and spherical particles to be used in further experiments. These particles were analysed again with AFM, UV/Vis and SEM to derive their shape and size. fig. 3.5 B displays the AFM taken from the big batch of prisms, the height distribution derived from two separate images was around 5.32 ± 2.99 nm. In the AFM image it can be clearly seen that most of the objects have a low intensity. For spherical particles the density of the wafers was lower, however, still a distribution was made. 35.27 ± 9.85 nm was the size of the average particle. The histogram of fig. 3.5 B shows a wide distribution of sizes.

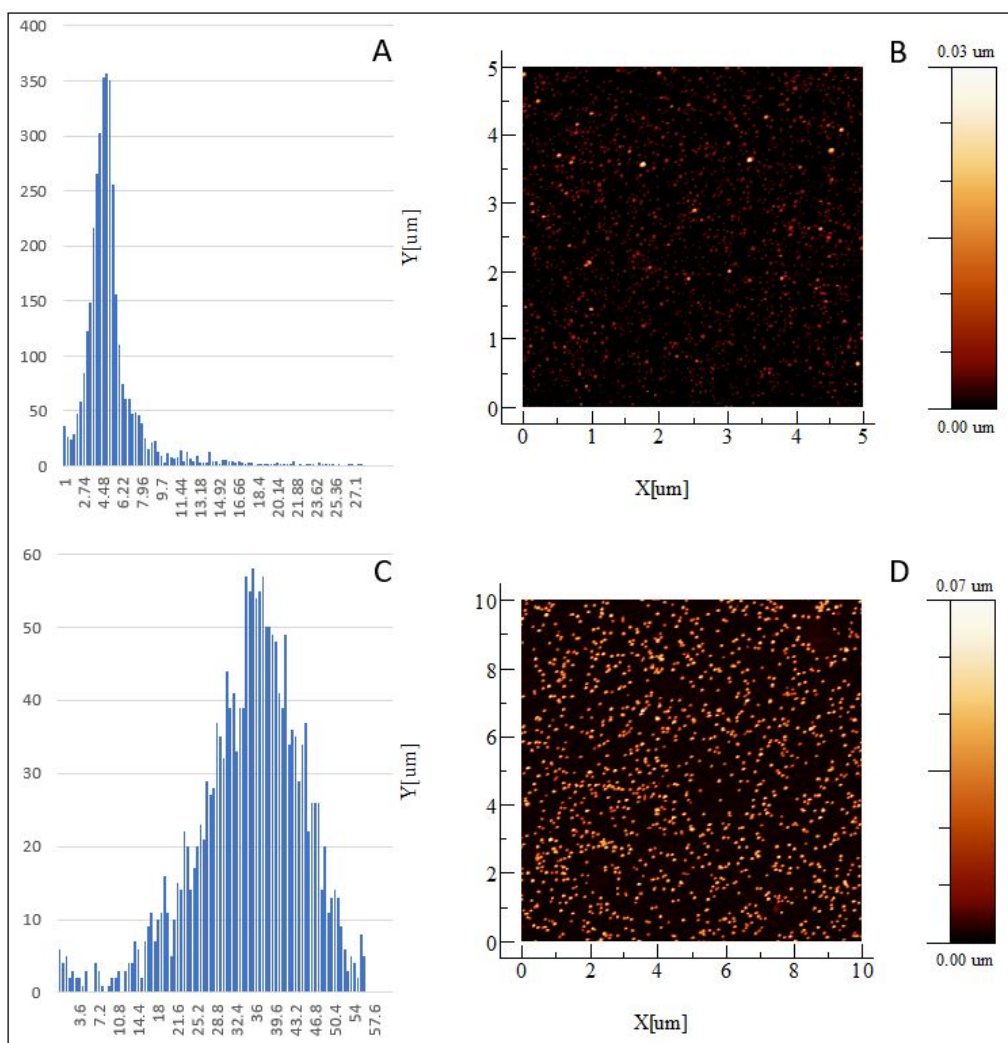


Figure 3.5: AFM imaging of big batch synthesis of spherical and prism particles. Histograms for A) prisms and C) spherical particles were compiled from two separate areas, imaged on the same silicon wafer. B) For prism two areas of $5 \times 5 \mu\text{m}$ were used, D) for spherical particles $2 \times$ and area of $10 \times 10 \mu\text{m}$.

Both SEM and AFM was used for analysing the particle size. AFM was useful measuring heights whereas SEM could measure width. The size distribution is seen in fig. 3.6.

The SEM analysis was done by taking the Feret diameter of the particles. The value was associated with the edge length of prisms and diameter of the particles. The prism had an average Feret diameter of $59.8 \pm 22.8 \text{ nm}$ and the spherical particles had an average Feret diameter of $16.97 \pm 12.37 \text{ nm}$.

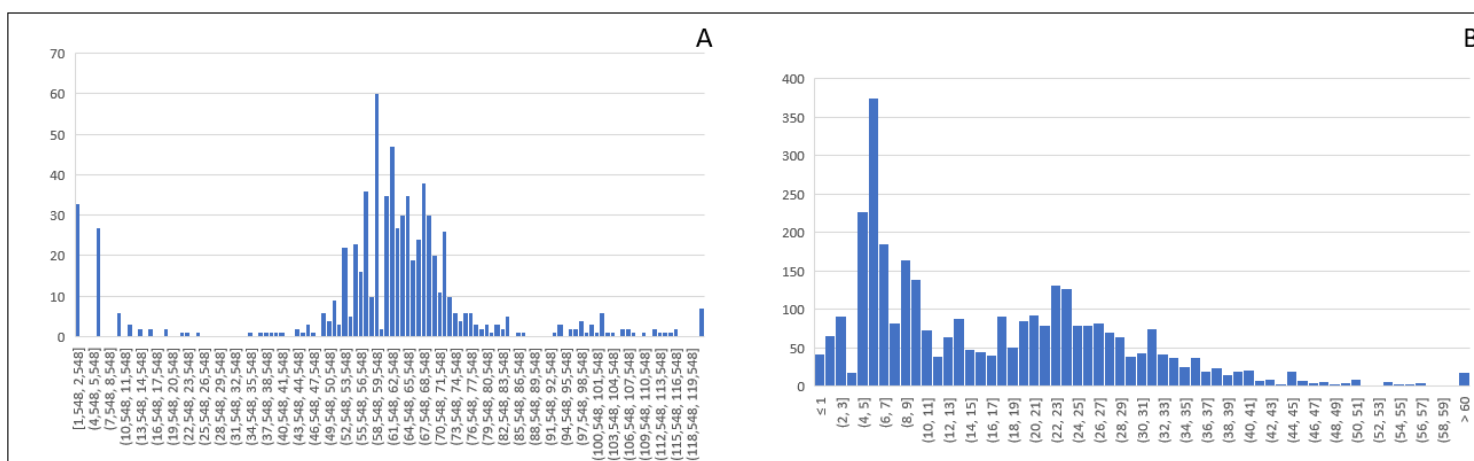


Figure 3.6: The Feret diameter distribution for A) the prism and B) seeds nanoparticles used for further experimentation

3.2 TPO nanoparticles characterisation

NTA was used to determine the size of the synthesised TPO nanoparticles, fig. 3.7 A shows the average of five samples where three regions were imaged for 45 seconds per sample. The results per region can be seen in fig. 3.7 B. 255 nm was the highest peak observed in all samples. When combining the results for the separate regions a global average shows a peak at 256.8 nm with a high size distribution between 100 and 400 nm.

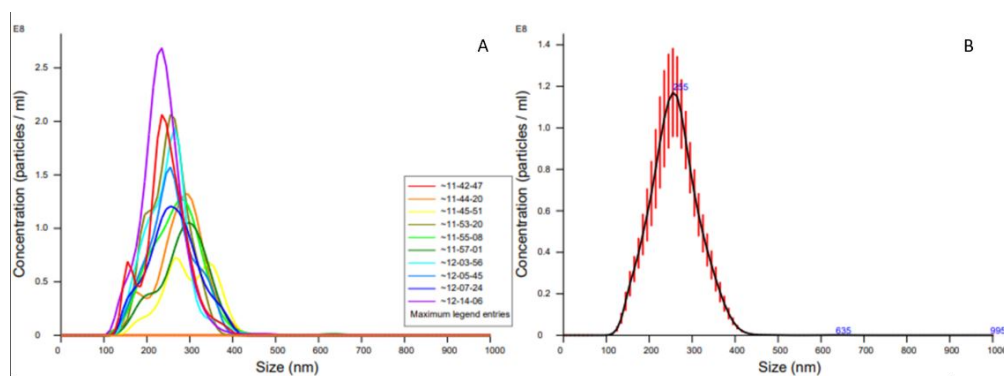


Figure 3.7: Size distribution of TPO nanoparticles measured with NTA, A) separate regions were imaged for 45 seconds in five different samples, concentration was plotted against the calculated size. B) The tracks were combined for an average size distribution. Current temperature measured at the end of imaging a region and entered into the software. Track length was set to 12 frames and the jump distance to 5 pixels.

When comparing different analysis parameters such as letting the software confine the track length and jump distance of tracked particles. The distribution stays similar when jump distance is set to auto, peaks at 195 and 105 appear showing an increase in

higher concentrations of smaller particles fig. A.3. The total amount of particles tracked per frame increases as does the concentration calculated for the sample. The largest population of particles stays the same in size, 253.8 nm.

When both jump distance and track length are set to auto, a smaller peak at 75 nm almost forms a separate peak with a size distribution from 50 nm to 400 nm fig. A.4. The result is that the average size of particles decreases to 205.1 nm. Also the largest fraction of the particles has a size around 227.1 nm. The concentration increases in regard to when the track length and jump distance were set manually, but decreased compared to when only jump distance was set to automatic.

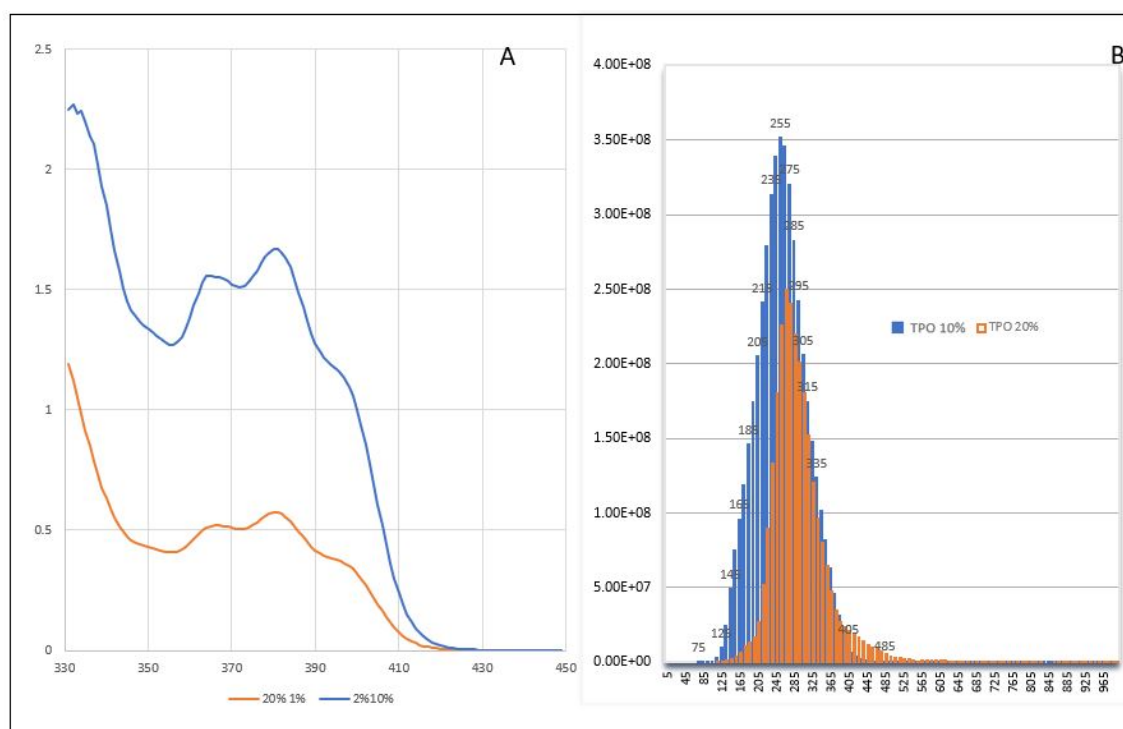


Figure 3.8: TPO particle characterisation. Solubility was probed with UV/Vis spectra to see the intensity of TPO characteristic peaks at 360 nm and 380 nm. B) TPO_{20%} and TPO_{10%} particles were analysed with NTA for average particle size. Three samples were measured for both particles, per sample 3 areas were imaged over a 60 second time period.

A new TPO NPs solution was made with 20% TPO and new NTA measurements were done. In figure fig. 3.8 the particle size distribution of TPO_{20%} is compared to TPO_{10%}. The distribution is the average value of three experiments that measured three positions over a time period of 1 minute. The particles counts from the measurement were summed to form the particle size distribution. For TPO_{20%} the highest peak is 288 nm and the average size is 298.47 nm. The particles size distribution ranged between 125 and 450 nm.

Dissolving the particles in water, resulted in cloudy solutions that were filtrated with a 400 μm filter, producing clear solutions. $TPO_{20\%}$ was able to solve at a concentration of 1% w/w in water. Increasing the w/w ratio did not result in a stronger effect. $TPO_{10\%}$ was solvable at 2% w/w which resulted in a high intensity on the UV/Vis spectrum after filtration (fig. 3.8 A) .

3.3 Hydrogels

Hydrogels were made with different concentrations of 20, 15, 10 and 5% AAm monomers with a cross-linking density of 1.56% PEGDA. The gels were photo-polymerized at 405nm UV light by using TPO as photo-initiator. 5% PAAm/PEGDA gels were discarded from measurements since the polymer content was not enough to form a gel and remained a thick viscose liquid. Mechanical properties, such as toughness, elasticity and rigidity of the gels were analysed with, compression, elongation and rheology testing. Furthermore pore sizes and Feret's diameter were derived from SEM images of freeze dried hydrogels.

3.3.1 SEM image of hydrogels

Hydrogel samples were prepared in two different ways for SEM analysis, either by freezing than lyophilization, or freeze snapping and than lyophilization.

For these SEM preparations different shapes were used. One used a flat gel, the other method used a cylindrical shaped gel. Each method gave different results. The gels which were frozen and dried are presented in fig. C.2 and snapped gels in figs. 3.10 and 3.11. The method giving the most consistently distributed pore size was the frozen, snapped and then freeze dried gel. These gels were used for the network analysis.

On the SEM-images of varying PEG concentration (fig. 3.10), polymer network can be observed, where as on the images with varying PEG length and concentration (fig. 3.11) It was observed different network when changing the concentration from 0.78 to 3.12% for both PEGDA₂₅₀ and PEGDA₇₀₀. Especially when the SEM images where magnified further to 614x. The 614x magnification of all the gels shows further the heterogeneity of pore sizes with area of large pores, and clusters with small pores (figs. 3.9 and C.5).

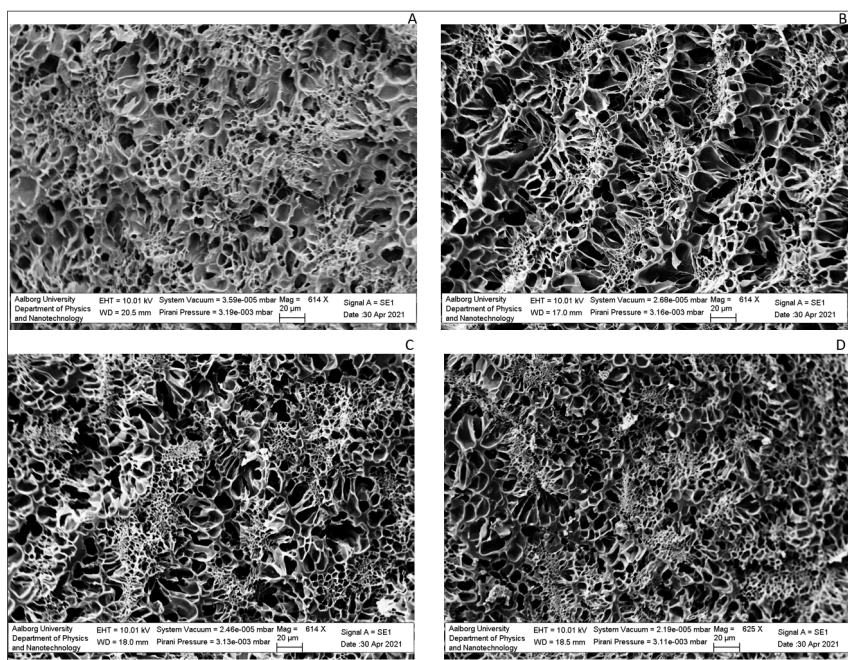


Figure 3.9: SEM image of the hydrogel magnified by 614x consisting of A) 0.78, B) 1.56, C) 2.34 and D) 3.12% PEGDA₅₇₅

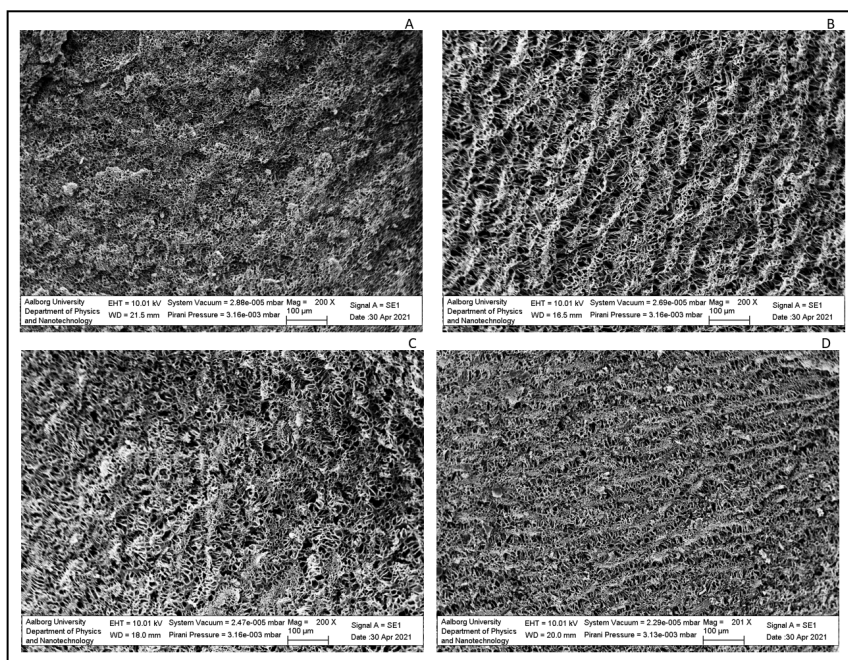


Figure 3.10: All the gels consist of 15% AAm and A) 0.78% PEGDA/AAm ratio, B) 1.56% PEGDA/AAm ratio, C) 2.34% PEGDA/AAm ratio D) 3.12% PEGDA/AAm ratio. PEG is 575 Mn

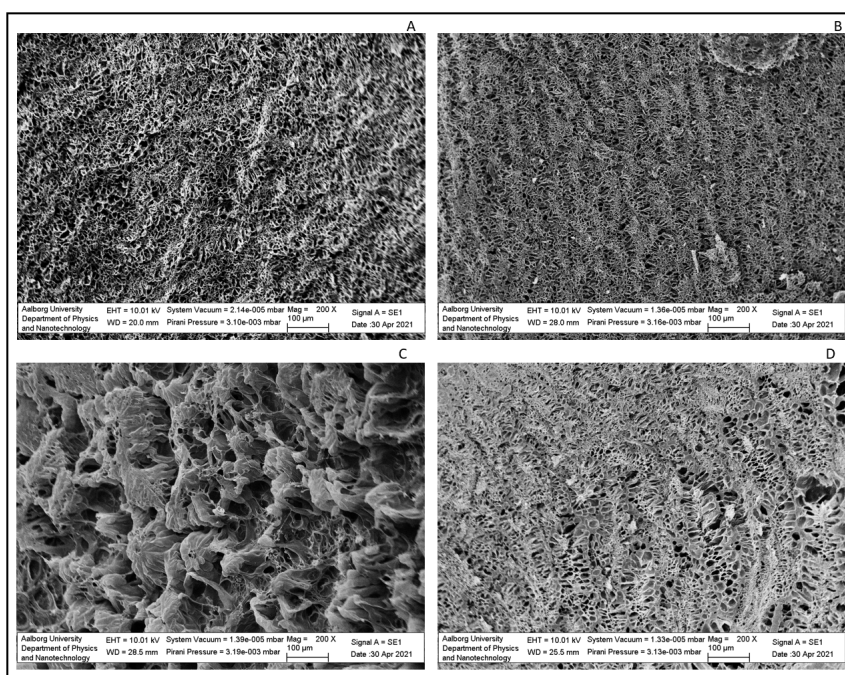


Figure 3.11: All the gels consist of 15 % AAm and A) 0.78% PEGDA/AAm ratio with PEG 250 Mn, B) 0.78% PEGDA/AAm ratio with PEGDA 700 Mn, C) 3.12% PEGDA/AAm ratio with PEGDA 250 Mn and D) 3.12% PEG/AAm ratio with PEGDA 700 Mn.

Table 3.3: The average area and Feret's diameter of the pores in the gels consisting of different concentration and length of PEG at magnification 200x

	0.78% PEGDA ₅₇₅	1.56% PEGDA ₅₇₅	2.34% PEGDA ₅₇₅	3.12% PEGDA ₅₇₅
Area 200x	17.42 ± 93.23 μm^2	25.23 ± 73.13 μm^2	29.89 ± 110.83 μm^2	24.87 ± 74.98 μm^2
Feret's diameter	6.35 ± 7.22 μm	6.37 ± 7.45 μm	6.95 ± 8.39 μm	6.57 ± 7.53 μm
	0.78% PEGDA ₂₅₀	3.12% PEGDA ₂₅₀	0.78% PEGDA ₇₀₀	3.12% PEGDA ₇₀₀
Area 200x	26.79 ± 52.67 μm^2	70.87 ± 298.59 μm^2	22.04 ± 61.97 μm^2	26.56 ± 70.11 μm^2
Feret's diameter	6.4 ± 7.73 μm	6.95 ± 7.26 μm	6.36 ± 6.92 μm	6.25 ± 5.59 μm

The histograms shows distributions of pore sizes, and from the same data set average pore sizes, feret diameter and the standard deviations have been calculated to get an better overview. For the average calculations the fully data set were used, so the pores above 80 μm was taken into account.

To check how the pore sizes were affected by change in monomer and cross-linker concentration or cross-linker length, Feret diameters and pore area were extracted from imageJ [69] and size distributions were made in Excel. To make the histograms more clear, only the pores ranging from 1 to 80 μm^2 were displayed. In fig. C.6. Many pore sizes were counted. 20% AAm gels had above 2500 pores in the size range 1 - 7 μm^2 , 15%

had above 1500 in the size range 1 - 7 μm^2 and 10% had under 1500 in the size range 1 - 7 μm^2 . The average pore size diameters were $16.39 \pm 33.99 \mu\text{m}^2$, $17.34 \pm 42.34 \mu\text{m}^2$ and $15.82 \pm 46.30 \mu\text{m}^2$ for 20, 15, and 10% AAm gels, respectively.

An additional experiment was done to compare swollen vs non-swollen gels. Here 0.78% PEGDA₅₇₅ was frozen and snapped before drying. Two areas are seen on the gel as a result of the snapping, a smooth surface and a rough one (fig. 3.12 A). When the different areas are magnified (200x) a surface with stretched pores and a surface with intact pores can be seen (fig. 3.12 B and C, respectively). Swollen gel of 0.78% PEGDA₅₇₅ was also presented (D), and fig. C.9 shows the difference in pore size of swollen vs non swollen.

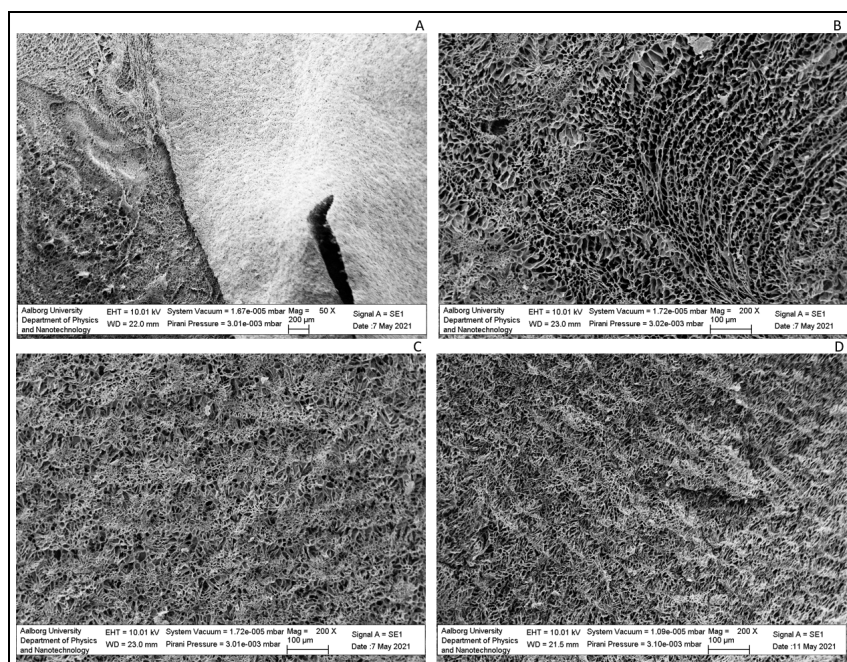


Figure 3.12: All the gels consist of 15% AAm and 0.78% PEGDA/AAm ratio with PEGDA 575. A) SEM image of the 0.78% PEGDA gel, B) pores of the gel seen in A, C) pores of the gel seen in A but another area and D) SEM image of same type of gel but swollen for 72 hours. B, C and D was taken at 200x magnification

The effect of increased concentration of cross-linker on pore size are presented in (fig. C.7 A to D) The pore size in range 1 to 3 μm^2 for 0.78, 1.56, 2.34 and 3.12% was above 3500, 4000, 5000 and 4000 ,respectively.

SEM analysis was also done for PEGDA₂₅₀ and PEGDA₇₀₀ fig. 3.11. The pore size in the range of 1-3 μm^2 was just under 7000 for 0.78% PEGDA₂₅₀ and when increasing the concentration to 3.12% the count of the pore size in in the range of 1-3 μm^2 was between 500 and 600 (fig. C.8 A and B). The pore size in the range of 1-3 μm^2 was just above 8000 for 0.78% PEGDA₇₀₀ and when increasing the concentration to 3.12%, the count of the pore size in the range of 1-3 μm^2 was just above 2500 (fig. C.8 C and D).

For all the gels made the average pore size and Feret's diameter can be found in table 3.3

3.3.2 Compression

Compression was tested to see how changing concentration of monomer would affect the toughness of the gel. Small disks of 5 mm high 15 mm in diameter was used to measure the compression modulus. The average results are represented in fig. 3.13 A. In the figure the mechanical response of gels of varying monomer concentrations with a cross-linking density of 1.56% PEGDA₅₇₅ was reported. PAAm_{10%} has a flat curve, low increase in stress with increasing strain. The applied stress at 60% strain was used to make the curves comparable to each other table 3.4. At this point PAAm_{10%} requires a stress of $3.06 \cdot 10^{-3}$ MPa. AAm_{15%} needs a compression pressure of $6.14 \cdot 10^{-3}$ MPa. AAm_{20%} has a very steep curve which starts increasing rapidly after 40% strain. This was also seen at 60% strain where the stress was $1.60 \cdot 10^{-2}$ MPa.

AAm_{15%} was chosen to test the influence of cross-linker density and the length of the cross-linker were also investigated to see whether they affected gel strength (fig. 3.13 B). Stress at 60% was used to compare as well. The stress for the gels starts to increase at the same level of strain, at 20% strain the applied pressure starts rising. At 60% a stress of $5.70 \cdot 10^{-3}$ MPa was measured for 0.78% PEGDA₅₇₅. 1.56% PEGDA₅₇₅ has a stress of $6.41 \cdot 10^{-3}$ MPa, 2.34% PEGDA₅₇₅ $9.93 \cdot 10^{-3}$ MPa. 3.12% PEGDA₅₇₅ demonstrates the highest pressure at 60%, $1.51 \cdot 10^{-2}$.

The gels with different cross-linkers PEGDA₂₅₀ and PEGDA₇₀₀ are depicted in fig. 3.13 C. For these gels the higher cross-linking densities of 3.12% were prone to breaking at high strain levels as can be seen for the slight 'jumps' at the highest point of the graph (fig. 3.13 C). The other density tested for these cross-linkers was 0.78% showed a less steep curve in general for all cross-linkers. Therefor, there was also a difference seen at 60% strain. The lower cross-linking densities showed $4.68 \cdot 10^{-3}$ and $4.19 \cdot 10^{-3}$ MPa for PEGDA₂₅₀ and PEGDA₇₀₀ respectively. The higher cross-linking densities showed stresses of $1.40 \cdot 10^{-2}$ and $1.55 \cdot 10^{-2}$ MPa for PEGDA₂₅₀ and PEGDA₇₀₀.

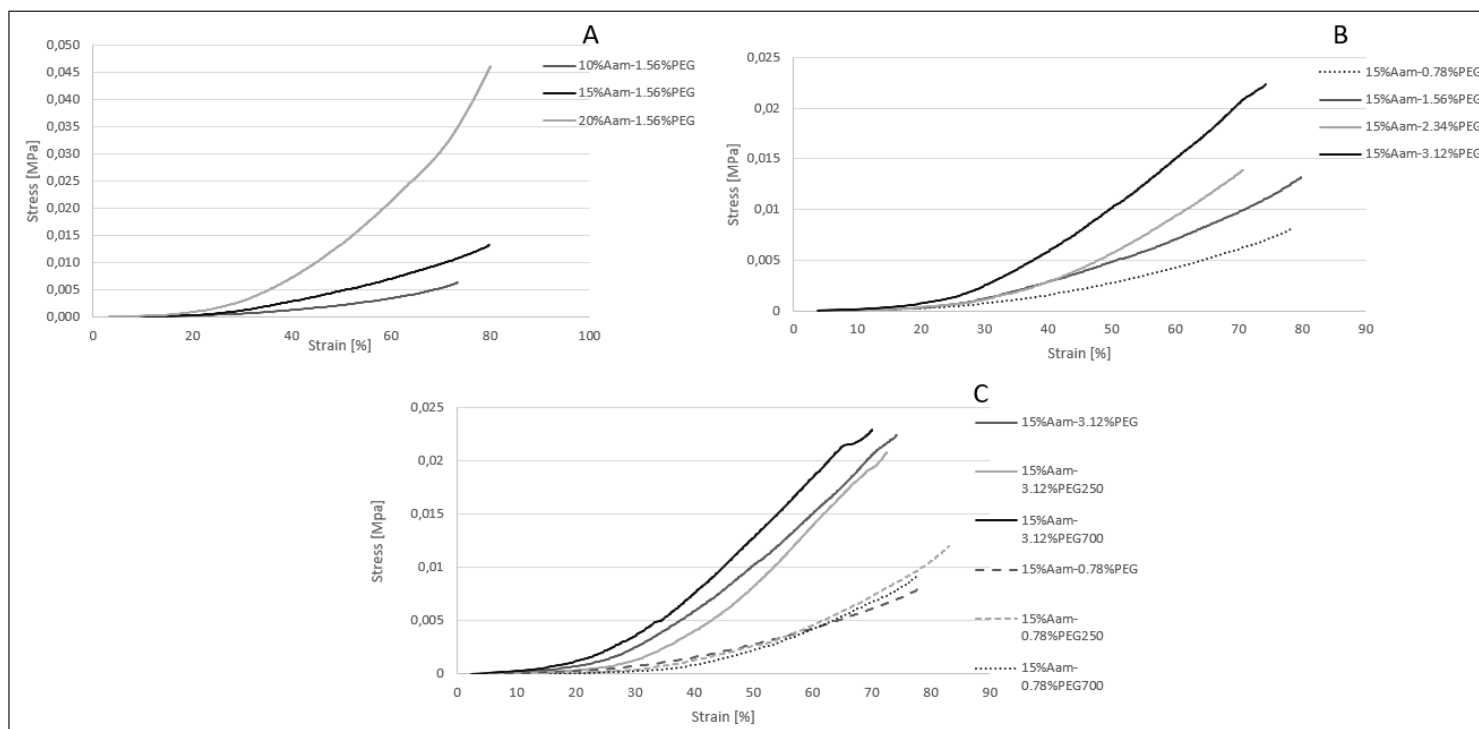


Figure 3.13: The average graph for the different compression test. A) show the strain-stress curve for changing the amount of acrylamide monomer, B) the amount of cross-linker was changed and C) amount and length of the cross-linker was changed. PEG has the average molecular number of 575, whereas PEG250 and PEG700 have the average molecular number of 250 and 700, respectively. All lines are the average from 3 experiments.

Table 3.4: Average stress measured at a strain of 60% for hydrogels with varying monomer concentrations, cross-linking densities and cross-linker length

Hydrogel	MPa
PAAm _{10%} /PEGDA ₅₇₅ 1.56%	0.00306 ± 0.00199
PAAm _{20%} /PEGDA ₅₇₅ 1.56%	0.0160 ± 0.00206
PEGDA ₅₇₅ 0.78%	0.00570 ± 0.00252
PEGDA ₅₇₅ 1.56%	0.00641 ± 0.00058
PEGDA ₅₇₅ 2.34%	0.00993 ± 0.00429
PEGDA ₅₇₅ 3.12%	0.0151 ± 0.00330
PEGDA ₂₅₀ 0.78%	0.00468 ± 0.00268
PEGDA ₂₅₀ 3.12%	0.0140 ± 0.00360
PEGDA ₇₀₀ 0.78%	0.00419 ± 0.00216
PEGDA ₇₀₀ 3.12%	0.0155 ± 0.00755

More compression tests were conducted, however, this time the gels were cured with

either AgNP_{Prism} or AgNP_{Spherical}. The results are shown in fig. 3.14. Unlike the compression testing for cross-linking densities and length this experiment was only conducted once. In general the curves generated by the gels containing spherical particles show gradual increase of stress with increasing strain (fig. 3.14 A and B). Stress/strain curves produced by gels polymerized with AgNP_{Prism} have a rapid increase in strain to 40-60% depending on the cross-linking density before the stress rapidly increases. Breaking of the gel was observed for the higher cross-linking densities of AgNP_{Spherical} gels at higher levels of strain, + 65%, similar values were observed for AgNP_{Prism} gels (fig. 3.14 C and D). Although the stress in these gels rise at higher levels of strain and the higher concentration cross-linked gels break, the stress at 60% strain was still used as a reference point table 3.5. For AgNP_{Spherical} gels cross-linking densities of 0.78% PEGDA₅₇₅ needs $1.23 \cdot 10^{-2}$ MPa to reach a 60% strain, PEGDA₂₅₀ required $7.20 \cdot 10^{-3}$ MPa and PEGDA₇₀₀ $7.60 \cdot 10^{-3}$ MPa.

Table 3.5: Stress measured at 60% strain for gels polymerized in the presence of either AgNP_{Spherical} or AgNP_{Prism} at different cross-linking densities and by using different length cross-linkers.

Hydrogel	Ag _{Spherical} (MPa)	AgNP _{Prisms}
PEGDA ₅₇₅ 0.78%	0.0121	0.00566
PEGDA ₅₇₅ 1.56%	0.0101	0.00931
PEGDA ₅₇₅ 2.34%	0.0148	0.00150
PEGDA ₅₇₅ 3.12%	0.0184	0.00134
PEGDA ₂₅₀ 0.78%	0.0072	0.000337
PEGDA ₂₅₀ 3.12%	0.0181	0.00841
PEGDA ₇₀₀ 0.78%	0.0076	0.00219
PEGDA ₇₀₀ 3.12%	0.0191	0.00895

Increasing the cross-linking concentration to 3.12% resulted in an increase of force required to reach 60% for all PEGDA lengths. PEGDA₅₇₅ demonstrated $1.84 \cdot 10^{-2}$ MPa at 60% strain. PEGDA₂₅₀ and PEGDA₇₀₀ Showed $1.81 \cdot 10^{-2}$ and $1.90 \cdot 10^{-2}$ MPa respectively. The cross-linking densities in between, 1.56 and 2.34% for PEGDA₅₇₅ displayed $1.48 \cdot 10^{-2}$ and $1.01 \cdot 10^{-2}$ MPa at 60% deformation. For AgNP_{Prims} this difference between the cross-linkers was less clear. Here the lower cross-linking densities of 0.78% require stresses of $3.37 \cdot 10^{-4}$, $5.66 \cdot 10^{-3}$ and $2.19 \cdot 10^{-3}$ for PEGDA₂₅₀, PEGDA₅₇₅ and PEGDA₇₀₀ respectively. The higher cross-linking densities of 3.12% demonstrates strengths of, $8.41 \cdot 10^{-3}$ MPa for PEGDA₂₅₀, $1.34 \cdot 10^{-3}$ MPa to achieve 60% for PEGDA₅₇₅ 3.12% gel and $8.95 \cdot 10^{-3}$ for PEGDA₇₀₀. cross-linking at 1.56% and 2.34% PEGDA₅₇₅ reached 60% strain at stresses of $9.31 \cdot 10^{-3}$ and $1.50 \cdot 10^{-3}$ MPa.

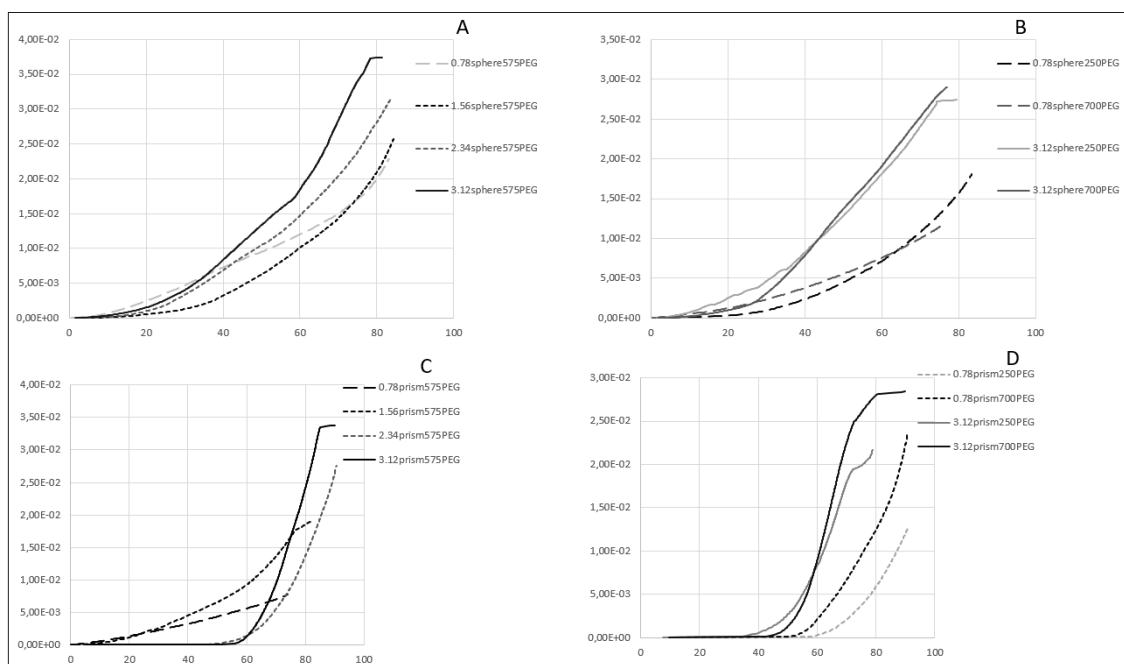


Figure 3.14: A) shows the compression of gel made with 0.78 to 3.12% PEGDA₅₇₅ cured with spherical silver nanoparticles, B) shows the compression of gel made with either 0.78 or 3.12% PEGDA₂₅₀ or PEGDA₇₀₀ cured with spherical silver nanoparticles, C) shows the compression of gel made with 0.78 to 3.12% PEGDA₅₇₅ cured with AgNP_{Prism}, D) shows the compression of gel made with either 0.78 or 3.12% PEGDA₂₅₀ or PEGDA₇₀₀ cured with AgNP_{Prism}. The lines in the graph represent 1 experiment

3.3.3 Elongation

A home made setup was used for the elongation testing of hydrogels. This resulted in gels often breaking at the edges connected to the clamp instead of in the middle. However, it was still useful to get an idea on which gel was the strongest and only gels that broke in the thinnest part were taken along in the results. Just like with compression, the concentration of monomer and cross-linker were changed and average molecular number of the cross-linker was changed too.

Force vs elongation curves for the gels differing in monomer concentration are shown in fig. 3.15. To compare the force required to break the gel and the elongation at which the gels broke are reported in table 3.6, in addition the Young's modulus was calculated from these variables according to eq. (1.4). AAm_{10%} broke at a force of 0.12 Newton where it was 201% elongated and Modulus of 4.11 kPa was calculated. Increasing the concentration to AAm_{15%} resulted in a force at break of 0.23 N and elongation of 199.6% with a modulus of 7.67 kPa. At the highest monomer concentration 20 w/w%, a 0.27N force elongated the gel 196% resulting in 9 kPa as elastic modulus. For further testing the gel consisting of 15% acrylamide was used.

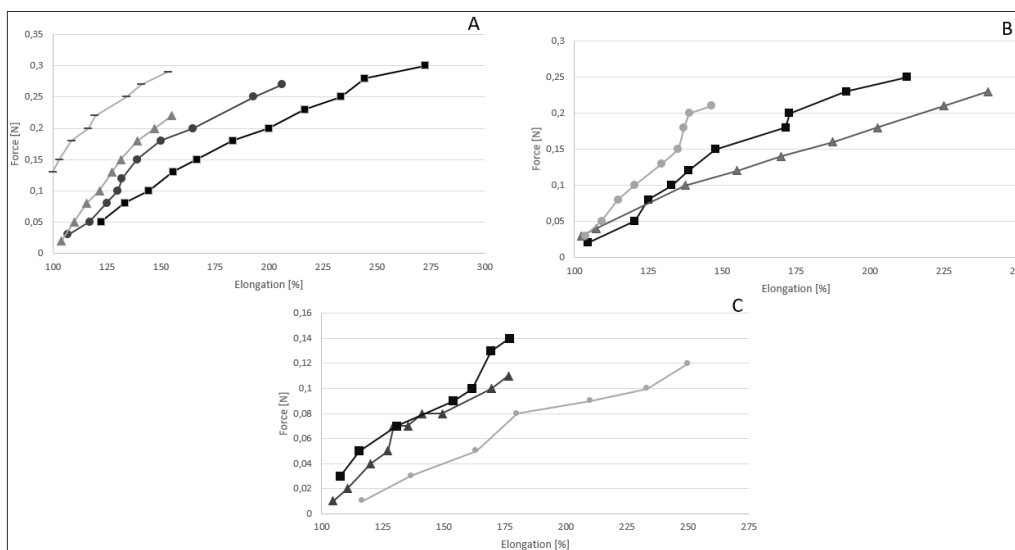


Figure 3.15: Shows the force it takes to elongate gels consisting of, A) 20% acrylamide, B) 15% and C) 10%. All gels have the same amount of PEG 1.56 % with and average molecular number of 575. The end of each graph is the breaking point of each gels.

When changing the length of the PEG to 250 the 3.12% gels were brittle and broke while trying to take them out of the dog bone mold, or trying to get them in the clamps, so no test was conducted on it.

15% AAm gels were made with varying cross-linking concentrations (fig. 3.16), in addition cross-linker length was changed (fig. 3.17), similar to the compression testing. Again gels were extended till the breaking point was reached, force and length of deformation were recorded at this point and used to compare (table 3.6. For the lower cross-linking densities of 0.78% varying results are found. PEGDA₂₅₀ required 0.33 N to break where it was extended to 190% of it's original length. PEGDA₅₇₅ broke at 62% with a applied force of 0.16 N where PEGDA₇₀₀ was elongated with 167% and a force op 0.39 N. Young's modulus was calculated for all three, 11.49, 5.34 and 13.56 kPa, for PEGDA₂₅₀ PEGDA₅₇₅ and PEGDA₇₀₀ respectively. Increasing the cross-linking to 3.12% demonstrated forces of 0.40 N for PEGDA₅₇₅ and 0.39 N for PEGDA₇₀₀ and respective elongations of 90.84 and 35.17% with moduli of 14.02 and 13.45 kPa. For PEGDA₅₇₅ two additional cross-linking densities were tested in between 0.78 and 3.12%, namely 1.56 and 2.34%. 2.34% was the stronger gel, with a breaking force of 0.41 N at 90.68% extension. 1.56% needed 0.33N to break at 189.89%. Young moduli were calculated as 11.29 kPa for 1.56% and 2.34% had a modulus of 14.22 kPa.

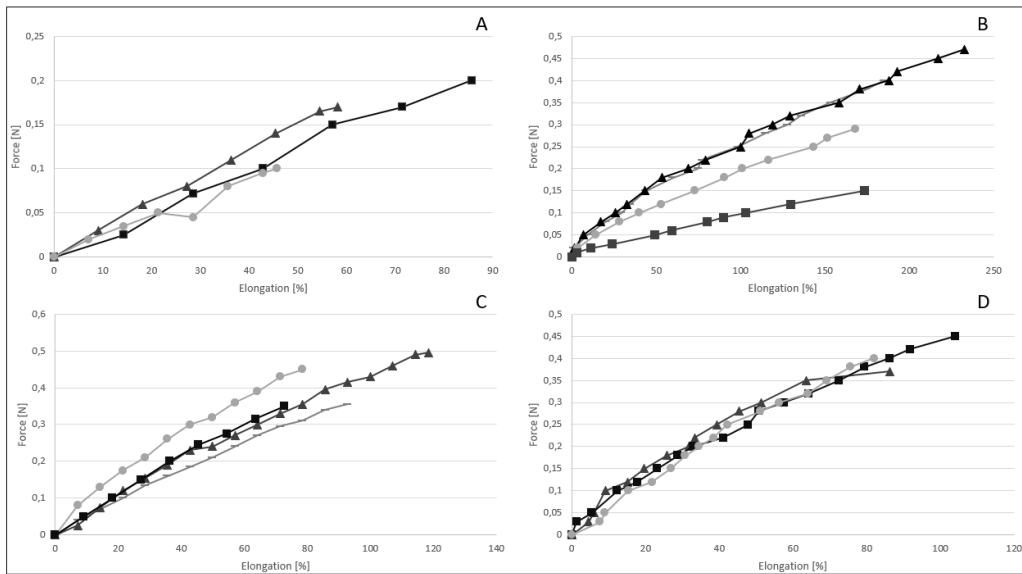


Figure 3.16: All gels consist of 15% acrylamide A Shows the force it takes to elongate gels consisting of 0.78% PEG, B 1.56% C 2.34% D 3.12%. The PEG used for all gels has an average molecular number of 575. The end of each graph is the breaking point of each gels.

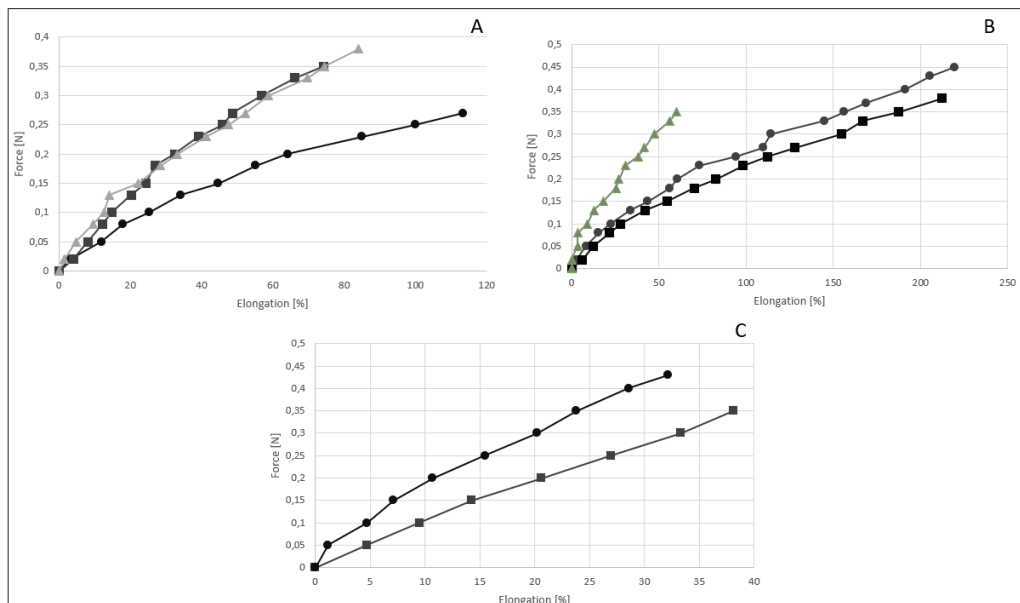


Figure 3.17: All gels consist of 15% acrylamide A) Shows the force it takes to elongate gels consisting of 0.78% PEGDA₂₅₀, B) 0.78% PEGDA₇₀₀ and C) 3.12% PEGDA₇₀₀. The end of each graph is the breaking point of each gels.

Table 3.6: The average force, calculated modulus and elongation from each type of gel made at their breaking point.

Force	0.78 % PEGDA ₂₅₀ 0.33 N	0.78 % PEGDA ₅₇₅ 0.16 N	0.78 % PEGDA ₇₀₀ 0.39 N	1.56 % PEGDA ₅₇₅ 0.33 N	2.34 % PEGDA ₅₇₅ 0.41 N	3.12 % PEGDA ₅₇₅ 0.40 N	3.12 % PEGDA ₇₀₀ 0.39 N	10 % AAm 0.12 N	15 % AAm 0.23 N	20 % AAm 0.27 N
Elongation	90.62 %	62.25 %	164.07 %	189.89 %	90.68 %	90.84 %	35.17 %	201.11 %	199.6 %	196.63 %
modulus	11.49 kPa	5.34 kPa	13.56 kPa	11.29 kPa	14.22 kPa	14.02 kPa	13.45 kPa	4.11 kPa	7.67 kPa	9 kPa

3.3.4 Rheology

To further understand the mechanical effect of cross-linking density and length of cross-linker in a PAAm/PEGDA hydrogel, rheology measurements were done. From these measurement the G modulus was derived and plotted against increasing strain (fig. 3.18 A). From the amplitude test it was determined to use 1% strain during the frequency test, where the rad/s is increased while keeping the strain constant (fig. 3.18 B). For all gels it goes that the when the G storage decreases, the G storage loss increases (not depicted on the graph). The amplitude was taken to understand the amount of strain could be used during the frequency sweep. This strain was set at 1%, this was a strain for all gels. The frequency sweep show constant values for the G modulus storage against increasing frequencies. Indicating that the measurements were conducted in the linear visco elastic region and only the elasticity of the polymer strands was tested. The values of the G' are given in table (table 3.7), showing similar values for the higher density gels, PEGDA₂₅₀ 3.12% 0.563 kPa, PEGDA₅₇₅ 3.12% 0.527 kPa and for PEGDA₇₀₀ 3.12% 1.003. The intermediate cross-linking densities for PEGDA₅₇₅ had G' of 0.506 and 0.538 kPa for 1.56% and 2.34% respectively. The lower density gels PEGDA₂₅₀ 0.78%, PEGDA₅₇₅ 0.78% and PEGDA₇₀₀ 0.78% had the lowest G' , namely 0.246, 0.325 and 0.341 kPa

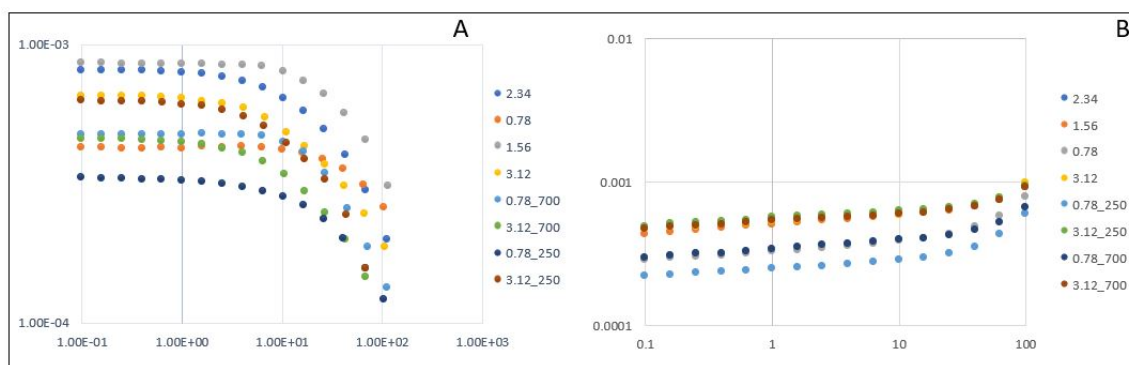


Figure 3.18: Rheology was done for PEGDA₅₇₅, PEGDA₂₅₀ and PEGDA₇₀₀. At the different cross-linking w/w% 0.78%, 1.56%, 2.34% and 3.12%. For each gel an A) amplitude and B) frequency sweep was taken. Amplitude curve shows the G storage modulus vs increasing strain %, whereas the frequency curve depict the Storage modulus vs increasing frequency of oscillation at 1% strain. every curve is an average of three experiments.

Table 3.7: Shear modulus storage (G') and loss (G'') obtained during frequency sweep, the values were taken at 1 rad/s

Hydrogel	G' (kPa)	G'' (kPa)
PEGDA ₅₇₅ 0.78%	0.325	0.0340
PEGDA ₅₇₅ 1.56%	0.506	0.0515
PEGDA ₅₇₅ 2.34%	0.538	0.0460
PEGDA ₅₇₅ 3.12%	0.527	0.0534
PEGDA ₂₅₀ 0.78%	0.246	0.0452
PEGDA ₂₅₀ 3.12%	0.563	0.0231
PEGDA ₇₀₀ 0.78%	0.341	0.0310
PEGDA ₇₀₀ 3.12%	1.003	0.0771

3.3.5 Hydrogel swelling

The swelling rate of the hydrogels was established by measuring the water uptake every hour by weighing the gels and calculating the percentile increase of weight. For this experiment three different number average molecular weights of PEGDA were used, 250, 700 and 575 Mn at 4 different cross-linking concentrations, 0.75%, 1.56%, 2.34% and 3.12%. The swelling of these gels was measured for 48 hours to make sure equilibrium was attained. For all gels there is a fast increase in weight, where the gels gained 90% of their total weight in the first 8 hours. More liquid is taken up the next 16 hours and at 48 hours no more uptake is observed and the gels are in equilibrium state. PEGDA₅₇₅ as said (fig. 3.19 A), grow fast in the first 8 hours and then slowly to their maximum volume in 48 hours. Low density cross-linking, 0.78% shows the largest increase in size, 288% of the volume/weight at cross-linking. 1.56%, 2.34% and 3.12% have a lower increase in weight of 148%, 123% and 144% respectively. When the lower Mn weight PEGDA, PEGDA₂₅₀ (fig. 3.19 B), is used, 0.78% shows the highest increase as well with an increase of 300%. Increasing the cross-linking density to 1.56% reduces swelling percentages to 231%. Gels with 2.34% and 3.12% cross-linking swell with 175% and a 150% respectively.

Using PEGDA₇₀₀ the weight of 0.78% cross-linked gel increases with 340%. 3.12% PEGDA₇₀₀ increased with 160%. 2.34% and 1.56% PEGDA₇₀₀ both grew with 175% (fig. 3.19 C). The overall swelling ratios of the gel (fig. 3.19D), show 4x increase for the 0.78% gels, 2.7x for the 1.56% gels. 2.34 and 3.12% have ratios close to 2.5x.

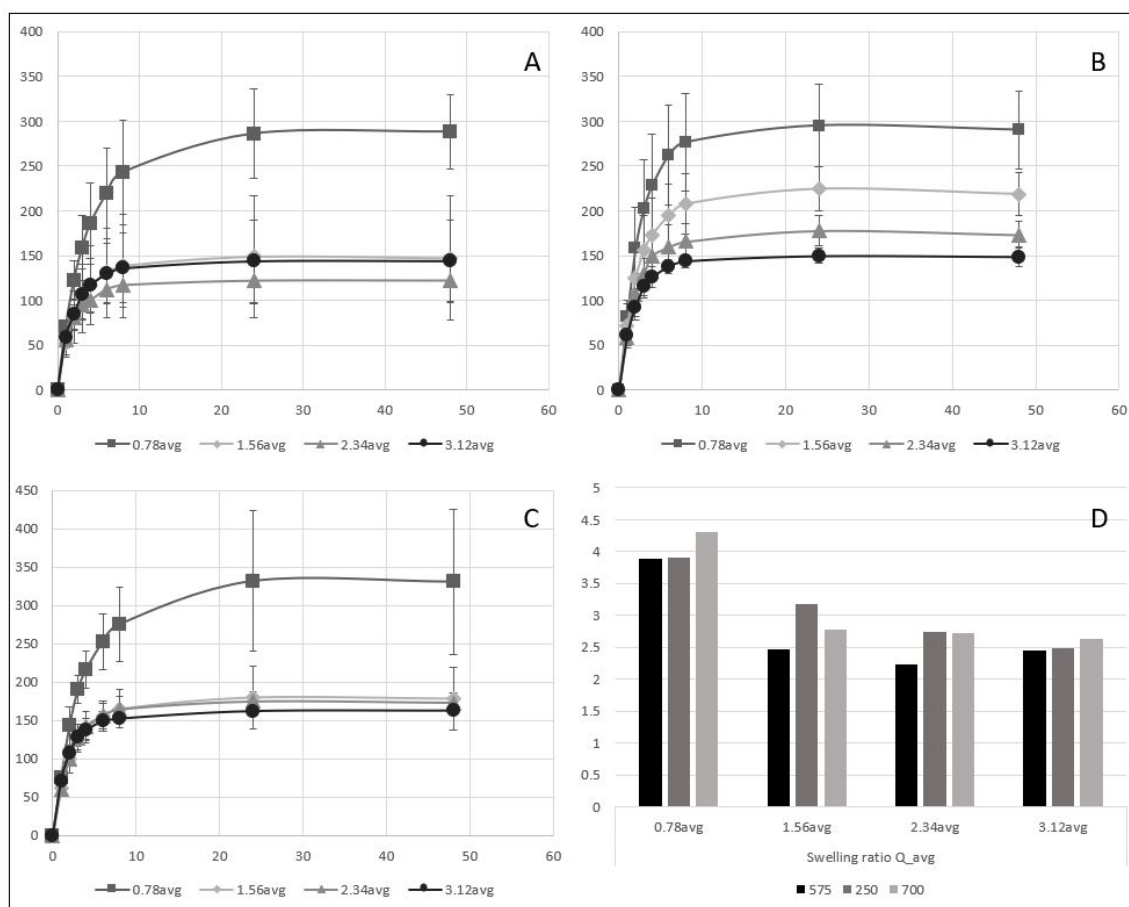


Figure 3.19: Hydrogel swelling was assessed over a period of 48 hours. Hydrogels with different cross-linker size were used, A) PEGDA₅₇₅, B) PEGDA₂₅₀ and C) PEGDA₇₀₀. For every gel 4 different cross-linker w/w% to monomer were used, 0.78%, 1.56%, 2.34% and 3.12%. D) Final swelling ratios for the separate gels are given as the ratio between the weight at the start of the experiment and the final weight after 48 hours. All data points are the average of 3 separate experiments.

3.4 cross-link dependent diffusion

Gels loaded with tetracycline, prisms and spherical particles were placed in water. The liquid was measured with a UV/vis spectrometer. The maximum absorbance at characteristic wavelengths, 360 nm for tetracycline, 415 nm for spherical AgNP and 550nm for AgNP Prisms, were used to calculate the concentration from standard curves of the respective substances. Concentrations released per gram of gel were plotted against time, over a period of days. During the diffusion of the AgNP_{Prism} a release was not enough to observe with the UV/Vis spectra. Spherical particle diffusion showed a burst release in the first 8 hours releasing 7.64% of total AgNP concentration in the gel. Where the concentration of particles in water increased 3.48x for 0.78% PEGDA₅₇₅ in 96 hours

compared to the measurement at hour 1, for a total release of 9.07% (fig. 3.20 A). After 8 hours 1.56% PEGDA₅₇₅ released 5.09% which further increased to 5.70% in 96 hours. 2.34% PEGDA₅₇₅ AgNP release was 4.22% after 8 hours and in 96 hours 5.93%. For 3.12% PEGDA₅₇₅ 2.8% of the total AgNP was released after 8 hours, resulting in 3.60% in 96 hours. Final concentrations for the gels, 0.78% PEGDA₅₇₅, 1.56% PEGDA₅₇₅, 2.34% PEGDA₅₇₅ and 3.12% PEGDA₅₇₅, were $0.038 \mu\text{g}\cdot\text{mL}^{-1}g_{\text{gel}}^{-1}$, $0.027 \mu\text{g}\cdot\text{mL}^{-1}g_{\text{gel}}^{-1}$, $0.028 \mu\text{g}\cdot\text{mL}^{-1}g_{\text{gel}}^{-1}$ and $0.016 \mu\text{g}\cdot\text{mL}^{-1}g_{\text{gel}}^{-1}$ respectively.

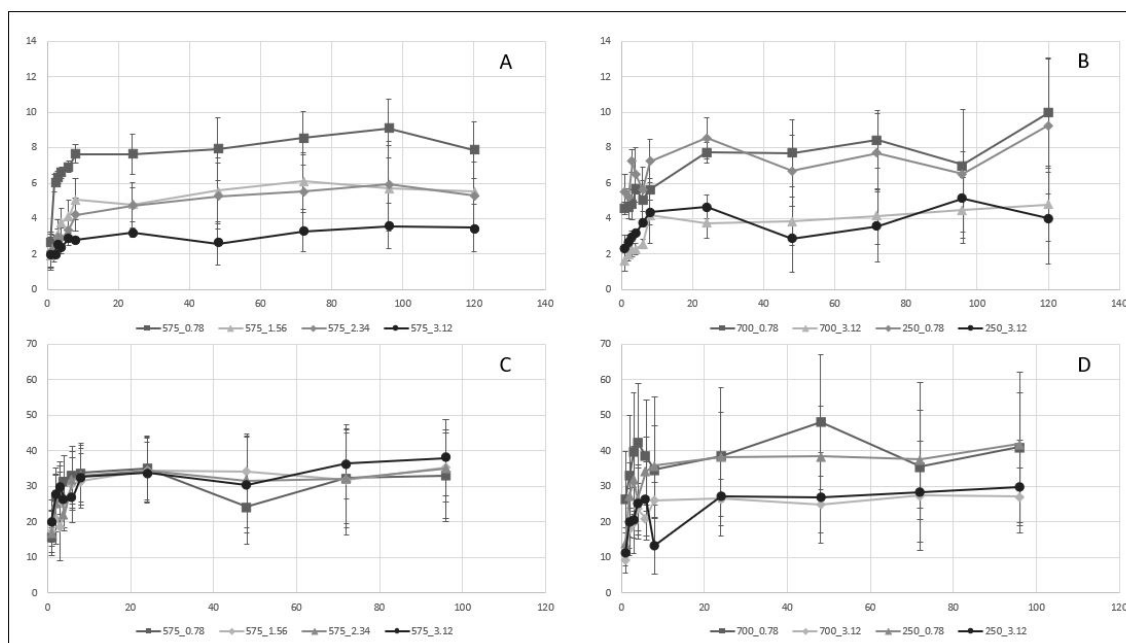


Figure 3.20: Diffusion of loaded drugs. Gels loaded with nanoparticles and tetracycline were placed in water, diffusion occurred over a period of 96 hours. Gels with PEGDA₅₇₅ 0.78%, 1.56%, 2.34% and 3.12% cross-linking, loaded with A) spherical particles and C) tetracycline. For PEGDA₂₅₀ and PEGDA₇₀₀ the lowest and highest cross-linking densities, 0.78% and 3.12%, were used and loaded with B) spherical particles and D) tetracycline. Curves show the increase of percentage released (of original content) versus time. All values are an average of 3 experiments.

When changing the PEGDA Mn the first 8 hours still show the highest release, which continues to 96 hours. At 72 hours 0.78% PEGDA₂₅₀ and 0.78% PEGDA₇₀₀ show a higher release rate than their more densely cross-linked counterparts 3.12% PEGDA₂₅₀ and 3.12% PEGDA₇₀₀ (fig. 3.20 B). 5.6% was released in the first 8 hours for 0.78% PEGDA₇₀₀ increasing to 7.03% in 96 hours, equal to a concentration of $0.027 \mu\text{g}\cdot\text{mL}^{-1}g_{\text{gel}}^{-1}$. 3.12% PEGDA₇₀₀ released 4.47% in 96 hours, $0.021 \mu\text{g}\cdot\text{mL}^{-1}g_{\text{gel}}^{-1}$, of which 4.18% was released in the first 8 hours. 0.78% PEGDA₂₅₀ released 7.22%, decreased to 6.52%, $0.036 \mu\text{g}\cdot\text{mL}^{-1}g_{\text{gel}}^{-1}$, 3.12% PEGDA₂₅₀ the total amount release from 3.12% PEGDA₂₅₀ grew to 4.37 % in 8 hours, with a final concentration of $0.023 \mu\text{g}\cdot\text{mL}^{-1}g_{\text{gel}}^{-1}$, 5.15% in 96 hours.

Similar to the spherical particles the majority of tetracycline release took place in the first 8 hours. After these first hours the speed of release slowed down. Over a period of 96 hours the 575 gels showed similar increase in tetracycline concentration, 0.066, 0.71, 0.70 and 0.076 $\text{mg}\cdot\text{mL}^{-1}\text{g}_{\text{gel}}^{-1}$ for increasing cross-linking density. These concentrations are represented in fig. 3.20 C as percentages of total tetracycline content of the respective gels. For 0.78% PEGDA₅₇₅ 33.88% was released after 8 hours, decreasing to 33.04%. 1.56% PEGDA₅₇₅ released 31.50% in 8 hours time, while after 96 hours this increased to 35.31%. 2.34% PEGDA₅₇₅ and 3.12% PEGDA₅₇₅ released 33.05 and 32.69% in 8 hours respectively and after 96 hours 34.93 and 38.06%.

For PEGDA₂₅₀ and PEGDA₇₀₀ there was a bigger difference between the cross-linking densities (fig. 3.20 D), 0.78% PEGDA₇₀₀ with a total release of 0.097 $\text{mg}\cdot\text{mL}^{-1}\text{g}_{\text{gel}}^{-1}$, 40.98% of the total tetracycline content, and 3.12% PEGDA₇₀₀ with 0.043 $\text{mg}\cdot\text{mL}^{-1}\text{g}_{\text{gel}}^{-1}$ equal to 27.07%. A similar difference was observed while using the 250 Mn PEGDA cross-linker, the concentration for 0.78% PEGDA₂₅₀ was 0.084 $\text{mg}\cdot\text{mL}^{-1}\text{g}_{\text{gel}}^{-1}$ and 3.12% PEGDA₂₅₀ 0.060 $\text{mg}\cdot\text{mL}^{-1}\text{g}_{\text{gel}}^{-1}$ corresponding to 41.94% and 29.89% after 96 hours.

The total swelling ratio of the gels used in diffusion was also measured by weighing them before and after the experiment (fig. 3.21). PEGDA₅₇₅-Seed composite gels at cross-linking densities of 0.78, 1.56, 2.34 and 3.12% showed swelling ratios of 2.79, 2.40, 2.24 and 2.12. For PEGDA₅₇₅-AgNP_{prism} these ratios were slightly higher for the respective gels, 3.08, 2.46, 2.58 and 1.92. Tetracycline containing PEGDA₅₇₅ of the different cross-linking densities had swelling ratios of 3.57, 3.03, 2.76 and 2.27 for increasing cross-linking percentage.

Swelling of the different M_n PEGDA, were 3.38 and 2.00 for PEGDA₂₅₀-AgNP_{spherical} at densities of 0.78 and 3.12%, AgNP_{prism} showed and volume increase of 3.60 and 2.00 where tetracycline gels had an increase of 3.25 and 2.18. PEGDA₇₀₀-AgNP_{spherical} had swelling ratios of 3.15 and 1.95 for the cross-linking percentages 0.78 and 3.12%. The ratios for PEGDA₇₀₀-AgNP_{prism} 0.78% and 3.12% were 3.19 and 2.01. PEGDA₇₀₀-tetracycline showed a swelling ratio of 3.69 and 1.92 for the respective cross-linking densities of 0.78% and 3.12%.

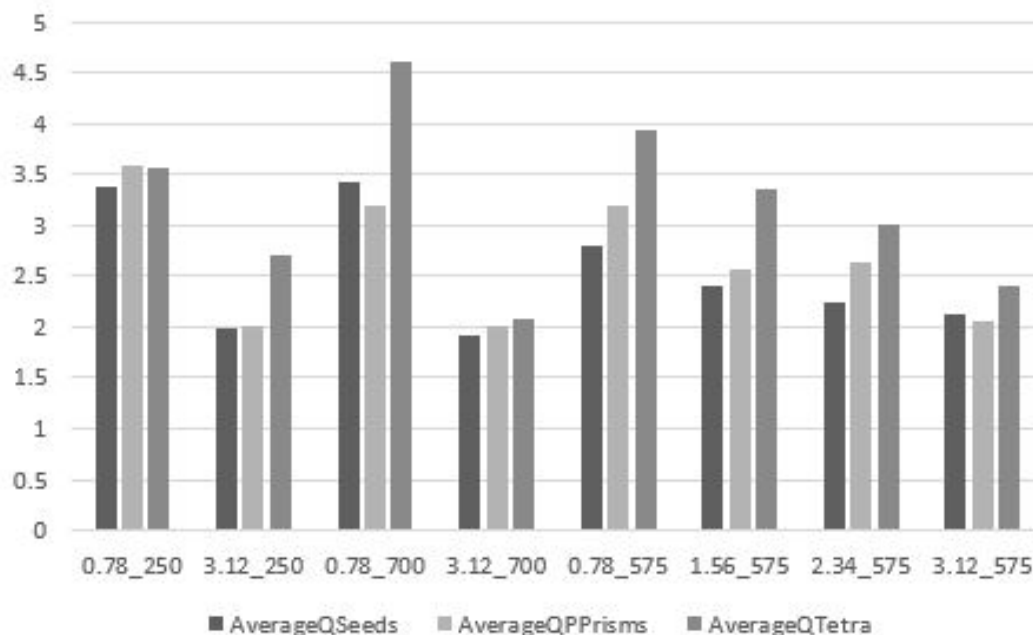


Figure 3.21: Swelling ratio's of gels loaded with tetracycline, $AgNP_{Prism}$ and $AgNP_{Spherical}$. The values were taken as an average of three experiments.

3.5 Bacterial growth and inhibition

3.5.1 Minimal inhibitory concentration

The antibacterial effect of $AgNP_{Prism}$ and $AgNP_{Spherical}$, was tested on *E.coli* in liquid cultures. Four different concentrations of AgNP were used and the cultures were incubated over night. After 2 hours a difference in growth was observed for $AgNP_{Prism}$ and the cultures were plated on LB agar plates. After 18 hours of incubation growth was observed in all cultures, including those that showed a difference after 2 hours. The plates that were plated 2 hours after initiation of the experiment showed an inhibitory effect (see table 3.8) when counting the CFU. From this data the MIC for $AgNP_{Prism}$ was in between 1x(47.73 $\mu\text{g}/\text{mL}$) and 2x(95.46 $\mu\text{g}/\text{mL}$). $AgNP_{Spherical}$ did not show a inhibitory effect at the highest concentration of 1.944 $\mu\text{g}/\text{mL}$.

Table 3.8: Colony forming units per concentration of AgNPs after two hours of incubation

	$AgNP_{prism}$	$AgNP_{Spherical}$
2x	$1.00 \cdot 10^7$	$2.60 \cdot 10^8$
1x	$2.60 \cdot 10^6$	$5.70 \cdot 10^8$
0.5x	$7.27 \cdot 10^7$	$2.40 \cdot 10^8$
0.25x	$1.30 \cdot 10^8$	$4.80 \cdot 10^8$

3.5.2 Zone of inhibition

To see if the drug or particle could diffuse out of a PAAm/PEGDA hydrogel and prevent growth of *E. coli* and *S. cerevisiae*. The gels cured with either tetracycline, water, AgNP_{Prism} or AgNP_{Spherical} were tested on agar plates with either LB or YPD-medium.

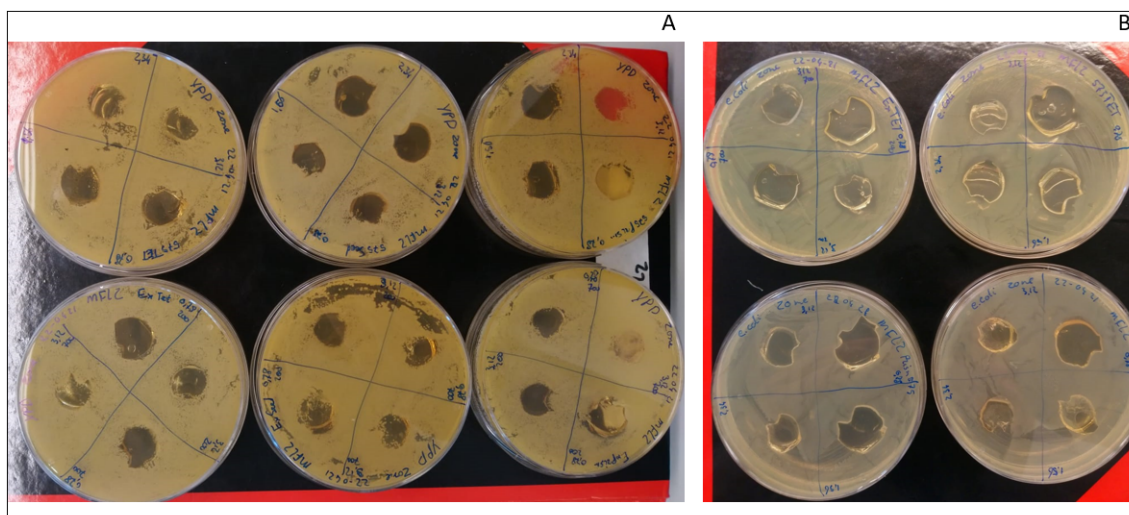


Figure 3.22: Zone of inhibition experiment. A) all the yeast experiment with different length and concentration of PEG gel and cured with either AgNP_{Prism}, AgNP_{Spherical} or tetracycline. B) same experiment but on *E. coli* instead.

All types of gels inhibit growth under them but not around them. In fig. 3.22 It is seen that yeast grow well on all the agar plates. For *E. coli*, however, a small zone without any colonies can be observed around the gels cured with tetracycline. The zone of inhibition was better visible in fig. 3.23.

For the gels consisting out of PEGDA₅₇₅ cured with tetracycline, the concentration 0.78, 1.56, 2.34 and 3.12% had a zone of inhibition with a length of 3.49, 2.59, 2.35 and 4.28 mm, respectively. For the gels with PEG of average weight 250 or 700 and concentration of 0.78 or 3.12% the zone of inhibition was 1.21 mm (0.78% PEGDA₂₅₀), 2.84 mm (3.12% PEGDA₂₅₀), 2.07 mm (0.78% PEGDA₇₀₀) and 1.3 mm(3.12% PEGDA₇₀₀)

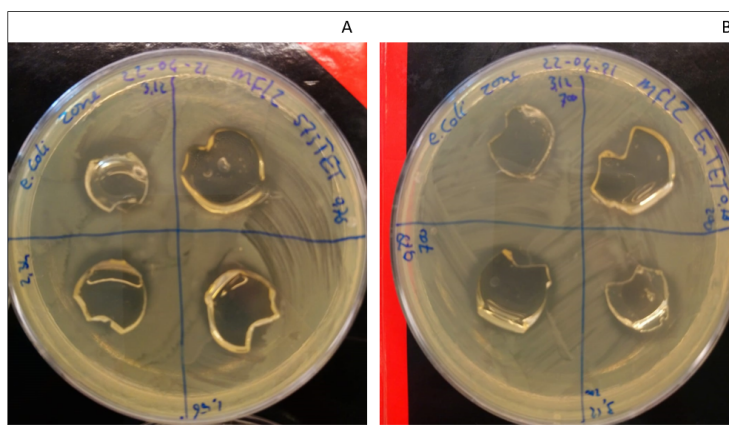


Figure 3.23: A) agar plates with gels made with different concentration of PEGDA with a molecular weight of 575 MN. Concentrations of PEGDA are 0.78, 1.56, 2.34 and 3.12% clockwise rotation. B) made from PEGDA with molecular weight of 250 or 700 MN with either a concentration of 0.78 or 3.12%. all gel consist of 15% PAAm

3.5.3 Segmented growth experiment

The antibacterial effect of the gels was also tested in pre-culture tubes with different concentrations of *E. coli* diluted from an O/N culture, $10^{-2} - 10^{-7}$. These concentrations were then co-incubated with hydrogels loaded with, $\text{AgNP}_{\text{Prisms}}$, $\text{AgNP}_{\text{Spheres}}$ and tetracycline for 8 hours.

The starting amount of the bacterium from each dilution of the negative control was counted from the agar plates and are seen in table 3.9. From these plates it could be determined that O/N culture on average contained a 10^9 cells/mL. In all three experiment it was seen that an inhibitory effect from the gels when the dilutions are equal or bigger than 10^{-3} . The results of the first experiment as seen in fig. 3.24 shows almost no growth at different dilutions for *E. coli* with tetracycline gel, the same goes for the other experiments as seen in figs. 3.25 and 3.26.

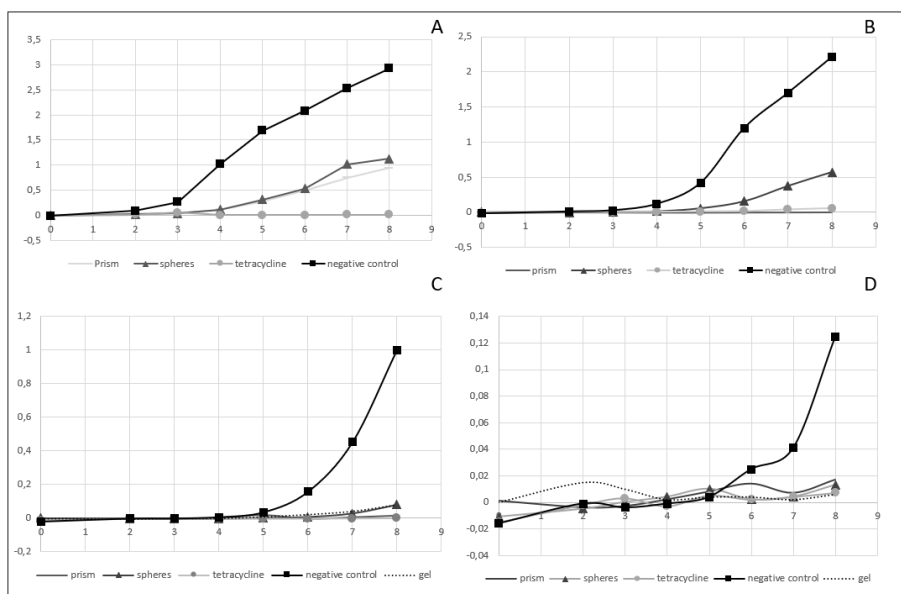


Figure 3.24: OD_{600} of the different gels cured with either tetracycline, water, prism or spherical nanoparticles and their effect on bacterial growth in different dilutions. One measurement was taken every hour for 8 hours. The dilutions of O/N culture are A) 10^{-3} , B) 10^{-4} , C) 10^{-5} and D) 10^{-6} . The gels used had a volume of 1 ml

The experiment was repeated 2 times, however, the 0.78 % PAAm/PEGDA₅₇₅ were placed in tubes with higher concentrations of *E. coli*.

Looking at the inhibitory effect of AgNP_{prism} and AgNP_{spheres}, it was observed after 8 hours an OD_{600} absorbance under 2 and just above 2.5 respectively. For the gel control an absorbance of 1 was measured at OD_{600} (fig. 3.25 A). At a dilution of *E. coli* 10^{-6} (fig. 3.25 D) the OD_{600} value for all sample except for negative control seem to be at the same value after 8 hours, under 0.02

For the third experiment the gel control had an absorbance of 1 was measured at OD_{600} (fig. 3.26 A). At a dilution of *E. coli* 10^{-6} (fig. 3.26 D) the OD_{600} value for all sample except for negative control seem to be at the same value after 8 hours, under 0.05

Table 3.9: The colonies counted for each dilution of the negative control from each experiment. 100 μ L was put on the agar plates

	10^{-8}	10^{-7}	10^{-6}	10^{-5}	10^{-4}
Experiment 1	1	181	84	679	2812
Experiment 2	0	17	126	242	3336
Experiment 3	3	14	157	809	3432

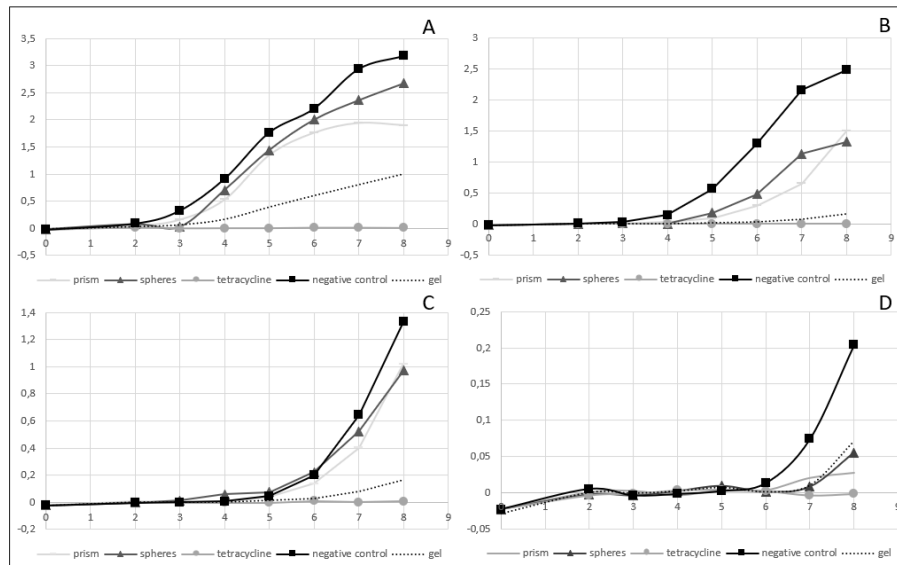


Figure 3.25: OD_{600} of the different gels cured with either tetracycline, water, $AgNP_{Prism}$ or $AgNP_{Spherical}$ nanoparticles and their effect on bacterial growth in different dilutions. The lowest concentration of cross-linking was used 0.78%, to produce an anti bacterial effect since diffusion would be the highest for these gels. One measurement was taken every hour for 8 hours. The dilutions of O/N culture are A) 10^{-3} , B) 10^{-4} , C) 10^{-5} and D) 10^{-6} . The gels used had a volume of 0.5 ml

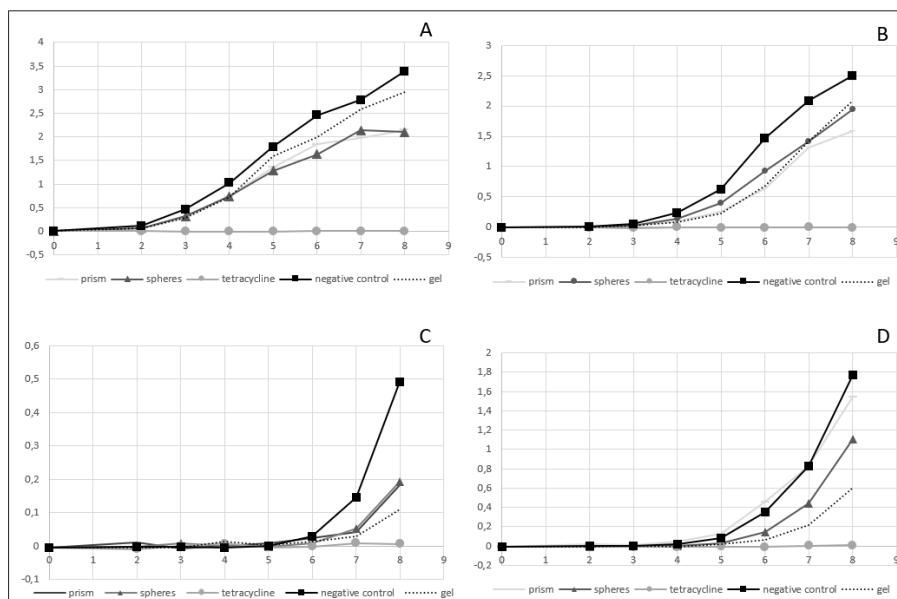


Figure 3.26: OD_{600} of the different gels cured with either tetracycline, water, $AgNP_{Prism}$ or $AgNP_{Spherical}$ nanoparticles and their effect on bacterial growth in different dilutions. One measurement was taken every hour for 8 hours. The dilutions of O/N culture are A) 10^{-3} , B) 10^{-4} , C) 10^{-5} and D) 10^{-6} . The gels used had a volume of 0.5 ml

After the eight hours the cultures tubes were left over night in incubator 37 ° to see if all bacterium was death or not. No OD_{600} was measured but as seen in fig. 3.27 only the tube with tetracycline gel was clear compared to rest.

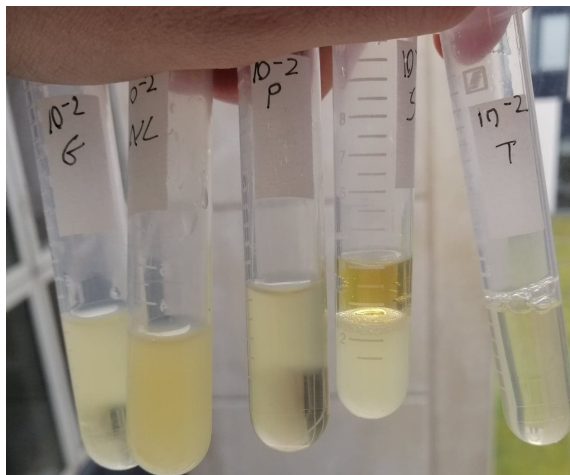


Figure 3.27: The culture tubes after 24 hours incubation. From left to right was culture with 0.78 % PEG and 15 % AAm gel, negative control, gel with AgNP_{Prism}, gel with AgNP_{Spherical} and lastly a gel with tetracycline.

Chapter 4

Discussion

4.1 Particle synthesis

4.1.1 AgNP synthesis

A fast chemical synthesis was chosen to produce AgNP_{Prism} and AgNP_{Spherical}. The Produced NPs were examined with Uv/vis spectra, AFM and SEM to define shape and size.

Right after synthesis of AgNP_{Prisms} UV measurements were done and the maximal absorbance was assessed. It was shown that the maximal absorbance grew with decreasing seed volume used. In addition it was seen that the broadness of the peak also grew with decreasing seed volume, suggesting a larger distribution of sizes. Since there was a big red shift between seed particles and the produced particles, it was assumed that these particles was shaped as a prism. This was confirmed with SEM and topography (AFM), where both triangular and hexagonal shapes were present. Most importantly, topography combined with SEM, showed a low height compared to the edge-lengths, with an average height below 10 nm (table 3.2). Lower seed concentration resulted in larger AgNP_{Prism}, hence, a longer average edge-length.

Arhene et al. showed the increase in maximum absorbance wavelength for bigger AgNP_{Prism} and decrease in intensity [52]. Transmission electron microscopy done by them showed that 90% of the particles were shaped as a prism. Results presented here show a high distribution in shape, where high percentage of the particles have a hexagonal shape fig. A.2. This might have been due to the stability of the AgNP_{Prism} solutions. Where particles seem to grow over time (table 3.1).

Diffusion of particles through a hydrogel was to be tested and the antibacterial effect of particles Prism₂₀₀μL were used for further experimentation with the AgNP_{Spherical}, since they were comparable in size.

The increase in hexagonal particles is especially seen in particles produced in bigger reaction volumes. Where an even higher number of hexagonal particles were seen.

These particles were bigger and had a higher deviation, to what was expected from the small volume reaction. These difference are undesirable and might have been caused by keeping the addition speed of the AgNO_3 the same for the smaller volume and the bigger volume. The result might be due to the addition of a to small volume, leading to improper mixing of the Ag^+ throughout the reaction resulting in uneven growth.

4.1.2 Spherical particles

Multiple methods were used to produce $\text{AgNP}_{\text{spherical}}$, such as seed depended growth with seeds capped with either, TSC, or PSSS. TSC resulted in flat particles with a high variety in shapes. PSSS capping showed more $\text{AgNP}_{\text{spherical}}$, however, were not reproducible. Therefor, $\text{AgNP}_{\text{spherical}}$ were produced from ammonia-Ag complexes. This method produced particle seed particles with high ellipticity. The obtained sizes in the topography differed from what has been shown in Xing et al. [59]. Here we found sizes of 40 and 44 nm, whereas they concluded sizes of 45 and 60 for the same seed volume added. This might be explained by the amount of precipitation that is visible in the reaction volumes during the reaction. Precipitation of silver ions resulting in fewer ions aggregating to seeds in the solution, leading to smaller particles. Due to the presence of Cl^- in the reaction volume, it can lead to the formation of AgCl . This salt is not solvable in water and thus leads to the aggregation and precipitation of silver. Xing et al. used Cl^- to increase the control over the shape of particles formed and mention a maximal concentration that can be used [59, 70]. Removing the salt from the initial seed formation leads to an increased polydispersity of formed seed particles. Further growth reactions show no difference compared to the presence of Cl^- , the aggregation of silver remains. Increasing the concentration of TCS seems to increase the stability of the reactions.

When increasing the scale of the AgNP production, an increase in aggregation is observed. Reducing the molarity of ascorbic acid seemed to alleviate this problem for 20 mL reaction volumes. Further increasing the reaction volume resulted once more in aggregation. Due to increasing effort to produce particles where size could be controlled. It was opted to use the seeds produced in the ammonia-complex method, however, the addition of NaCl was removed, resulting in an increased concentration of particles with a bigger size distribution.

4.1.3 TPO nanoparticles

Monodisperse TPO nanoparticles were required to initiate the polymer radicalization evenly throughout the solution. Size should be relatively small, however the main point is increasing the solubility of TPO. The solubility was increased to 2% w/w with water, which is a large improvement from 0.01% w/w solubility of TPO powder. This solubility was only found for particles with a TPO content of 10%. $\text{TPO}_{20\%}$ were barely solvable in 1% w/w in water.

Analysis with nanosight offered several adjustable parameters within the software [71]. Adjusting these parameters, blur size, jump distance and track length greatly influence the data representation. This is clearly shown in the figs. 3.7, A.3 and A.4, using the right parameters to remove background signal from particles is important. Resulting in one smooth peak representing the hydrodynamic size distribution of the TPO particles, ranging from 150 to 400 nm with an average size of 255 nm. When leaving these parameters for the algorithm to decide the curve loses its smoothness, showing more size populations within the 150 to 400 nm range. When closely observing how the algorithm tracks the particles it shows that some artifacts are included, such as the accumulation of particles <100 nm when there is no minimum track length which could be noise. These are mostly small spots of signal that appear for a few frames before disappearing again, either produced by background noise or small fast moving particles. By setting the minimum track length to 12 frames the 75nm peak disappeared.

When the particles are hit by the laser, the light scatters often results with blurring of the signal shown as multiple spots that represent the same particle. The algorithm occasionally jumped between these spots, increasing the average speed of the Brownian motion resulting in a smaller particle readout. Increasing the jump distance to 5 pixels removes the jumping between the blurred spots reducing the particle populations at 105 and 185 nm. The tweaking of these parameters does come with a risk, adjusting to much where the data is no longer representative for imaged sample. Therefore, it is important how the parameter adjustments change your data representation. In this case the peak at 255 nm stays constant with changing parameter settings, leaving the conclusion that TPO_{10%} have an average hydrodynamic size of 255 nm. For TPO_{20%} a value of 288 nm was found. This size does differ from [23] where they found a hydrodynamic size of 250 nm for 10% w/w TPO nanoparticles. For Higher TPO concentration particles they showed significant deviation in size ranging from 180 to 350.

Pawar et al. [23] also shows that the concentration of TPO in the nanoparticles can be increased to 25% w/w, this was valuable for their research to increase the speed on curing during 3D printing. In this study increasing the TPO concentration affected the solubility of the particles, reducing the total amount of TPO in the solution upon polymerisation. Simply increasing the concentration of Particles with lower TPO content had a higher effect.

4.2 Mechanical characteristics of PAAm/PEGDA hydrogel

12 gels were made with change in either AAm, PEGDA concentration or PEGDA chain length to see how it affected mechanical properties of hydrogels. In general the gels felt more stiff and brittle when increasing PEGDA concentration. Reducing the PEGDA chain length had a similar effect where smaller chains produced more brittle gels. First the amount of AAm was changed, 5, 10, 15 or 20% AAm, cross-linked with 1.56% PEGDA. 5% w/w AAm was not used for measurements, although polymerization oc-

curred the result could not hold shape, therefore, it could not be considered a gel. During the handling of the gels it was noticed that the adhesion of gels to surfaces decreased with increasing concentrations of AAm.

Compression and elongation experiments were conducted on the gels to see how the mechanical properties changed as a result of the increasing AAm concentration. In fig. 3.13 A, it was observed that it takes more force to deform the gels with higher percentages of AAm. Even though, the strongest gel consisted out of 20% AAm, the 15% AAm gel was chosen for further research. This was due to the adhesion were better, which is important when used in wound dressing and it is stronger than the 10% AAm gel.

Increasing the concentration of PEGDA (fig. 3.13 B) increased the strength while decreasing the adhesion of PAAm/PEGDA gels. Lastly the PEGDA chain length were changed from 575 Mn to 250 or 700 Mn using 0.78 and 3.12 w/w% ratio's of PAAm/PEGDA (fig. 3.13 C). At lower concentrations of cross-linker, it seems that the PEGDA chain length does not affect the strength, however, at higher concentrations the length of PEGDA seems to have an effect where larger chains produced a stiffer gel. The effect of chain length is not as dominant compared to the change in PEGDA concentration.

The gel consisting of 0.78% PEGDA₅₇₅ is the weakest and highest strain occurs at an applied stress between 0.005 and 0.01 MPa. The strongest gel is 3.12% of PEGDA₅₇₅ and PEGDA₇₀₀ at a stress applied between 0.02 to 0.025 MPa.

The elongation of gels (figs. 3.15 to 3.17 tests their tensile strength. For gels consisting of 10, 15 and 20% AAm a force of 0.12, 0.23 and 0.27 N were applied, respectively, before the gels broke. Increase total polymer content in the gel makes it stronger, since it takes more force to stretch the gels. The average forces presented in table 3.6 were used to calculate the Young's modulus. The elasticity is reduced with increasing AAm. Increasing the PEGDA concentration the elongation becomes bigger from 0.78% to 1.56% PEGDA, where it becomes smaller between 1.56% and 3.12%. The force increases with the increase of PEGDA concentration which stops at where 2.34% is comparable to 3.12% in regard to force and elongation at breaking point. This is also seen in fig. 3.16. The resemblance of 2.34 and 3.12% of PEGDA₅₇₅ might indicate that the PEGDA concentration of 2.34% is the minimum concentration needed to make the strongest gel with 15% AAm.

In (fig. 3.17) Both PEGDA₂₅₀ and PEGDA₇₀₀ require more force to stretch compared to PEGDA₅₇₅ with cross-linking densities of 0.78%. Increasing the amount of PEGDA₇₀₀ to 3.12% takes the same amount of force to break as 0.78% but stretches less than the gels with 3.12% PEGDA₅₇₅. Since the 3.12% PEGDA₂₅₀ gels were brittle and broke before testing, there were no stretching tests conducted for this gel.

Mechanical studies of PAAm-PEGDA gels were also conducted by Zhang et al. [18] who 3D printed their gels. They concluded that increase in PEGDA concentration resulted in a more stiff gel at the cost of being less stretchable. When they decreased the PEGDA length to either 250 or 550 Mn the gel became less stretchable and increased in

modulus. The opposite was observed when increasing the PEGDA length.

The increase in PEGDA concentration results in a stronger gel, due to a higher cross-linking density. As a result of the increased cross-linking density, the average PAAm chain becomes smaller because of more cross-linking points. This shorter chain length reduces the elasticity of individual polymer strands. Increased PEGDA length also results in a more stretchable gel since the chain is longer, which leads to decline in stiffness of the gels. Our results show the the same effect, however, not as consistent as Zhang et al. [18]. As mentioned they use 3D printed gels, whereas our gels are photo-polymerised in bulk. Perhaps the fact when getting the gels out of the mold it gets more damaged, thus introducing weak spots in the polymer network, compared to taking it off a 3D-printer. Their gels also consisted out of 20% AAm which is stronger than 15% AAm. They further used a lower cross-linking concentration of 0.625 w/w% PEGDA/AAm ratio and as Norioka et al. [20] observed, tougher gels were made with higher concentration of AAm and a low concentration of cross-linker, since a to high cross-linking density lead to a brittle gel. Another factor beside monomer/cross-linker ratio could be, that 3D-printed gels have an altered polymer network compared to gels photo-polymerised in bulk, due to the layer by layer polymerisation. The compression test are more in agreement with Zhang et al. [18], which might be because the compression tests were made by a machine and the tensile tests were done by hand giving human errors like the pulling speed and dragging forces. There are automated options to measure tensile strength but not available to us.

Mechanical testing were also performed on the gel loaded with AgNPs. It was seen during the compression that the gels with AgNPs are more though compared to the gels without AgNPs. It is inconclusive which type of particle stabilised the most since it varied from sample to sample. The reason for more though gels could be that the particles interact with the polymeric network by H-bond or entanglement as suggested by Yissar et al. [66].

4.3 Swelling of hydrogels

Swelling studies were conducted on all of the gels made (see fig. 3.19). It was observed that lower amounts of cross-linker lead to a higher degree in swelling. As the concentration of cross-linker increases it seems that the length of PEGDA had less influence on the swelling. Especially, if the lowest concentration, 0.78%, is compared with the highest concentration, 3.12% PEGDA. Here a clear difference can be seen after 48 hours, where the lower concentration swells 2x more than the highest concentration. A similar difference is observed for the different PEGDA lengths. At 0.78% PEGDA₂₅₀ and PEGDA₅₇₅ swell almost 4 times bigger compared to their original, relaxed state, whereas PEGDA₇₀₀ almost becomes 4.5 times bigger. At 3.12% there is still a difference between the PEGDA length but less prominent compared to 0.78%.

Caykara et al. [17] did similar swelling experiment but with longer cross-linkers at

higher concentrations of PEGDA. They concluded that change in PEG length has bigger influences over swelling compared to change in concentration. The results in fig. 3.19 show a clear difference in swelling when comparing 0.78% PEGDA to the rest of the PAAm/PEGDA w/w% (fig. 3.19 A and C). In fig. 3.19 B the deviation in swelling of the different PEGDA₂₅₀ gels becomes more noticeable. At higher concentrations of PEGDA, the length of the cross-linker seems to decrease its effect on swelling. This is clearly seen in fig. 3.19 D when the swelling of 0.78% PEGDA is compared to 3.12%. The reason of inconsistency between Caykara et al. [17] results and those obtained here, might be due to the concentrations used. They used 4.8 w/w% PAAm/PEGDA as their lowest cross-linking concentration. As discussed for fig. 3.19 A and C there seems to be less of an influence on the swelling when increasing the PEGDA w/w% from 2.34 and above. A suggestion for these results might be that at a certain point of PEGDA concentration, the gels cannot be more densely packed, hence the gels cannot swell less. Another factor is their usage of 4000, 6000 and 10000 Mn PEG, which is longer compared to the PEGDA used in this project. Swelling of a gel is determined by two forces, water interaction with the hydrophilic chain, and the counter force of the cross-linked network trying to pulling the chain together [30]. The longer chains used compared to our experiment enable their gels to swell more due to the increased elasticity of the polymer chains.

The swelling experiments can also be used to indicate which gels have the largest or smallest mesh size, which normally correlates with cross-linking density [31]. Since the mesh size was calculated based on volume fractions of polymer and the swelling ratios, 0.78% PEGDA₇₀₀ which has the highest swelling ratio, should also have the largest mesh size [36, 31]. At higher concentrations of PEGDA the structure of the gels becomes tighter and hinders the mobility of polymer chains, minimizing their water uptake. Yacob and Hashim [19] tested this phenomena on hydrogels and saw more dense structures led to lower water uptake. Caykara et al. [17], mention that smaller PEG also leads to lower water uptake. They further state that the polymerisation process leads to heterogeneous structures. This heterogeneity might explain the big standard deviation seen in table 3.3.

4.3.1 Diffusion through PAAm/PEGDA gels

This experiment was made to check at which rate the particles or antibiotic were released from the gels and how the PEGDA length and concentration affect the diffusion. The data from AgNP_{prism} showed no release and it might be due to their shape and size making it harder for the prisms to travel through the gel. This is observed by the difference in concentrations for AgNP_{prisms} and AgNP_{spherical} that were used to polymerise the hydrogel-composite gels. Even when AgNP_{prisms}-hydrogels contained 50x more total silver content, hardly any release was observed.

Most of the release takes place during the first eight hours, which coincides with rapid swelling of the hydrogels. In fig. 3.20 A, B, a slow increase can be seen after 24 Hours for AgNP_{spherical}. For tetracycline fig. 3.20 C and D, the concentration is fluctuat-

ing after 24 hours, indicating equilibrium of tetracycline concentration within the gel and water. At equilibrium just as much that comes in comes out of the gels which is why the intensity seems to be pretty similar throughout the experiments after 24 hours. A bigger initial release was observed for tetracycline compared to AgNP_{Spherical}. This is most likely due to the smaller size of tetracycline. This makes it less likely to get entrapped in the polymeric network of the gel, resulting in a faster release. PEGDA₅₇₅ 0.78% has the highest release rate over time and continues releasing nanoparticles after the first 8 hours. This release rate, however, was low. As the concentration of PEGDA₅₇₅ increases the amount of particles released decreases. This is seen in the initial burst which is lower for increasing cross-linking densities (fig. 3.20 A). For tetracycline it is different, where the release seems to be the same for all PEGDA₅₇₅ concentrations used (fig. 3.20 B).

For PEGDA₂₅₀ and PEGDA₇₀₀ a similar trend was observed. A clear difference between the initial burst of the 0.78% and the 3.12%, where 0.78% shows a higher release (fig. 3.20 C and D). This release did not appear to be dependent on the cross-linker length, since the release percentages are similar for PEGDA₂₅₀, PEGDA₅₇₅ and PEGDA₇₀₀ at the same amount of cross-linker concentration (fig. 3.20 C and D). PEGDA length also did not influence the release rate of AgNP_{Spherical} (fig. 3.20 B).

The intensity drops at 8 hour before increasing again in addition high standard deviations are recorded for tetracycline release (fig. 3.20 C and D). This fluctuation is explained by the swelling we see for the tetracycline gels, which is higher than that of the particle gels. Swelling increases the distance between polymer chains, leading to the reduction in steric hindrance of particles and eventually the release of particles or tetracycline. It might also be the interaction of AgNPs which either get entrapped or binds to the polymeric network due to its capping agent.

When comparing the swelling of particles loaded gels (fig. 3.21) with unloaded gels (fig. 3.19) the ones with AgNP_{Prism} and AgNP_{Spherical} have swelled less compared to their counter parts without any particles. As discussed, a more dense structure inhibits the mobility of polymer chains (section 4.3) and as a result less water is able to penetrate the gel. The addition of AgNPs into the gels makes them tougher and more stress is needed to be applied to deform the gels (fig. 3.14). A reason for that might be the nanoparticles binds to the polymeric network stabilising it even more compared to gel without the particles. However, stabilising the polymer chains means a lower mobility, offering an explanation as to why the gels with particles have a decreased swelling ratio compared to unloaded hydrogels. A decrease in swelling ratio for gels loaded with AgNPs was also observed by Masood et al. [65]. No effect of tetracycline is seen for swelling of PAAm/PEGDA hydrogels.

4.4 Polymer network structure

Deriving pore size from SEM images of hydrogels depends on the sample handling during the freeze drying process. It is well known that deformations to network can occur

during the freezing process [27]. Further, during the lyophilization water evaporates through the pores on the surface which can cause a collapse of pores. Since liquid nitrogen has a low heat capacity, it is important to freeze the gel sample long enough, not doing so will result in large shrinkage of the gel. Not doing so will still leave a surface which shows pores, however, the interior of the gel is entirely collapsed. Freezing them longer, preserves the inner structure better while freeze drying.

Other than freeze drying the gels could be dried via super critical drying, This technique is commonly used to produce aerogels, of which the gels retain most of their 3D structure. In order to use supercritical drying, water needs to be removed from the hydrogel, prior to the supercritical drying. Removal of water is essential for the liquid CO₂ to fill the gel, since liquid CO₂ cannot exchange with water in the gel. Water was extracted with several a-polar solvents with lower densities such as, ethanol acetone and isopropanol. All of them resulted in a collapsed gel. The a-polar solvent used were not useful for drying the gels due to the collapse.

When SEM images were taken of the surface, collapse or debris of the pore structure was quite often observed, resulting in images that were not possible to correctly analyse. This coincided with frequent collapse of small pores leading to a approximation of the average pore size being bigger than it should be.

By freezing the gels for a longer period, 5-15 minutes, and subsequently breaking them indiscriminately, shards were collected and freeze dried. This process obtained representative images of how the polymer network is formed. Where no dangling ends can be seen, as in fig. C.1 C and D, which are present on the surface of the gel. Removing these artifacts results in a better image analysis that is more representative for the polymer network.

Still it is not without flaws in fig. 3.12 A, the surface has a rough and a smooth side. Magnification on 200x was made on both sides, where B displaces the rough side and C the smooth side. C has a more uniform surface and B a smeared surface. The difference of those two sides is due to before freezing the gel many small cuts are made along the cylindrical shaped gel to make weak spots when breaking it.

Table 4.1: Mesh size in Å calculated from swelling and rheology data compared to w/w% molar ratio and Feret's diameter obtained from SEM analysis

	PEGDS ₅₇₅				PEGDS ₂₅₀				PEGDS ₇₀₀			
%	0.78	1.56	2.34	3.12	0.78	1.56	2.34	3.12	0.78	1.56	2.34	3.12
Mesh _{swelling} eq. (1.30)	443.40	199.93	158.44	191.57	446.26	312.12	234.56	196.07	535.41	244.63	233.68	217.69
Mesh _{Rheology} eq. (1.34)	59.98	48.14	47.00	47.16	69.21	x	x	46.06	58.90	x	x	34.58
Mesh _{Rheology} eq. (1.35)	34.63	27.79	27.14	27.23	39.96	x	x	26.59	34.00	x	x	19.96
Mesh _{w/w%}	249.95	176.74	144.31	124.97	164.81	x	x	82.41	275.78	x	x	137.89
Feret's diameter _{pore} μm	6.35 ± 7.22	6.37 ± 7.45	6.95 ± 8.39	6.57 ± 7.53	6.4 ± 7.73	x	x	6.95 ± 7.26	6.36 ± 6.92	x	x	6.25 ± 5.59

Table 4.2: Mesh size in Å, derived from swelling data of hydrogels containing particles and tetracycline

	PEGDS ₅₇₅				PEGDS ₂₅₀		PEGDS ₇₀₀	
%	0.78	1.56	2.34	3.12	0.78	3.12	0.78	3.12
Prism	329.68	225.89	228.19	156.68	440.19	159.05	293.48	151.99
Spherical	248.83	243.311	194.94	150.40	354.31	161.66	402.83	140.272
Tetracycline	487.51	418.49	325.543	223.86	424.52	392.65	478.88	199.53

Pore size for hydrogels of different cross-linking density are reported in table 3.3 and are compared to values calculated for mesh size using equation (eq. (1.30) eq. (1.33)) and shown in table 4.1. These calculations used values obtained during the swelling and rheology experiments. Additionally the mesh was calculated for gels containing silver nanoparticles shown in table 4.2. It is important to note that the mesh size is not equal to pore diameter and only correlates with the increase in pore size. From table 4.1 it can be seen that there is a difference in mesh size between the cross-linking densities of 0.78% and 3.12% for the cross-linking densities in between 1.56 and 2.34% only a difference is seen for PEGDA₂₅₀, where there appears to be a linear dependency on the cross-linking density and mesh size. For PEGDA₅₇₅ and PEGDA₇₀₀ there were little difference in swelling between the higher cross-linking density and only a significant difference was seen in the 0.78% which showed a higher swelling ratio. This difference is translated into mesh sizes. For rheology a difference can be seen again between the two cross-linking densities of 0.78% and 3.12% for the all 3 PEGDA cross-linker lengths. The cross-linking densities of 1.56% and 2.34% of PEGDA₅₇₅ seem to affect the mesh length in the same line, increasing in cross-linking density, resulting in a smaller mesh size. However, the impact on the mesh above a density of 1.56% is low.

$Mesh_{Rheology}$ calculated with the Young's modulus shows an obvious decrease in mesh size compared when using the G modulus. Where the G modulus is generally 3x lower than the elastic modulus, although, the same trend holds (table 4.1).

When both the mesh calculated from the rheology and swelling are compared to the mesh size calculated based on the molar ratio between PAAm and PEGDA a difference is seen. $Mesh_{w/w\%}$ has a clear dependence on the concentrations used. This cross-link concentration dependence was missing in the experimental data for swelling and rheology. The difference between 0.78% and 3.12% for the experimental does hold up. The values of the different calculations clearly differ. $Mesh_{Rheology}$ is much lower than $Mesh_{w/w\%}$ and $Mesh_{swelling}$ approximates the mesh slightly higher. Both are relatively close to the simple calculation for M_C based on the w/w%. It has to be said that the $Mesh_{w/w\%}$ is a crude approximation of the mesh size since it only considers the ratio of monomer vs cross-linker molecules, whereas swelling introduces the change in free energy in the system and the expansion of the network upon dilution with a number of solvent molecules. For both swelling and rheology other forces are included in the experimental values, such as physical cross-linking and polymer entanglement.

$Mesh_{swelling}$ was also calculated for the gels cross-linked with particles and tetracycline (table 4.2). Here a increase in mesh can be seen dependent on cross-linker density,

similar to what was seen for PEGDA₂₅₀ swelling. In addition there was a difference seen between the AgNPs and the tetracycline gels, where AgNP_{Spherical} showed the overall smallest mesh sizes. 0.78 w/w% PAAm/PEGDA showed the biggest difference where AgNP_{Spherical} had a mesh of 249, AgNP_{Prism} 330 and with no particles 443 Å. Seemingly the particles increase the cross-linking density of the hydrogels.

All mesh sizes are considerably smaller than the Feret diameter. This is not surprising because of how cross-linked networks forms. Where mesh size gives an approximation where the polymer backbone is intersected with a cross-linking molecule and thus where it is connected to. The actual formation of the network can produce big pores since the cross-linker is not limited in 2D space fig. 1.5.

From average pore size in μm^2 a similar trend, growing pore size with decrease in cross-linking density, was not found. On the contrary it seems that the average pore remains the same with cross-linking density when we look at images with 200x magnification table 3.3. It has to be noted that all values have very high standard deviations due to the big variation in pore sizes that can be seen on the SEM images in fig. 3.10. The large distribution in pore sizes might have been caused by improper mixing of the gel components, monomer, cross-linker and photo-initiator before polymerization. Clusters of high density of small pores were observed for all hydrogels. A possible reason for these clusters could be higher concentrations of radicals were formed in these areas, or the concentration of cross-linker was higher in these regions. PEGDA₅₇₅ and PEGDA₇₀₀ solutions had a high viscosity. During the preparation of hydrogel reaction volumes it was made sure that these were properly mixed in the reaction volume. TPO was made soluble by emulsification and soluble up to 2 w/w%, resulting in a clear solution after filtration. It might have been that the TPO particles were not evenly spread throughout the reaction volume.

The histograms of the gels were made from multiple SEM-images of same magnification (200x). Since there was a high spread in pore size μ^2 (hence the big value for standard deviations) the histograms were made from values of 1 to 82 μ^2 and represented in figs. C.6 to C.8. The 20% AAm gel has more small pores compared to the 15% AAm gel and the 10% AAm gel has the lowest amount of small pores fig. C.6.

A similar trend is observed when PEGDA concentration is increased, except when the concentration is increased from 2.34 to 3.12%. As seen and discussed for the elongation results, these two are comparable in their results (see table 3.6). This indicates again that 2.34% PEGDA might be the minimum concentration needed for the optimal strength of 15% AAm gels. For PEGDA₂₅₀ and PEGDA₇₀₀ the opposite was observed, which might have been due to the freeze drying process. In the representative figures fig. 3.11 C and D The pores are less compared to A and B and there is more collapsed area resulting in lower amount of pores measured. This might explain why the 3.12% PEGDA₅₇₅ has less pores and does not follow the trend like 0.78, 1.56 and 2.34% PEGDA₅₇₅. With higher concentration of cross-linker more cross-linking points follows which should results in smaller pores, reducing the permeability of water. When freeze drying the water is

removed due to sublimation, so the smaller pores reducing the permeability of water might collapse which would explain lesser pores on the SEM-image.

Difference between swollen and non swollen gels are represented in figs. C.2 and C.3. These gels were freeze dried. Because of different sample handling these gels cannot be compared to the gels that were frozen, snapped and dried figs. 3.10 and 3.11. The comparison was still made between swollen and non-swollen gels, see fig. 3.12, that were treated in the same way here it was demonstrated that a swollen gel had a higher amount of smaller pores (see fig. C.9). This should not be the case since when the gel takes water up it swells and stretches both the PAAm and PEGDA resulting in bigger pores.

4.5 Antibacterial effect PAAm/PEGDA hydrogel

Although hydrogels can seal off a wound and protect the region from bacterial growth, increasing the antibacterial effect would be an great asset, for uses in an infected wound or for drug delivery purposes. The antibacterial effect of silver particles is widely discussed in current literature and used in real world applications [5, 41, 42, 46]. Particles are also being used in combination with hydrogels for a stronger effect of the wound dressing [64, 65, 66]. In this study AgNP_{spherical} and AgNP_{prism} particles were used in combination with PAAm/PEGDA hydrogels of varying concentration in a effort to control diffusion of said particles. MIC experiments were done to investigate the antibacterial effect of the particles on their own. Although, the particles were not able to completely stop the bacterial growth, there was a difference after 2 hours in colony forming units, most notably for the AgNP_{prism}, AgNP_{spherical} showed no impact on growth. The difference between particles can be explained by difference in concentration, where the AgNP_{prism} were at a higher concentration when starting the experiment. During the MIC it showed that the particles were interacting with the cells in the media, where grey aggregates were visible 16 hours after incubation in the media, This grey pellet was not seen in LB media with particles incubated for the same duration. This is a strong indication that the particles do interact with bacterial cells, most likely by aggregating to the cell wall [43, 44].

Concentrations of the particles were not adjusted when used in the synthesis of the hydrogels. An experiment was designed to observe the effect of gels loaded with particles at different concentrations of bacterial cells. While observing growth over a period of 8 hours, all gels showed an effect, including the negative gel control. For every bacterial concentration the growth observed with AgNP-composite gels showed a slight inhibitory effect compared to when no gel was present. However, the effect of the neutral gel was stronger than what was seen for either particles gels (specially for the higher concentration cell cultures, as seen in fig. 3.26). Therefor, the antibacterial effect was attributed to the gel itself and not the particles involved. Presumably the swelling of the gel allows for bacteria to enter the cells or get stuck on the porous surface of the hydrogel, reduc-

ing the number of bacteria in the media from the start. Resulting in a slower growth whenever a gel is present in the media [72]. When a bigger volume gel was used in the same volume of culture, 1 mL, a bigger effect was visible for the particle gels (comparing fig. 3.24 and fig. 3.25). Increasing the total amount of particles should have an effect on bacterial growth, instead, the increased volume of the gel has a negative impact on the experiment, where the gel takes up a big portion of the culture volume. Therefore, the volume of the gel was reduced to 0.5 mL.

Zone of inhibition is another method used in literature to showcase the effect of loading a drug into a hydrogel and demonstrating a zone of inhibition. Hydrogel will seal the area beneath it from air, resulting in no growth of bacteria underneath. A gel loaded with a drug will show a zone of inhibition. This effect is clearly visible for tetracycline where clear regions are depicted and measured. For the particle gels this is lacking. No zones are observed, showing that the particles have no suppressing effect on the bacterial cells. A similar thing was observed by Ferrag et al. where they used PAAm/PEGDA-AgNP composite gels and no zone of inhibition was observed [47]. However, they showed that no bacteria were able to grow on top of the gel [47]. For both the segmented growth and zone of inhibition no obvious effect is displayed by the particle gels. This might be explained by the diffusion we see relating to the gels. Diffusion is strongly related to the swelling in the first 8 hours, where the majority of the drug/particle was released. Here it can also be seen that the burst release of AgNP_{Spherical} is lower than the tetracycline, this difference is assumed to be linked to the size of the particles. More clearly demonstrated for the AgNP_{Prism}, where the release of particles was not possible to measure. Another possibility is that a smaller concentration is released compared to AgNP_{Spherical}, even though, the gel itself contains a higher concentration of silver.

After the initial burst release a slow release is observed over 96 hours, after which, the measurements become unreliable due to a loss of water, which affects the UV/vis measurements. No matter how big the burst is, the total amount of silver released is 8% of the total content inside 0.78% PEGDA₅₇₅ after 8 hours. Where a considerable amount of particles are trapped in the polymer network, it becomes hard to obtain a concentration sufficient enough to prevent bacterial growth through the release mechanism. This makes it difficult to obtain a concentration sufficient enough to prevent bacterial growth through the release mechanism. This method to demonstrate the bactericidal effect might also not be sufficient. Loo et al. demonstrated that incorporation of AgNP in the gel prior to polymerisation can have a negative effect on the bactericidal effect of the nanoparticles, despite high diffusion of particles [72]. In addition they report that hydrogels with a higher surface concentration of AgNPs are more effective against bacterial cells. These bacteria were derived from the gel after swelling in a culture media. The medium in the gel was squeezed out and re-cultured on agar plates to count CFU's.

4.6 Particle interaction with PAAm/PEGDA network

From the compression and swelling data it can be seen that gels with particles behave differently. They become tougher and swell to a lower degree. Since they gels take up less water it seems that the network elongation is restricted when particles are in them. Indicating an interaction between the particles and the polymers in the hydrogel. Possible interactions that the particles can form with the gel are electrostatic, hydrogen bonding and van der Waals interactions. Since there no charges in the polymer network it is not possible to form electrostatic interaction. Citrate that is present as capping agent on the AgNPs can potentially form hydrogen bonds with the amide groups of the PAAm fig. 4.1. Although not many sources mention AgNPs capped with citrate as a potential cross-linker, it has been mentioned that there might be interactions with hydrogen bonds. For example a breathing in, breathing out method, developed to load gels, or polymer networks with particles based on swelling is explained through this principle. Citrate capped particles enter the gel during swelling, deswelling in acetone extracts the water, however particles remain inside the gel due to steric hindrance of the network and hydrogen interaction between citrate and polymer network [72]. in Ferrag et al. breathing in and out is used to load hydrogels with citrate-capped AgNPs. Gels with these particles show an increase in tensile strength, no explanation is given [47]. Hydrogen bond cross-linking has shown to be able to increase the strength of a gel. Particles with hydroxyl groups that increase in branching, more hydroxyl groups, have shown to increase tensile strength [73]. Since particles without hydroxyl groups were unable to show a similar result, the increase was dependent on the hydrogen-bonds. Hydrogen-bond cross-linking mediated by citrate could explain the increase in strength seen in [47] and in compression tests shown here. Citrate by itself is also mentioned as a chemical cross-linker in conjunction with a host of polymers, however, PAAm is not mentioned [74]. Since chemical cross-linking with citrate would involve the formation of an ester bond, this is unlikely to happen in PAAm/PEGDA hydrogel.

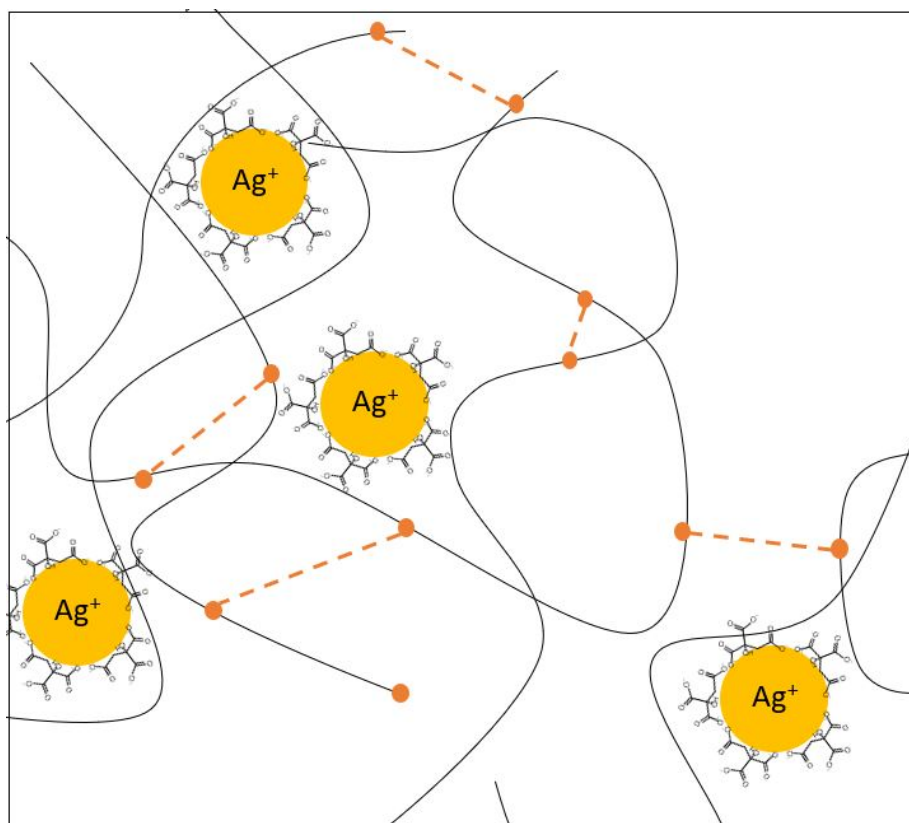


Figure 4.1: Schematic representation of the cross-linked polymer network including $\text{AgNP}_{\text{spherical}}$. $\text{AgNP}_{\text{spherical}}$ can act as additional cross-linker through hydrogen bonds forming between the polymer network and the capping agent, PAAm and citrate.

It is not unreasonable to assume that these also hinder the release of the AgNPs. Yissar et al. [66] used breath in breath out technique to encapsulate nanoparticles and they also suggest h-bond formation between polymer chain and the citrate or just physically entanglement with the network. Diffusion of the particles is dependent mostly on the interruptions made by the polymer network. In the PAAm-PEGDA the mesh size is sufficiently large compared to the particles that this should not affect the diffusion that much. Also shown in the burst release that is present. However, only 8% of the particles was released. The remaining 90% seems to be stuck in the gel, hydrogen bonding can be a possible explanation for the low amount of release. Swelling of the particle gels is also reduced. This ultimately results in the lack of bactericidal effect that is visible in the segmented growth experiment. The reduced swelling ratio due to AgNPs, was also reported by et al. [65], whom suggested the AgNPs can form interaction with polymeric networks.

Chapter 5

Conclusion

The PAAm/PEGDA gels were cross-linked by TPO nanoparticles. The mechanical properties were tune-able by either increasing the concentration of monomers (AAM) or increasing the concentration of cross-linker (PEGDA). In general more force was required to break or deform the gels with higher concentration of either AAM or PEGDA. This increase in strength came at the cost of elasticity. The change of concentration had an impact on swelling too. Length of cross-linker did not show a clear effect, where there was an increased swelling of PEGDA₇₀₀ compared to the shorter cross-linkers. However, compression and similarly rheology did not show a clear difference between the cross-linker lengths. Showing that cross-linking density is a more dominant factor deciding hydrogel strength compared to cross-linkers of different length. This change in mechanical properties was not reflected in the polymer network observed in the SEM images. Here pore sizes were analysed and found to be the same for all gels. The structure itself showed patterns of small pores clustered together separated by big pores. This was caused by unequal distribution of the photo-initiator throughout the gel. When the gels were cured with AgNPs (AgNP_{Spherical} with Feret's diameter 40 nm and AgNP_{Prism} with Feret's diameter of 24.89 nm) their mechanical strength increased. Furthermore, curing the gel with particles decreased their swelling ability compared to normal gels.

This decreased swelling affected the diffusion of particles where a lower percentage was released with increasing cross-linker concentration. Only 10 % of the AgNP_{Spherical} were released. No release was observed for AgNP_{Prism}. Although containing the smaller tetracycline released up to 50% this difference was not only contributed to the size of the components.

Bactericidal capabilities of the gel cured/uncured were tested on *E. coli*. A zone of inhibition was only observed for the gels cured with tetracycline. In LB-medium the observed inhibition of growth seen for the particle cured gels was due to the swelling of the gels. At the highest concentration of bacteria used only tetracycline had an visible effect. Although AgNP_{Prism} particles were able to impede bacterial growth, the release from the hydrogel was to low.

It has been shown that drug release from a PAAm/PEGDA hydrogel polymerized with TPO can be regulated by cross-linking density. This is strongly dependent to the size of the loaded drug as can be seen for the particles. However, the concentration particles released from the hydrogel do not contribute to the killing effect of the gel itself, independent of shape.

Bibliography

- [1] Naeema Mayet, Yahya E. Choonara, Pradeep Kumar, Lomas K. Tomar, Charu Tyagi, Lisa C. Du Toit, and Pillay Viness. "A Comprehensive Review of Advanced Biopolymeric Wound Healing Systems". In: *Journal of Pharmaceutical Sciences* 103 (2014), pp. 2211–2230. DOI: 10.1002/jps.24068.
- [2] Julia Koehler, Ferdinand P.Brandl, and Achim M.Goeperich. "Hydrogel wound dressings for bioactive treatment of acute and chronicwounds". In: *European Polymer Journal* 100 (2018), pp. 1–11. DOI: <https://doi.org/10.1016/j.eurpolymj.2017.12.046>.
- [3] Alexandra Elena Stoica, Cristina Chircov, and Alexandru Mihai Grumezescu. "Hydrogel Dressings for the Treatment of Burn Wounds: An Up-To-Date Overview". In: *Materials* 13.12 (2020), p. 2853. ISSN: 1996-1944. DOI: 10.3390/ma13122853.
- [4] Wei Zhang, Ruixing Wang, ZhengMing Sun, Xiangwei Zhu, Qiang Zhao, Tengfei Zhang, Aleksander Cholewinski, Fut (Kuo) Yang, Boxin Zhao, Rattapol Pinnaratip, Pegah Kord Forooshani, and Bruce P. Lee. "Catechol-functionalized hydrogels: biomimetic design, adhesion mechanism, and biomedical applications". In: *Chemical Society Reviews* 49.2 (2020), pp. 433–464. ISSN: 0306-0012. DOI: 10.1039/C9CS00285E.
- [5] Praveen Thoniyot, Mein Jin Tan, Anis Abdul Karim, David Jame Young, and Xian Jun Loh. "Nanoparticle–Hydrogel Composites: Concept, Design, and Applications of These Promising, Multi-Functional Materials". In: *Advanced science* 2.1 (2015), pp. 1–13. DOI: 10.1002/advs.201400010.
- [6] Fahem Ullah, Muhammad Bisyrul Hafi Othman, Fatima Javed, Zulkifli Ahmada, and Hazizan Md. Akil. "Classification, processing and application of hydrogels: A review". In: *Materials Science and Engineering: C* 57.1 (2015), pp. 414–433. DOI: <https://doi.org/10.1016/j.msec.2015.07.053>.
- [7] Enas M Ahmed. "Hydrogel: Preparation, characterization, and applications: A review". In: *Journal of Advanced Research* 6.2 (2015), pp. 105–121. DOI: <http://dx.doi.org/10.1016/j.jare.2013.07.006>.

- [8] Tzu-Yun Cheng, Ming-Hong Chen, Wen-Han Chang, Ming-Yuan Huang, and Tzu-Wei Wang. "Neural stem cells encapsulated in a functionalized self-assembling peptide hydrogel for brain tissue engineering". In: *Biomaterials* 34.8 (2013), pp. 2005–2015. DOI: <http://dx.doi.org/10.1016/j.biomaterials.2012.11.043>.
- [9] Kaustabh Ghosh, Zhi Pan, E. Guan, Shouren Ge, Yajie Liu, Toshio Nakamura, Xiang-Dong Ren, Miriam Rafailovich, and Richard A. F. Clark. "Cell adaptation to a physiologically relevant ECM mimic with different viscoelastic properties". In: *Biomaterials* 28.4 (2007), pp. 671–679. DOI: [10.1016/j.biomaterials.2006.09.038](https://doi.org/10.1016/j.biomaterials.2006.09.038).
- [10] Amtul Jamil Sami, Madeeha Khalid, Tahir Jamil, Saira Aftab, Sermaid Ahmad Mangat, A.R. Shakoory, and Sara Iqbal. "Formulation of novel chitosan guar gum based hydrogels for sustained drug release of paracetamol". In: *International Journal of Biological Macromolecules* 108.1 (2018), pp. 324–332. DOI: <https://doi.org/10.1016/j.ijbiomac.2017.12.008>.
- [11] Diana Elena Ciolacu, Raluca Nicu, and Florin Ciolacu. "Cellulose-Based Hydrogels as Sustained Drug-Delivery Systems". In: *materials* 13.22 (2020), pp. 1–37. DOI: [doi: 10.3390/ma13225270](https://doi.org/10.3390/ma13225270).
- [12] S. H. Aswathy, U. Narendrakumar, and I. Manjubala. "Commercial hydrogels for biomedical applications". In: *Helvion* 6.4 (2020), pp. 1–11. DOI: <https://doi.org/10.1016/j.helivon.2020.e03719>.
- [13] Jeanie L. Drury and David J. Mooney. "Hydrogels for tissue engineering: scaffold design variables and applications". In: *Biomaterials* 24.24 (2003), pp. 4337–4351. DOI: [https://doi.org/10.1016/S0142-9612\(03\)00340-5](https://doi.org/10.1016/S0142-9612(03)00340-5).
- [14] Yung-Hao Tsou, Joe Khoneisser, Ping-Chun Huang, and Xiaoyang Xu. "Hydrogel as a bioactive material to regulate stem cell fate". In: *Bioactive Materials* 1.1 (2016), pp. 39–55. DOI: <https://doi.org/10.1016/j.bioactmat.2016.05.001>.
- [15] Saahil Sheth, Era Jain, Amin Karadaghy, Sana Syed, Hunter Stevenson, and Silviya P. Zustiak. "UV Dose Governs UV-Polymerized Polyacrylamide Hydrogel Modulus". In: *International Journal of Polymer Science* 2017 (2017), pp. 1–9. DOI: <https://doi.org/10.1155/2017/5147482>.
- [16] Ilya Levental, Penelope C. Georgesa, and Paul A. Janmey. "Soft biological materials and their impact on cell function". In: *Soft Matter* 3 (2007), pp. 299–306. DOI: [10.1039/b610522j](https://doi.org/10.1039/b610522j).
- [17] Tuncer Caykara, Melek Bulut, Nursel Dilsiz, and Yüksel Akyüz. "Macroporous Poly(Acrylamide) Hydrogels: Swelling and Shrinking Behaviors". In: *Journal of Macromolecular Science* 43.6 (2006), pp. 889–897. DOI: [0.1080/10601320600653699](https://doi.org/10.1080/10601320600653699).

- [18] Biao Zhang, Shiya Li, Hardik Hingorani, Ahmad Serjouei, Liraz Larush, Amol A. Pawar, Amir Hosein Goh Wei Huang Sakhaei, Michinao Hashimoto, Kavin Kowsari, Shlomo Magdassi, and Qi Ge. "Highly stretchable hydrogels for UV curing based high-resolution multimaterial 3D printing". In: *Journal of Materials Chemistry B* 6.20 (2018), pp. 3246–3253. DOI: 10.1039/c8tb00673c.
- [19] Norzita Jacob and Kamaruddin Hashim. "Morphological effect on swelling behaviour of hydrogel". In: *AIP Conference Proceedings* 1584.1 (2014), pp. 153–158. DOI: <https://doi.org/10.1063/1.4866123>.
- [20] Chisa Norioka, Yuino Inamoto, Chika Hajime, Akifumi Kawamura, and Takashi Miyata. "A universal method to easily design tough and stretchable hydrogels". In: *NPG Asia Materials* 13.34 (2021), pp. 1–10. DOI: <https://doi.org/10.1038/s41427-021-00302-2>.
- [21] M. B. Browning, T. Wilems, and M. E. Cosgriff-Hernandez Hahn. "Compositional control of poly(ethylene glycol) hydrogel modulus independent of mesh size". In: *Journal of Biomedical Materials Research part A* 98a.2 (2011), pp. 268–273. DOI: <https://doi.org/10.1002/jbm.a.33109>.
- [22] N. Ranganathan, R. Joseph Bensingh, Kader M. Abdul, and S.K. Nayak. "Synthesis and Properties of Hydrogels Prepared by Various Polymerization Reaction Systems." In: *Mondal M. (eds) Cellulose-Based Superabsorbent Hydrogels. Polymers and Polymeric Composites: A Reference Series* (2018). DOI: https://doi.org/10.1007/978-3-319-76573-0_18-1.
- [23] Amol A. Pawar, Gabriel Saada, Liraz Cooperstein Ido Larush, Joshua A. Jackman, Seyed R. Tabaei, Nam-Joon Cho, and Shlomo Magdassi. "High-performance 3D printing of hydrogels by water-dispersible photoinitiator nanoparticles". In: *Science Advances* 2.4 (2016), pp. 1–7. DOI: 10.1126/sciadv.1501381.
- [24] Mohammed Abdul Hadis. "POLYMERISATION KINETICS AND OPTICAL PHENOMENA OF PHOTOACTIVE DENTAL RESINS". PhD thesis. Faculty of Medicine and Dentistry of the University of Birmingham, 2011.
- [25] Inc Advanced Chemistry Development. *ACD/ChemSketch version 2020.2.1*. 2021. URL: www.acdlabs.com.
- [26] Aude Autissier, Catherine Le Visagea, Cécile Pouzetc, and Didier Chaubet Frédéric Letourneur. "Fabrication of porous polysaccharide-based scaffolds using a combined freeze-drying/cross-linking process". In: *Acta Biomaterialia* 6.9 (2010), pp. 3640–3648. DOI: <https://doi.org/10.1016/j.actbio.2010.03.004>.
- [27] Nasim Annabi, Jason W. Nichol, Xia Zhong, Chengdong Ji, Sandeep Koshy, Ali Khademhosseini, and Fariba Dehghani. "Controlling the Porosity and Microarchitecture of Hydrogels for Tissue Engineering". In: *Tissue Engineering. Part B, Reviews* 16.4 (2010), pp. 371–383. DOI: 10.1089/ten.teb.2009.0639.

- [28] Lei Qian and Haifei Zhang. "Controlled freezing and freeze drying: a versatile route for porous and micro-/nano-structured materials". In: *Journal of Chemical Technology and Biotechnology* 86 (2011), pp. 172–184. DOI: 10.1002/jctb.2495.
- [29] Stephen C. Cowin. *Mechanics of materials*. 2001, pp. 6–1–6–24. ISBN: 9781420036589. DOI: 10.4324/9781315636764-23.
- [30] Paul J. Flory and John Rehner. "Statistical mechanics of cross-linked polymer networks II. Swelling". In: *The Journal of Chemical Physics* 11.11 (1943), pp. 521–526. ISSN: 00219606. DOI: 10.1063/1.1723792.
- [31] Nicholas A. Peppas, J. Zach Hilt, Ali Khademhosseini, and Robert Langer. "Hydrogels in biology and medicine: From molecular principles to bionanotechnology". In: *Advanced Materials* 18.11 (2006), pp. 1345–1360. ISSN: 09359648. DOI: 10.1002/adma.200501612.
- [32] Josef Schurz. "Rheology of polymer solutions of the network type". In: *Progress in Polymer Science* 16.1 (1991), pp. 1–53. ISSN: 0079-6700. DOI: [https://doi.org/10.1016/0079-6700\(91\)90006-7](https://doi.org/10.1016/0079-6700(91)90006-7). URL: <https://www.sciencedirect.com/science/article/pii/0079670091900067>.
- [33] Polymerdatabase.com. *Characteristic Ratio of Some Polymers*. 21 May 2021. URL: <http://polymerdatabase.com/polymer/%20physics/C%20Table2%20.html>.
- [34] Paul J. Flory and John Rehner. "Statistical mechanics of cross-linked polymer networks I. Rubberlike elasticity". In: *The Journal of Chemical Physics* 11.11 (1943), pp. 512–520. ISSN: 00219606. DOI: 10.1063/1.1723791.
- [35] James C Bray and Edward W Merrill. "Poly (vinyl Alcohol) Hydrogels. Formation by Electron Beam Irradiation". In: *Journal of Applied Polymer Science* 17 (1973), pp. 3779–3794.
- [36] Donald L. Elbert, Alison B. Pratt, Matthias P. Lutolf, Sven Halstenberg, and Jeffrey A. Hubbell. "Protein delivery from materials formed by self-selective conjugate addition reactions". In: *Journal of Controlled Release* 76.1-2 (2001), pp. 11–25. ISSN: 01683659. DOI: 10.1016/S0168-3659(01)00398-4.
- [37] Andrea Doderò, Rhodri Williams, Simona Gagliardi, Silvia Vicini, Marina Alloisio, and Maila Castellano. "A micro-rheological and rheological study of biopolymers solutions: Hyaluronic acid". In: *Carbohydrate Polymers* 203 (2019), pp. 349–355. ISSN: 0144-8617. DOI: <https://doi.org/10.1016/j.carbpol.2018.09.072>.
- [38] L. R. G. Treloar. "The elasticity of a network of long-chain molecules. I". In: *Trans. Faraday Soc.* 39 (0 1943), pp. 36–41. DOI: 10.1039/TF9433900036.
- [39] Ana Salomé Veiga and Joel P. Schneider. "Antimicrobial hydrogels for the treatment of infection". In: *Biopolymers* 100.6 (2013), pp. 637–644. DOI: 10.1002/bip.22412.

- [40] Hongli Ye, Junwen Cheng, and Kun Yu. "In situ reduction of silver nanoparticles by gelatin to obtain porous silver nanoparticle/chitosan composites with enhanced antimicrobial and wound-healing activity". In: *International Journal of Biological Macromolecules* 121 (2019), pp. 633–642. DOI: <https://doi.org/10.1016/j.ijbiomac.2018.10.056>.
- [41] Chengzhu Liao, Yuchao Li, and Sie Tjong. "Bactericidal and Cytotoxic Properties of Silver Nanoparticles". In: *International Journal of Molecular Sciences* 20.2 (2019), p. 449. ISSN: 1422-0067. DOI: 10.3390/ijms20020449.
- [42] Christiane Beer, Rasmus Foldbjerg, Yuya Hayashi, Duncan S. Sutherland, and Herman Autrup. "Toxicity of silver nanoparticles—Nanoparticle or silver ion?" In: *Toxicology Letters* 208.3 (2012), pp. 286–292. ISSN: 03784274. DOI: 10.1016/j.toxlet.2011.11.002.
- [43] Pawinee Siritongsuk, Nuttaya Hongsing, Saengrawee Thammawithan, Sakda Daduang, Sompong Klaynongsruang, Apichai Tuanyok, and Rina Patramanon. "Two-Phase Bactericidal Mechanism of Silver Nanoparticles against *Burkholderia pseudomallei*". In: *PLOS ONE* 11.12 (2016). Ed. by Lisa A. Morici, e0168098. ISSN: 1932-6203. DOI: 10.1371/journal.pone.0168098.
- [44] Olesja M. Bondarenko, Mariliis Sihtmäe, Julia Kuzmičiova, Lina Ragelienė, Anne Kahru, and Rimantas Daugelavičius. "Plasma membrane is the target of rapid antibacterial action of silver nanoparticles in *Escherichia coli* and *Pseudomonas aeruginosa*". In: *International Journal of Nanomedicine* Volume 13 (2018), pp. 6779–6790. ISSN: 1178-2013. DOI: 10.2147/IJN.S177163.
- [45] Sukdeb Pal, Yu Kyung Tak, and Joon Myong Song. "Does the Antibacterial Activity of Silver Nanoparticles Depend on the Shape of the Nanoparticle? A Study of the Gram-Negative Bacterium *Escherichia coli*". In: *Applied and Environmental Microbiology* 73.6 (2007), pp. 1712–1720. ISSN: 0099-2240. DOI: 10.1128/AEM.02218-06.
- [46] Muhammad Raza, Zakia Kanwal, Anum Rauf, Anjum Sabri, Saira Riaz, and Shahzad Naseem. "Size- and Shape-Dependent Antibacterial Studies of Silver Nanoparticles Synthesized by Wet Chemical Routes". In: *Nanomaterials* 6.4 (2016), p. 74. ISSN: 2079-4991. DOI: 10.3390/nano6040074.
- [47] Celia Ferrag, Shaopei Li, Keuna Jeon, Nesha May Andoy, Ruby May A. Sullan, Svetlana Mikhaylichenko, and Kagan Kerman. "Polyacrylamide hydrogels doped with different shapes of silver nanoparticles: Antibacterial and mechanical properties". In: *Colloids and Surfaces B: Biointerfaces* 197 (2021), p. 111397. ISSN: 09277765. DOI: 10.1016/j.colsurfb.2020.111397.
- [48] Abbas Abbaszadegan, Yasamin Ghahramani, Ahmad Gholami, Bahram Hemmateenejad, Samira Dorostkar, Mohammadreza Nabavizadeh, and Hashem Sharghi. "The Effect of Charge at the Surface of Silver Nanoparticles on Antimicrobial Activity against Gram-Positive and Gram-Negative Bacteria: A Preliminary Study".

- In: *Journal of Nanomaterials* 2015 (2015), pp. 1–8. ISSN: 1687-4110. DOI: 10.1155/2015/720654.
- [49] Amro M. El Badawy, Rendahandi G. Silva, Brian Morris, Kirk G. Scheckel, Makram T. Suidan, and Thabet M. Tolaymat. "Surface Charge-Dependent Toxicity of Silver Nanoparticles". In: *Environmental Science & Technology* 45.1 (2011), pp. 283–287. ISSN: 0013-936X. DOI: 10.1021/es1034188.
- [50] Liang Chen, Meiyu Wu, Shan Jiang, Yanyun Zhang, Runzhi Li, Yongbo Lu, Lin Liu, Gang Wu, Ying Liu, Liming Xie, and Liming Xu. "Skin Toxicity Assessment of Silver Nanoparticles in a 3D Epidermal Model Compared to 2D Keratinocytes". In: *International Journal of Nanomedicine* Volume 14 (2019), pp. 9707–9719. ISSN: 1178-2013. DOI: 10.2147/IJN.S225451.
- [51] S. Iravani, H. Korbekandi, S. V. Mirmohammadi, and B. Zolfaghari. "Synthesis of silver nanoparticles: chemical, physical and biological methods." In: *Research in pharmaceutical sciences* 9.6 (2014), pp. 385–406. ISSN: 1735-5362.
- [52] Damian Aherne, Deirdre M. Ledwith, Matthew Gara, and John M. Kelly. "Optical Properties and Growth Aspects of Silver Nanoprisms Produced by a Highly Reproducible and Rapid Synthesis at Room Temperature". In: *Advanced Functional Materials* 18.14 (2008), pp. 2005–2016. ISSN: 1616301X. DOI: 10.1002/adfm.200800233.
- [53] Yugang Sun and Younan Xia. "Shape-Controlled Synthesis of Gold and Silver Nanoparticles". In: *Science* 298.5601 (2002), pp. 2176–2179. ISSN: 00368075. DOI: 10.1126/science.1077229.
- [54] Bahareh Khodashenas and Hamid Reza Ghorbani. "Synthesis of silver nanoparticles with different shapes". In: *Arabian Journal of Chemistry* 12.8 (2019), pp. 1823–1838. ISSN: 18785352. DOI: 10.1016/j.arabjc.2014.12.014.
- [55] Xiaohu Xia, Jie Zeng, Qiang Zhang, Christine H. Moran, and Younan Xia. "Recent Developments in Shape-Controlled Synthesis of Silver Nanocrystals". In: *The Journal of Physical Chemistry C* 116.41 (2012), pp. 21647–21656. ISSN: 1932-7447. DOI: 10.1021/jp306063p.
- [56] Zhi Zhang, Wenfei Shen, Jing Xue, Yuanmeng Liu, Yanwei Liu, Peipei Yan, Jixian Liu, and Jianguo Tang. "Recent advances in synthetic methods and applications of silver nanostructures". In: *Nanoscale Research Letters* 13.1 (2018), p. 54. ISSN: 1931-7573. DOI: 10.1186/s11671-018-2450-4.
- [57] Zhenjiang Zhang and Ping-Chang Lin. "Noble metal nanoparticles: synthesis, and biomedical implementations". In: *Emerging Applications of Nanoparticles and Architecture Nanostructures*. Elsevier, 2018, pp. 177–233. ISBN: 9780128135167. DOI: 10.1016/B978-0-323-51254-1.00007-5.
- [58] Sang Lee and Bong-Hyun Jun. "Silver Nanoparticles: Synthesis and Application for Nanomedicine". In: *International Journal of Molecular Sciences* 20.4 (2019), p. 865. ISSN: 1422-0067. DOI: 10.3390/ijms20040865.

- [59] Lixiang Xing, Yujiao Xiahou, Peina Zhang, Wei Du, and Haibing Xia. "Size Control Synthesis of Monodisperse, Quasi-Spherical Silver Nanoparticles to Realize Surface-Enhanced Raman Scattering Uniformity and Reproducibility". In: *ACS Applied Materials and Interfaces* 11.19 (2019), pp. 17637–17646. ISSN: 19448252. DOI: 10.1021/acscami.9b02052.
- [60] Houshen Li, Haibing Xia, Dayang Wang, and Xutang Tao. "Simple synthesis of monodisperse, quasi-spherical, citrate-stabilized silver nanocrystals in water". In: *Langmuir : the ACS journal of surfaces and colloids* 29.16 (2013), 5074–5079. ISSN: 0743-7463. DOI: 10.1021/la400214x.
- [61] Varsha Thomas, Murali Mohan Yallapu, B. Sreedhar, and S. K. Bajpai. "Breathing-in/breathing-out approach to preparing nanosilver-loaded hydrogels: Highly efficient antibacterial nanocomposites". In: *Journal of Applied Polymer Science* (2008), NA–NA. ISSN: 00218995. DOI: 10.1002/app.29018.
- [62] Mohamed A. Mekkawy Aml I. and El-Mokhtar, Sohair M. El-Shanawany, and Ehsan H. Ibrahim. "Silver Nanoparticles-loaded Hydrogels, A Potential Treatment for Resistant Bacterial Infection and Wound Healing: A Review". In: *British Journal of Pharmaceutical Research* 14.2 (2016), pp. 1–19. DOI: 10.9734/BJPR/2016/30525.
- [63] Maulida Zakia, Ja Min Koo, kim Dowan, Keunho Ji, Jinhwan Huh PilHo Yoon, and Seong Il Yoo. "Development of silver nanoparticle-based hydrogel composites for antimicrobial activity". In: *Green Chemistry Letters and Reviews* 13.1 (2020), pp. 34–40. DOI: 10.1080/17518253.2020.1725149.
- [64] Tan Dat Nguyen, Thanh Truc Nguyen, Khanh Loan Ly, Anh Hien Tran, Thi Thanh Ngoc Nguyen, Minh Thuy Vo, Hieu Minh Ho, Ngoc Thao Nhi Dang, Van Toi Vo, Dai Hai Nguyen, Thi Thu Hoai Nguyen, and Thi Hiep Nguyen. "In Vivo Study of the Antibacterial Chitosan/Polyvinyl Alcohol Loaded with Silver Nanoparticle Hydrogel for Wound Healing Applications". In: *International Journal of Polymer Science* 2019 (2019), pp. 1–10. DOI: <https://doi.org/10.1155/2019/7382717>.
- [65] Nosheen Masood, Rashid Ahmed, Muhammad Tariq, Zahoor Ahmed, Muhammad Shareef Masoud, Imran Ali, Rehana Asghar, Anisa Andleeb, and Anwarul Hasan. "Silver nanoparticle impregnated chitosan-PEG hydrogel enhances wound healing in diabetes induced rabbits". In: *International Journal of Pharmaceutics* 559 (2019), pp. 23–36. DOI: <https://doi.org/10.1016/j.ijpharm.2019.01.019>.
- [66] Vered Pardo-Yissar, Rachel Gabai, Andrew N. Shipway, Tatyana Bourenko, and Itamar Willner. "Gold Nanoparticle/Hydrogel Composites with Solvent-Switchable Electronic Properties". In: *Advanced Materials* 13.17 (2001), pp. 1320–1323. DOI: [https://doi.org/10.1002/1521-4095\(200109\)13:17<1320::AID-ADMA1320>3.0.CO;2-8](https://doi.org/10.1002/1521-4095(200109)13:17<1320::AID-ADMA1320>3.0.CO;2-8).

- [67] Jun Tian, Kenneth K.Y. Wong, Chi-Ming Ho, Chun-Nam Lok, Wing-Yiu Yu, Chi-Ming Che, Jen-Fu Chiu, and Paul K. H. Tam. "Topical Delivery of Silver Nanoparticles Promotes Wound Healing". In: *ChemMedChem* 2.1 (2007), pp. 129–136. doi: 10.1002/cmdc.200600171.
- [68] I. Horcas, J. M. Fernández R. Gómez-Rodríguez, J. Colchero, J. Gómez-Herrero, and A. M. Baro. "WSXM: A software for scanning probe microscopy and a tool for nanotechnology". In: *Review of Scientific Instruments* 78 (2007), pp. 1–8. doi: <https://doi.org/10.1063/1.2432410>.
- [69] C. Schneider, W. Rasband, and K Eliceiri. "NIH Image to ImageJ: 25 years of image analysis". In: *Nature Methods* 9.19 (2012), pp. 671–675. doi: <https://doi.org/10.1038/nmeth.2089>.
- [70] Jianyu Li and David J. Mooney. "Designing hydrogels for controlled drug delivery". In: *Nature reviews. Materials* 1.12 (2016), pp. 1–19. doi: 10.1038/natrevmats.2016.71..
- [71] MalvernInstruments. "NanoSight - NTA 2.1 Analytical Software". In: (2010), pp. 1–62.
- [72] Siew Leng Loo, William B. Krantz, Anthony G. Fane, Xiao Hu, and Teik Thye Lim. "Effect of synthesis routes on the properties and bactericidal activity of cryogels incorporated with silver nanoparticles". In: *RSC Advances* 5.55 (2015), pp. 44626–44635. ISSN: 20462069. doi: 10.1039/c5ra08449k.
- [73] Wenjin Xing, Amin Jamshidi Ghahfarokhi, Chaoming Xie, Sanaz Naghibi, Jonathan A. Campbell, and Youhong Tang. "Mechanical properties of a supramolecular nanocomposite hydrogel containing hydroxyl groups enriched hyper-branched polymers". In: *Polymers* 13.5 (2021). ISSN: 20734360. doi: 10.3390/polym13050805.
- [74] Rabiul Salihu, Saiful Izwan Abd Razak, Nurliyana Ahmad Zawawi, Mohammed Rafiq Abdul Kadir, Norjihada Izzah Ismail, Norhana Jusoh, Mohd Riduan Mohamad, and Nadirul Hasraf Mat Nayan. "Citric acid: A green cross-linker of biomaterials for biomedical applications". In: *European Polymer Journal* 146. January (2021), p. 110271. ISSN: 00143057. doi: 10.1016/j.eurpolymj.2021.110271.

Appendix A

Particle shape and size characterisation

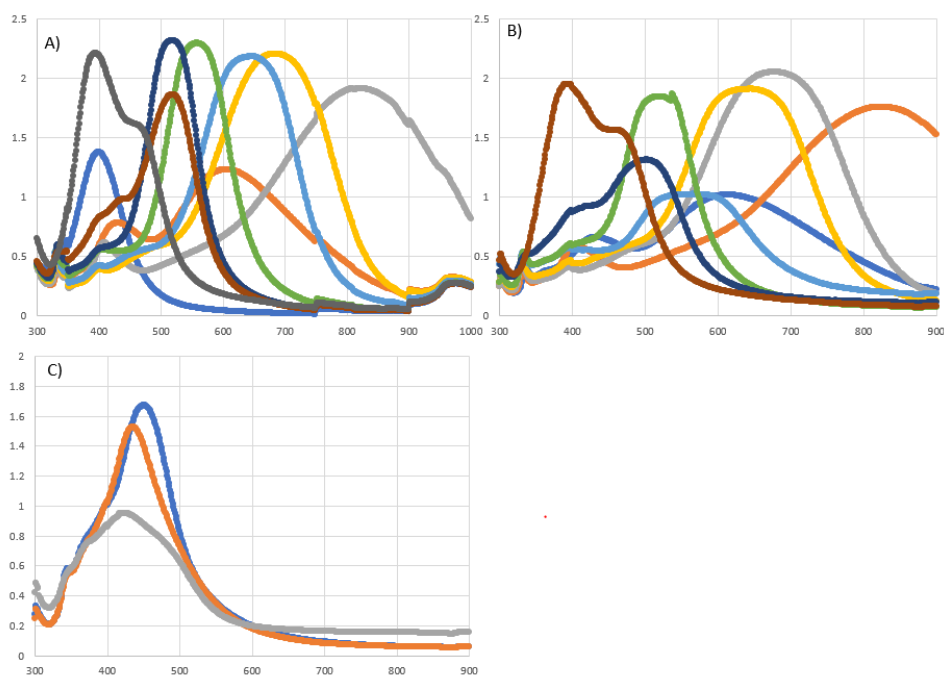


Figure A.1: UV vis spectra are depicted of a series of nanoparticles of varying sizes spherical (Dark grey), 600 μ L Prism (Maroon), 400 μ L Prism (Dark blue), 200 μ L Prism (Green), 150 μ L Prism (Light blue), 100 μ L Prism (Yellow), 50 μ L Prism (Light grey) and 25 μ L Prism (Orange) A) Right after synthesis the spectra was assessed B) and after 2 months the spectra was redone. C) the spectrum of spherical particles with different seed volumes, 400 μ L (Light grey), 200 μ L (Orange) and 100 μ L (Blue) with a 1 M PSSS concentration. On the y-axis the absorbance and x-axis the wavelength is given.

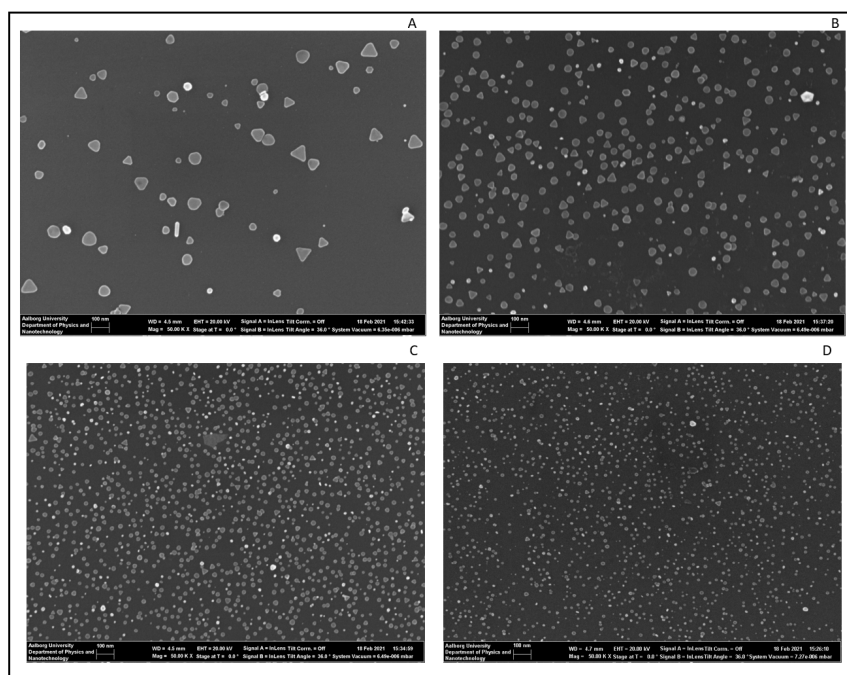


Figure A.2: SEM image of the different nanoparticles made with different seed amount added during growth. a) 50 μL , b) 100 μL , c) 200 μL and d) 400 μL

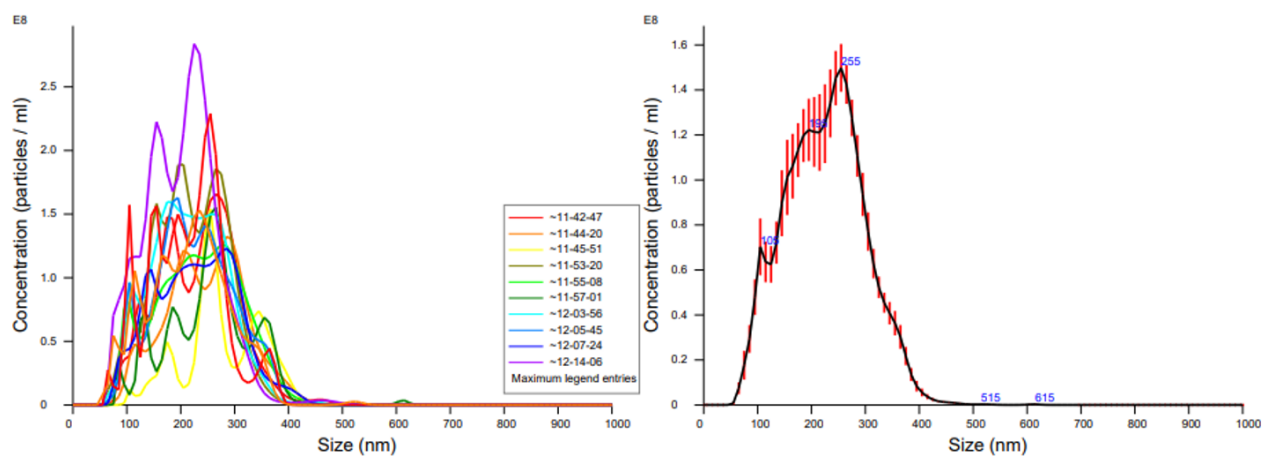


Figure A.3: Size distribution of TPO nanoparticles measured with NTA, a) separate regions were imaged for 45 seconds in five different samples, concentration was plotted against the calculated size. b) The tracks were combined for an average size distribution. Current temperature measured at the end of imaging a region and entered into the software. Track length was set to 12 frames and jump distance was set to automatic

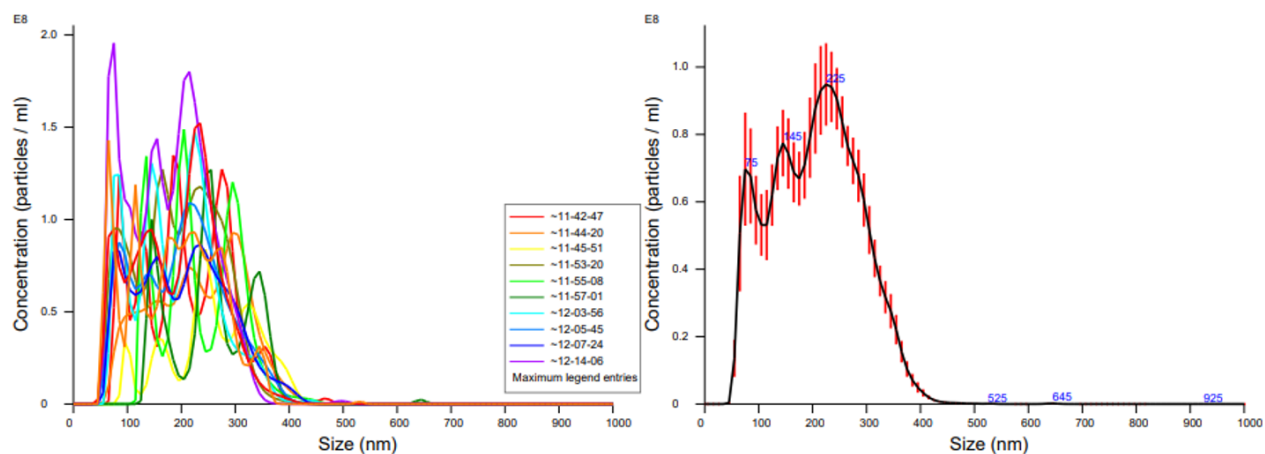


Figure A.4: Size distribution of TPO nanoparticles measured with NTA, a) separate regions were imaged for 45 seconds in five different samples, concentration was plotted against the calculated size. b) The tracks were combined for an average size distribution. Current temperature measured at the end of imaging a region and entered into the software. Track length and jump distance were set to automatic

Appendix B

Nanoparticle AFM and SEM image analysis

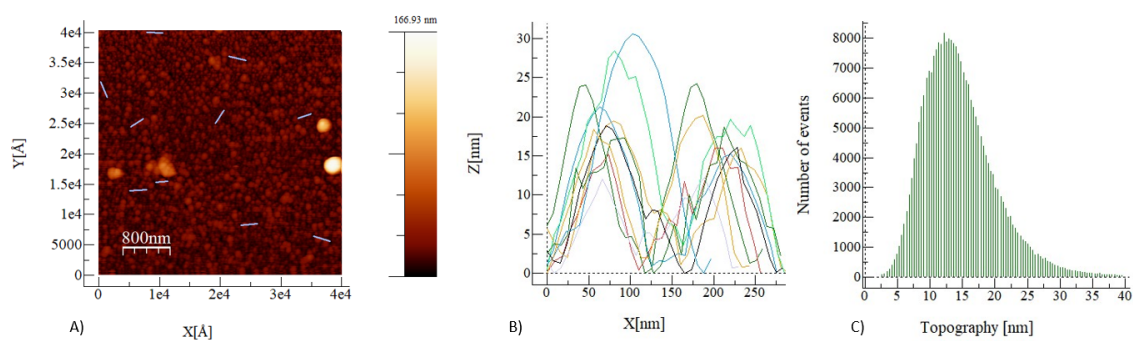


Figure B.1: a) shows the AFM image of the citrated capped spherical nanoparticles made from 400 μ L seed solution. Height measurement of selected particles is seen in b) where the selected particles measured is seen by the blue line in a). Height distribution is seen in c).

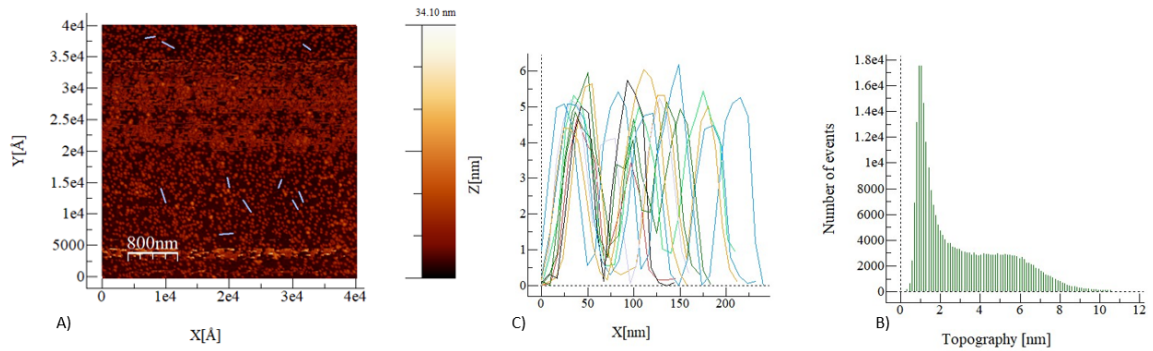


Figure B.2: a) shows the AFM image of the citrated capped spherical nanoparticles made from 200 μL seed solution. Height measurement of selected particles is seen in b) where the selected particles measured is seen by the blue line in a). Height distribution is seen in c).

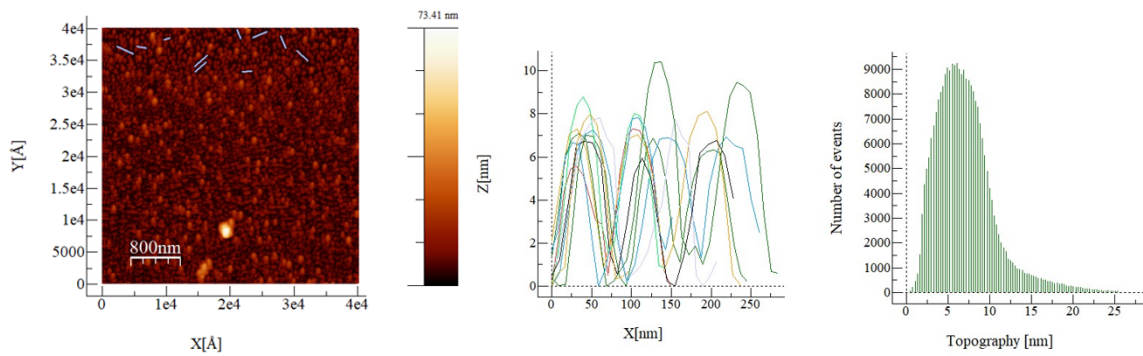


Figure B.3: a) shows the AFM image of the citrated capped spherical nanoparticles made from 100 μL seed solution. Height measurement of selected particles is seen in b) where the selected particles measured is seen by the blue line in a). Height distribution is seen in c).

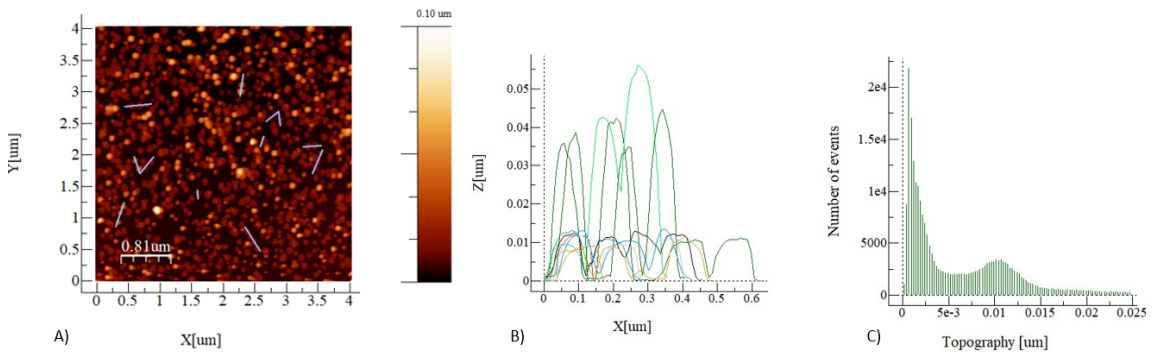


Figure B.4: a) shows the AFM image of the citrated capped spherical nanoparticles made from 50 μL seed solution. Height measurement of selected particles is seen in b) where the selected particles measured is seen by the blue line in a). Height distribution is seen in c).

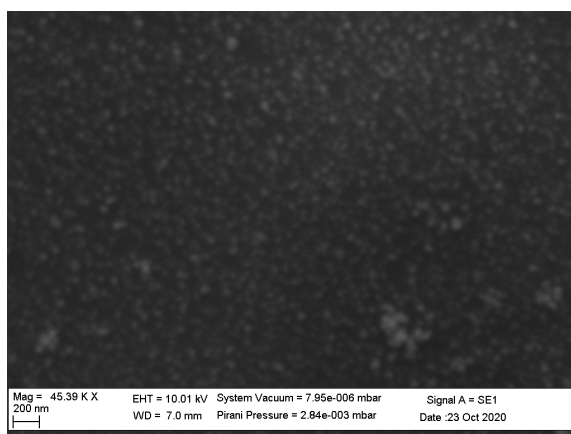


Figure B.5: SEM image of the spherical nanoparticles at 45.39 k magnification

Appendix C

SEM images and histogram of pore size

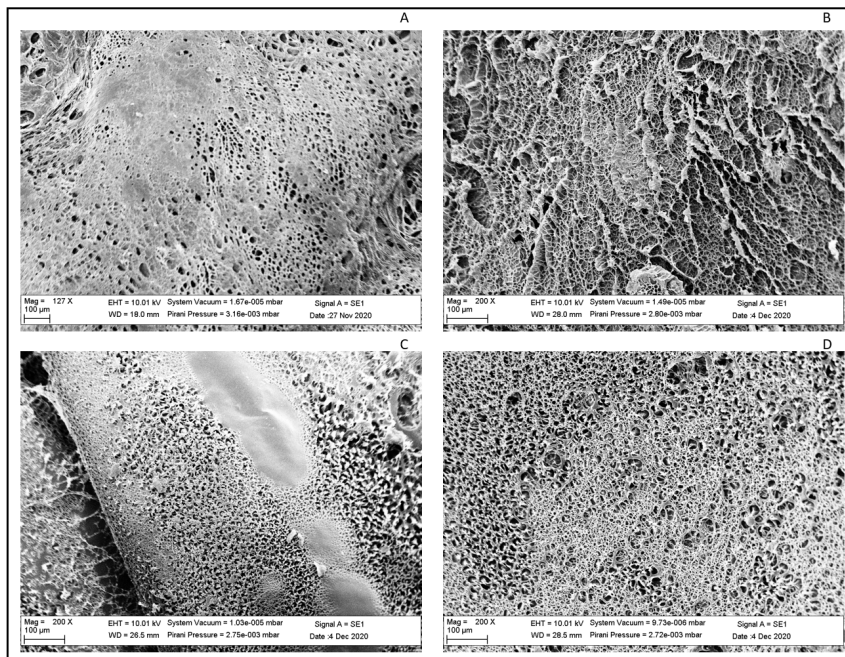


Figure C.1: SEM images of gels consisting of A) 5 % AAm, B) 10 % AAm, C) 15% AAm and D) 20 %

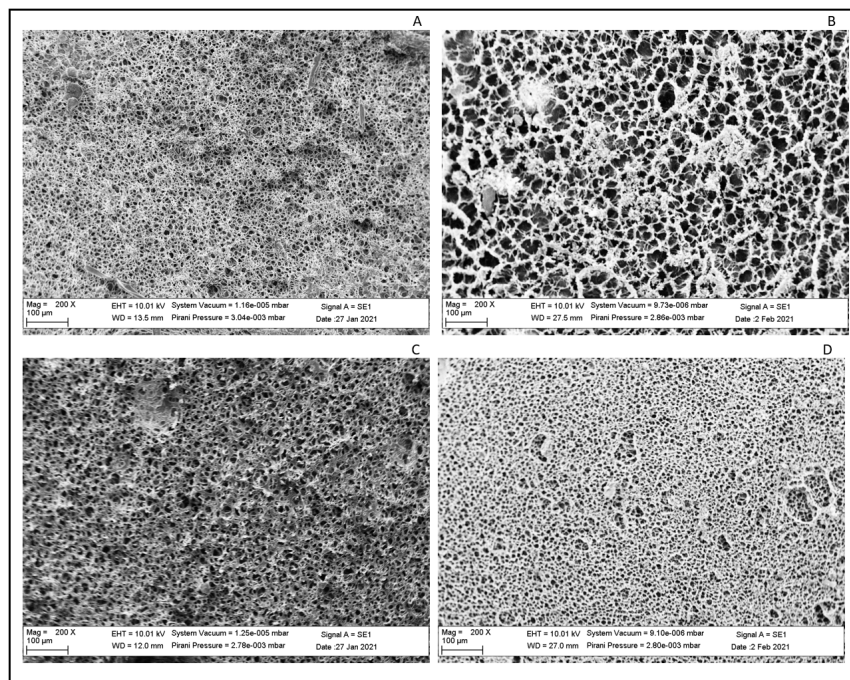


Figure C.2: Pores compared to each other at the same percentage of PEGDA non-swollen vs swollen for 24 hours. A) non swollen 0.78 % PEGDA/AAm ratio, B) swollen 0.78 % PEGDADA/AAm, C) non swollen 1.56 % PEGDA/AAm and D) swollen 1.56 % PEGDADA/AAm

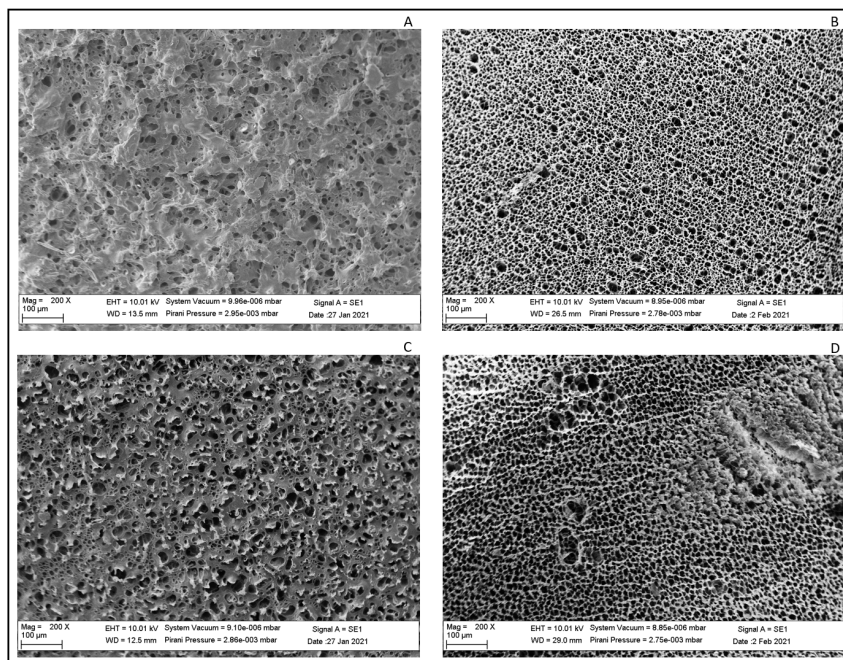


Figure C.3: Pores compared to each other at the same percentage of PEGDA non-swollen vs swollen for 24 hours. A) non swollen 2.34 % PEGDA/AAm ratio, B) swollen 2.34 % PEGDA/AAm, C) non swollen 3.12 % PEGDA/AAm and D) swollen 3.12 % PEGDA/AAm

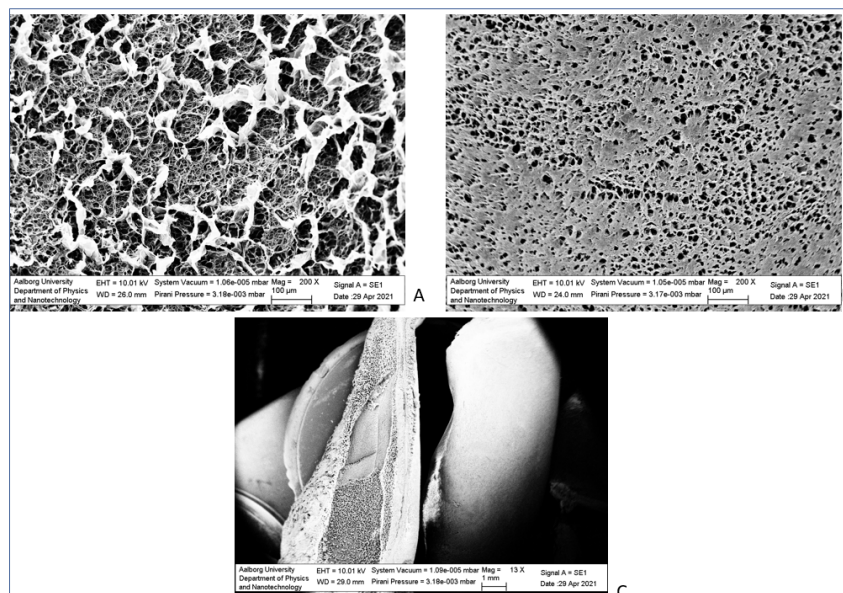


Figure C.4: The same gel but different sides C), A) the side which the water got sucked out and B) the side in contact with the Greiner tube.

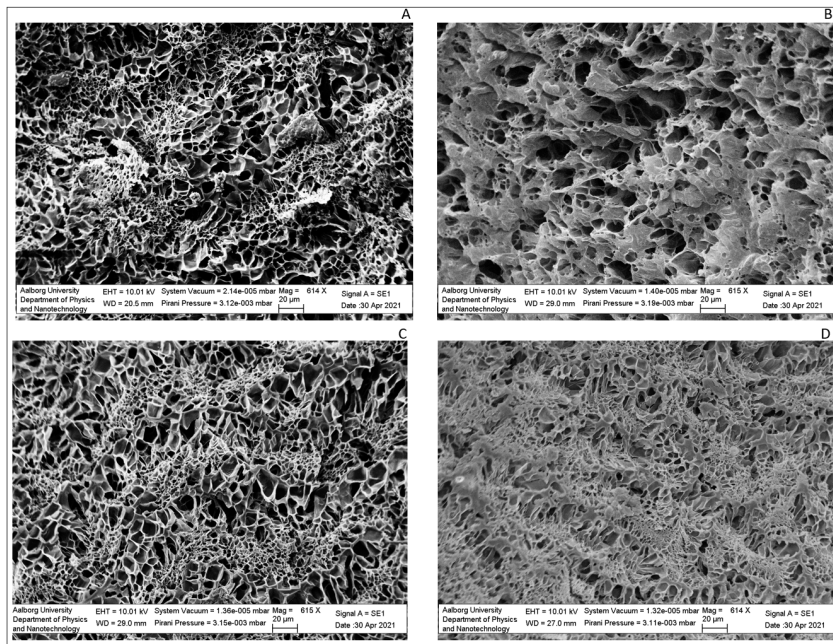


Figure C.5: SEM image of the hydrogel magnified by 614x consisting of A) 0.78 and B) 3.12 % PEGDA₂₅₀ whereas C) and D) consist of 0.78 and 3.12% PEGDA₂₅₀, respectively.

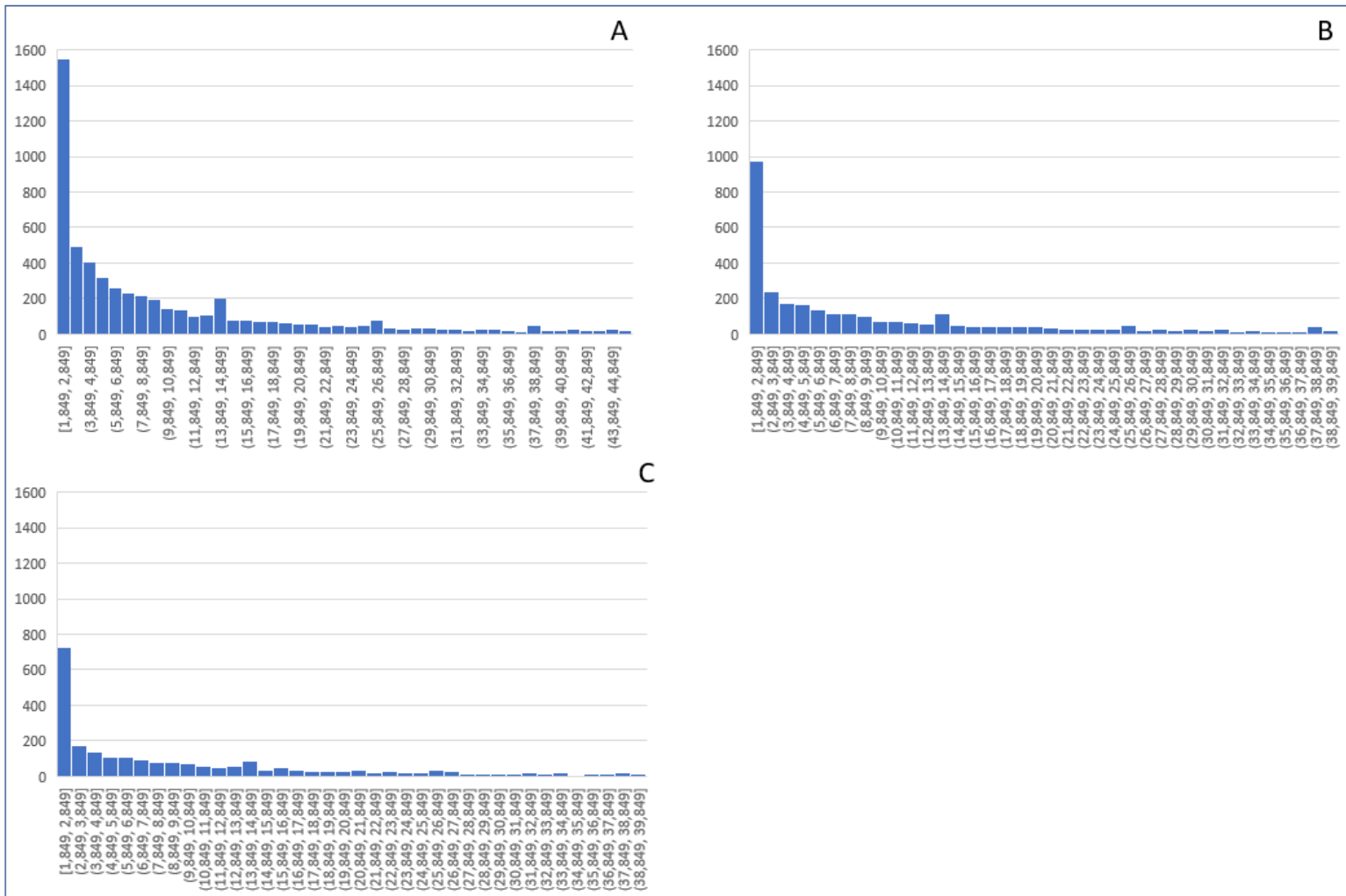


Figure C.6: All the gels consist of 1.56% PEGDA/AAM-ratio. The histograms are for gels consisting of A) 20, B) 15 and C) 10% AAm

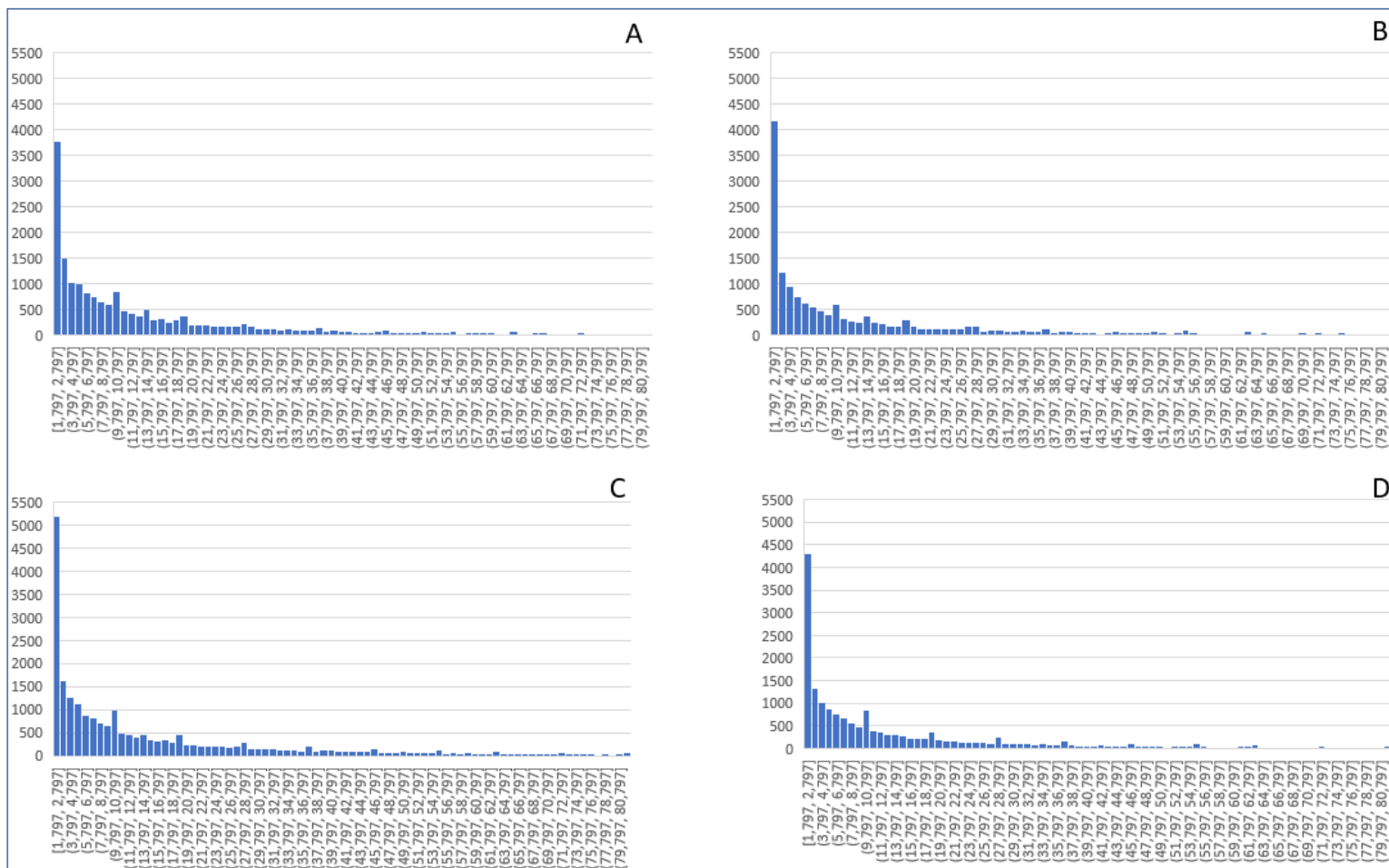


Figure C.7: All the gels consist of 15% AAm The histograms are for gels consisting of A) 0.78, B) 1.56, C) 2.34 and D) 3.12% PEGDA/AAM

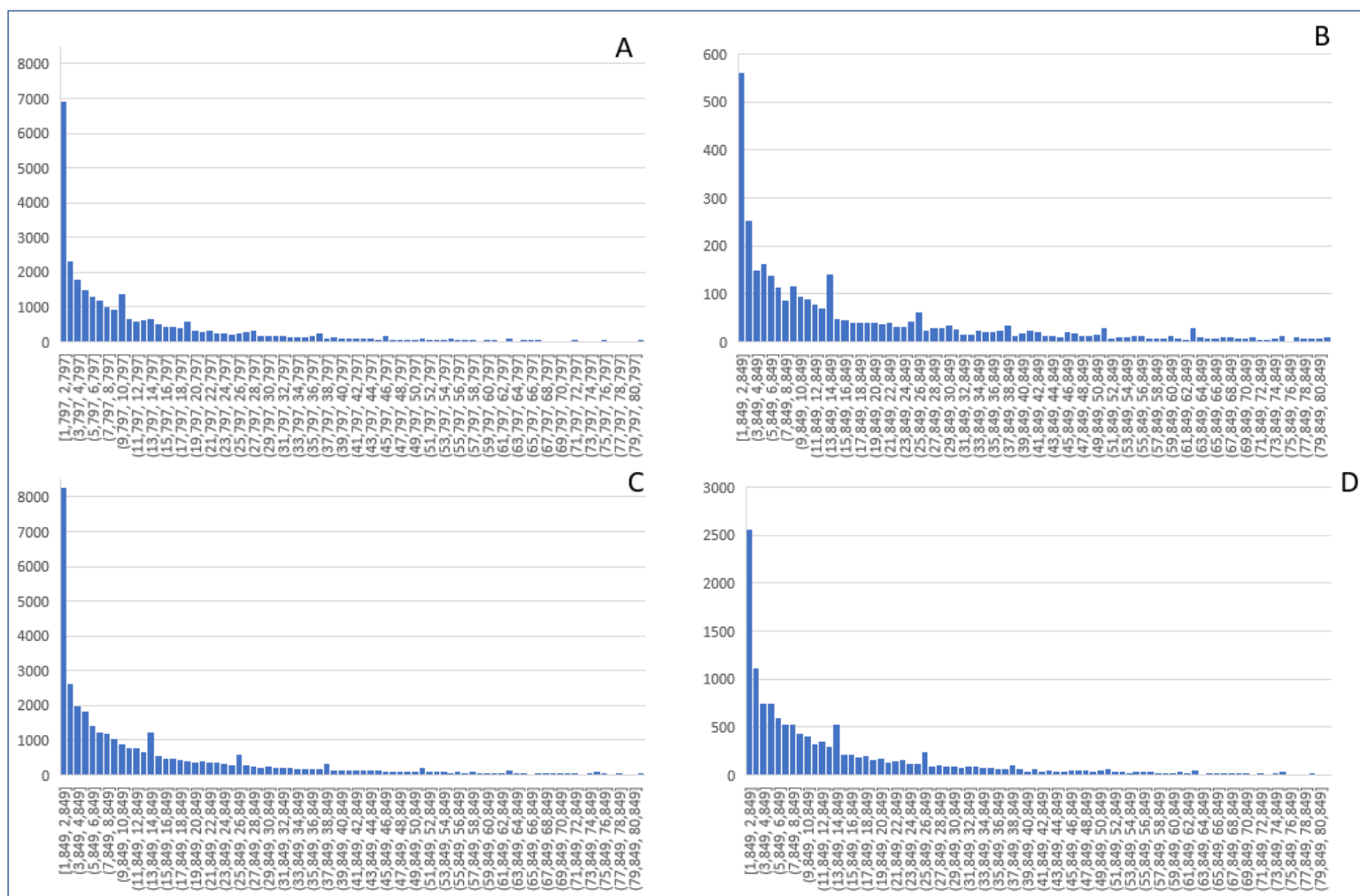


Figure C.8: All the gels consist of 15% AAm The histograms are for gels consisting of A) 0.78% PEGDA 250 Mn, B) 3.12% PEGDA 250 Mn, C) 0.78% PEGDA 700 Mn and D) 3.12% PEGDA 700 Mn

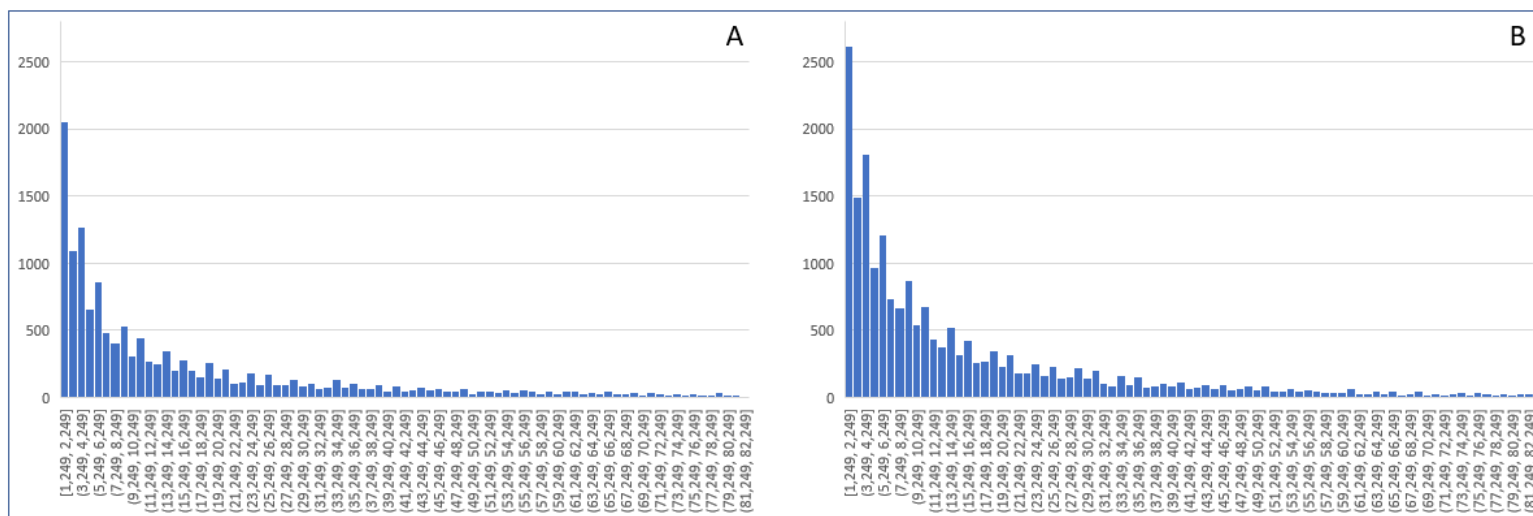


Figure C.9: The histograms show gels consisting of 15% AAm and 0.78% PEGDA/AAm ratio with PEGDA 575. A) histogram of 0.78% PEGDA gel and B) histogram for same type of gel but swollen for 72 hours